IN-PLANE BEHAVIOUR AND CAPACITY OF CONCRETE MASONRY INFILLS BOUNDED BY STEEL FRAMES

by

Sandra Soon

Submitted in partial fulfilment of the requirements
for the degree of Master of Applied Sciences

at

Dalhousie University
Halifax, Nova Scotia
October 2011

DALHOUSIE UNIVERSITY

DEPARTMENT OF CIVIL AND RESOURCE ENGINEERING

The undersigned hereby certify that they have read and recommend to the Faculty of Graduate Studies for acceptance a thesis entitled "IN-PLANE BEHAVIOUR AND CAPACITY OF CONCRETE MASONRY INFILLS BOUNDED BY STEEL FRAMES" by Sandra Soon in partial fulfilment of the requirements for the degree of Master of Applied Sciences.

Dated: October 28th, 2011

Supervisor: _____

_

Readers: _____

_

_____

DALHOUSIE UNIVERSITY

DATE: October 28th 2011

AUTHOR: Sandra Soon

TITLE: IN-PLANE BEHAVIOUR AND CAPACITY OF CONCRETE MASONRY INFILLS BOUNDED BY STEEL FRAMES

DEPARTMENT OR SCHOOL: Department of Civil and Resource Engineering

DEGREE: MASc **CONVOCATION:** May **YEAR**: 2012

_____

Signature of Author

For mom and dad

TABLE OF CONTENTS

LIST OF TABLES

LIST OF FIGURES

ABSTRACT

Masonry infilled walls have been commonly used as interior partitions as well as exterior walls infilled in either steel or reinforced concrete frames in the modern building constructions. In recent years, much research involving both experimentation and numerical modeling has been conducted in an effort to better understand the infill-frame interaction and to provide some rational design approaches. Studies have shown that infill walls can develop a number of possible failure mechanisms, depending on the strength and stiffness of the bounding frames with respect to those of the infills and the geometric configuration of the framing system. Most of models proposed for analysis of infill walls focused on one type of mechanism or the other, and they were not universally applicable to all infilled structures. Although the current Canadian and American masonry design standards provide some design guidelines in terms of evaluation of infills stiffness and strength, the efficacy of these guidelines has not been thoroughly examined.

An experimental program was therefore conducted to study the in-plane behavior of masonry infilled frames with the focus on the infills. Nine infilled frame specimens and one bare frame specimen were tested under a monotonic lateral load applied at the roof level of the frame. Parameters that were considered in this experimental program included the aspect ratio, grouting situation, opening and frame-to-infill stiffness. The initial stiffness, secant stiffness, failure mode and ultimate strength of the infill under the effects of the above mentioned parameters were obtained and discussed. Results from this experimental study as well as experimental studies by several other researchers were then used to evaluate the performance of equations provided by the current design standards.

In this experimental study, two failure modes including corner crushing and diagonal tension cracking were observed. It was found that increasing the grouting in the infill resulted in an increase in both stiffness and strength of the infill. The presence of openings located in the central region of the infill reduced the stiffness and strength of the infill. A frame with weaker columns showed lower stiffness and strength comparing with one with stronger columns. It is evident that gap, even small, between the frame and infill may significantly affect the stiffness and strength of the infill. Accurate estimation of the stiffness and strength could be compromised when gaps are present. Results from this study showed that equations by CSA S304 generally overestimate the stiffness and underestimate the ultimate strength whereas equations by MSJC 2011 provide an overall better agreement with test results in both stiffness and strength. However, it should be cautioned that MSJC 2011, in several cases, overestimated the ultimate strength but underestimated the stiffness. Experimental results by several other researchers were also compared with values provided by CSA S304 and MSJC 2011. Although the average design-to-test ratios for both stiffness and strength are acceptable in this comparison, large scatters of results are observed. It suggests that design based on CSA S304 may be conservative while using MSJC 2011 design method may lead to an unsafe design.

LIST OF ABBREVIATIONS AND SYMBOLS USED

The following is a list of notations and symbols used in this thesis. All symbols and notations used are also defined in the text when they first appear.

Symbols

A	Total diagonal strut area
A_b, A_c	Cross-sectional area of the beam, column
τ_b	Shear stress along the beam
b_w	Overall web width
C	Empirical constant that varies with the in-plane displacement
C_{AC}	Multiplication factor that accounts for aspect ratio
d	Diagonal length of a rectangular steel frame
d_v	Effective depth for shear calculations
E_b, E_c	Modulus of elasticity of beam, column
E_f, E_I	Young's elastic modulus of the frame, infill
f'_m	Compressive strength of the masonry
f'_{mV}	Compressive strength of vertically loaded prisms
f_t	Tensile strength of the masonry
H, h	Height of the frame, infill
H_{cr}	Calculated net cracking strength of the masonry infill
H_{ult}	Calculated corner-crushing load
I_b, I_c	Moment of inertia of the beam, column
I_f	Moment of inertia the frame
K_{cr}	Empirical constant for first crack strength calculations
Kcra	Secant stiffness at first crack obtained during experimental study
K_{CSA}	Stiffness calculated using CSA equations
K_{EURO}	Stiffness calculated using Eurocode 8
K_{INI}	Initial stiffness obtained during experimental study
K_{MSJC}	Stiffness calculated using MSJC 2011
K_{ULT}	Secant stiffness at ultimate obtained during experimental study
K_{ult}	Empirical constant for ultimate strength calculation
L, ℓ	Length of frame, infill
ℓ_d	Diagonal length of infill panel
m	Dimensionless parameter relating the ratio of beam to column stiffness
M_{pb}, M_{pc}	Plastic resisting moment of the beam, column
M_{pj}	Least of the beam, the column, and their connection plastic resisting moment
N_u	Factored compressive force acting normal to shear surface that is associated with the V_u loading combination case under consideration
P_1	Compressive force in the unreinforced masonry acting normal to the sliding plane
P_{CRA}	First crack load obtained during experimental study
P_d	Axial compressive load on the section under consideration
P_r	Factored axial load resistance

P_{ULT}	Ultimate load obtained during experimental study
t	Thickness of the infill
t_e	Effective thickness of the infill
t_f	Thickness of the flange of the concrete masonry unit
V_n	Nominal shear strength
V_r	Factored shear resistance
w	Effective width
z	Empirical constant
θ	Slope of the infill diagonal to the horizontal axis
μ	Coefficient of friction on the interface between the frame and infill
$\alpha_{b,}\ \alpha_c$	Contact length with the beam, column
$\alpha_{L,}\ \alpha_h$	Horizontal, vertical contact length between the frame and the diagonal strut
β_o	Nominal upper bound to a reduction factor to account for the non-ideal plasticity
γ	Effective width factor
γ_g	Factor to account for partially grouted walls or columns or ungrouted walls and columns when calculating the shear resistance
λ	Non-dimensional stiffness parameter
ν_m	Shear strength of masonry
$\sigma_{bo,}\ \sigma_{co}$	Upper-bound normal contact stresses on the face of the beam, column
υ	Poison ratio for the infill
ϕ_m	Resistance factor for masonry
χ	Factor used to account for direction of compressive stress in a masonry member relative to the direction used for the determination of $f'_{m.}$

Abbreviation

CB	Concrete block
CMU	Concrete masonry unit
CS	Concrete encased steel
DAB	Dense aggregate blocks
RC	Reinforced concrete
SCT	Structural clay tile

ACKNOWLEDGEMENTS

This dissertation would not have been possible without the guidance and the help of several individuals who in one way or another contributed and extended their valuable assistance in the preparation and completion of this study.

First and foremost, I owe sincere gratitude to my research advisor, Dr. Yi Liu, who made me believe in myself and guided me through the entire process of this research. I will never forget her generous contributions, understanding and encouragement as I overcome all the obstacles in the completion of this research.

My thanks also go to my thesis committee members Dr. John Newhook and Dr. Dmitry Garagash for their time spent on reviewing this thesis. I would like to express my thanks to the faculty and staff of the Department of Civil and Resource Engineering for their support during this research. I would also like to especially thank Mr. Brian Kennedy, Mr. Brian Liekens, and Mr. Blair Nickerson for their assistance and helpful contributions during the experimental stage of this research.

Acknowledgement is due to the Canadian Masonry Design Centre for providing the material for the fabrication of the wall specimens. A special thanks to Mr. Gerry Hubley for his hard work as well as providing practical guidance throughout the fabrication of the specimens.

Lastly, I would like to thank my friends and family, most importantly, my parents who provided me with unparalleled support and inspiration. A special thanks to Alex Bell, for his never-ending encouragement throughout this research.

CHAPTER 1 INTRODUCTION

1.1 BACKGROUND OF MASONRY

Masonry has been used to construct various structures since the beginning of civilization, dating back as early as ten thousand years ago (Drysdale and Hamid, 2005). Until late in the nineteenth century masonry has been one of the principal construction materials. The first masonry construction consisted of dry stacking suitably shaped natural stones with earth introduced as a binding material, as well as to provide uniform bedding for masonry units. Other materials such as clay bricks, calcium silicate units, and concrete masonry units were eventually introduced as knowledge of masonry increased. However, masonry construction experienced a serious decline in the past 100 years due to its slow development in construction techniques and more importantly, a rational design method. While rational design methods and building codes were rapidly developing for the other more modern construction materials such as concrete and steel, masonry was being designed by very conservative "rules of the thumb" based on its historical use. Such rules of thumb lead to inordinately high safety factors combined with unacceptably high construction costs in our modern engineering age. Not until the 1960s was masonry revived as a competitive construction material with the introduction of American Standards Association Building Code Requirement for Masonry (ASA A41.4-1953) and the National Building Code of Canada (1965) together with significant improvements in masonry manufacturing techniques.

1.2 MASONRY INFILLED PANELS

In modern building construction, masonry is often used together with concrete or steel. One example is masonry infilled frames where masonry walls are used to infill concrete or steel frames. These infilled frames are used either as partitions to separate spaces or as claddings to complete the building envelope. For the design and construction of these frames, a decision has to be made on whether to include the masonry wall as part of the framing structure or to treat it as a separate entity. The common practice at present is to treat masonry infills as non-structural elements and design surrounding frames for both gravity and lateral loading. By not taking advantage of infills' inherent large in-plane

stiffness, the design may not be an economical one since the lateral loading system has to rely upon other elements. On the other hand, if one is to incorporate the infill in the load sharing with the surrounding frame, the accurate estimation of infill frame stiffness and strength is crucial in the overall assessment of structural behavior and capacity.

Due to the lack of scientific information on the exact extent of interaction between the infill and the surrounding frame, the contribution of infill to the system stiffness and strength is often ignored. However, ignoring the interaction between the infill and the frame could cause detrimental effects where infill walls significantly stiffen the frame and thus reduce its ductility. This in turn attracts large forces to the infill frame region. If not designed properly for lateral loads, infill walls can be a contributing factor to catastrophic structural failures especially in earthquakes. Although the current Canadian masonry design standard CSA S304.1-04 (2004) provides equations for the consideration of infill stiffness and strength, the values obtained using these equations are found to be in large disparity with those obtained from experimental testing. In 2011, Masonry Standards Joint Committee (MSJC) in United States proposed design equations for the stiffness and strength of masonry infill. However, their validity has not been thoroughly examined.

In order to utilize the masonry infill in the in-plane lateral or gravity load resisting systems of a structure, the rational and accurate evaluation of their stiffness and strength is crucial to practical implementation. This research is therefore motivated to investigate experimentally the behavior and capacity of masonry infill walls with a focus on the concrete block masonry infills.

1.3 RESEARCH OBJECTIVES

The objectives of this experimental study include the following:

1. To conduct an extensive literature review on the research in the topic of masonry infilled steel frames;
2. To conduct an experimental study of concrete-masonry infilled steel frames under in-plane lateral load;

3. To analyze the effect of several key parameters on the stiffness and strength of the concrete masonry infilled steel frames using experimental results;
4. To assess the validity of design equations provided by various codes with the results of this experimental study;
5. To assess the validity of design equations provided by Canadian code CSA S304 and American code MSJC 2011 with reported experimental results by other researchers;
6. To present appropriate conclusions and recommendations resulting from this research.

1.4 ORGANIZATION OF DOCUMENT

A comprehensive literature review relevant to the subject of masonry infilled frames was conducted at the beginning of this research. Various strength and stiffness calculation methods, experimental studies conducted by other researchers along with a summary of the available design codes were presented in Chapter 2. Chapter 3 presents a detailed description of the experimental program which included the various auxiliary tests on the materials used in construction of the masonry infill, as well as large-scale tests of 9 masonry infilled steel frame specimens. Chapter 4 discussed the results obtained from the experimental program of the large-scale tests and auxiliary tests. Comparisons between the experimental and analytical results as well as example calculations were performed and discussed in Chapter 5. Chapter 6 presents the summary and conclusions of the research. Appendix A presents the stress-strain curves obtained from auxiliary tests.

CHAPTER 2 LITERATURE REVIEW

2.1 INTRODUCTION

Masonry infilled walls have been commonly used as interior partitions as well as exterior walls infilled in either steel or reinforced concrete frames in the modern building construction. The design philosophy and practice has been to treat masonry infilled walls as non-structural elements and design frames for both gravity and lateral loading. The contribution of masonry infilled walls to the frame stiffness and strength is therefore often ignored in design due to either a lack of design guidelines or the motivation for a simplistic design. However, ignoring the interaction between the infills and surrounding frames does not necessarily result in a safe design, quite on the contrary, it may cause detrimental effect to the frame and ultimately to the structure (Drysdale and Hamid, 2005). Infill walls have been identified as a contributing factor to catastrophic structural failures in earthquakes. Frame–infill interaction can induce brittle shear failures of reinforced concrete columns and short-column phenomena. Furthermore, infills can over-strengthen the upper stories of a structure and induce a soft first storey, which is highly undesirable from the earthquake resistance standpoint (Shing and Mehrabi, 2002). Unfortunately, there were neither well-developed design recommendations nor well-accepted analytical procedures for infilled frames.

In recent years, much research involving both experimentation and numerical analysis based on finite element modelling has been conducted in an effort to better understand the infill-frame interaction and to provide some rational design approaches. Studies have shown that infilled frames can develop a number of possible failure mechanisms, depending on the strength and stiffness of the bounding frames with respect to those of the infills and the geometric configuration of the framing system. Most analytical models proposed today focus on one type of mechanism or the other, and they were not universally applicable to all infilled structures. Hence, the design of engineered infilled frames and the evaluation of existing infilled structures still remain a challenge. The

following provides a summary of these recent findings and developments which were most relevant to this research.

2.2 STIFFNESS ANALYSIS

The stiffness of masonry infilled frames has been the focus of considerable experimental and numerical studies over the past five decades. Most research concluded that an adequate representation of the masonry infill was an equivalent diagonal strut. The area of the strut used to replace the wall would be the thickness of the wall times the width of the strut. After the width was established, a simple braced frame analysis can be conducted to determine the stiffness of the frame system. The following provides a summary of theoretical background and development of this so-called diagonal strut method in the calculation of infill stiffness.

Polyakov (1956) was the first to use the analogy of replacing the infill with an equivalent diagonal strut. He conducted experiments on a number of four-hinged infilled steel frames and provided early results on the equivalent strut concept (Tucker, 2007).

Holmes, M. (1961) continued with the equivalent strut analogy and performed experiments with small scaled wall specimens. He recommended an effective width, w, as follows:

$$w = \frac{d}{3} \qquad \textbf{[2-1]}$$

where d was the diagonal length of a rectangular steel frame.

Stafford-Smith (1966) developed the equivalent strut method for a square infilled frame from experimental investigation of diagonally-loaded infilled frames. Using the experimental results, he developed equations to determine the length of contact, effective width of the infill, diagonal stiffness and diagonal strengths as a function of a non-dimensional parameter, λH. The equation of λH was shown as

$$\lambda H = H\sqrt[4]{\frac{E_I t}{4E_f I_f h}} \qquad \textbf{[2-2]}$$

where E_I, t, and h are the elastic modulus, thickness, and height of the infill, and E_f, I_f, and H are the elastic modulus, second moment of area, and height of the frame.

Stafford-Smith and Carter (1969) further developed the method proposed by Stafford-Smith (1966) for rectangular infilled frame. They showed that when the infill frame was loaded laterally at the top of the frame, large portions of the frame separated from the infill except for the corners located at the end of compression diagonal. The resulted contact length with the column α_c as shown in Figure 2.1 satisfies with the following equation.

$$\frac{\alpha_c}{H} = \frac{\pi}{2\lambda H} \qquad \textbf{[2-3]}$$

The length of contact on the beam was observed to be roughly half of the span.

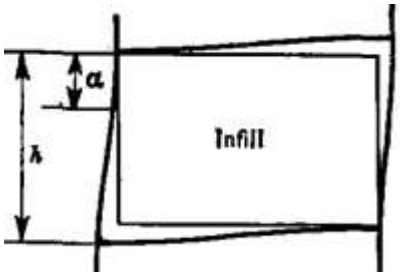

Figure 2.1 Location of the column length of contact for an infill.

(Adapted from Stafford-Smith and Carter, 1969).

Representing the relative stiffness between the infill and surrounding columns, λ was modified from equation [1-2] with θ being introduced to account for the effect of aspect ratio.

$$\lambda = \sqrt[4]{\left[\frac{E_I t \sin 2\theta}{4E_f I_f h}\right]} \qquad \textbf{[2-4]}$$

where θ is the slope of the infill diagonal to the horizontal axis. They then developed a series of design charts to determine the diagonal load for compressive failure, cracking failure and shearing failure of the infill in terms of the non-dimensional parameter, λH, in order to predict the ultimate lateral load for the infill.

Jamal et al. (1992) proposed a diagonal strut width based on diagonal strut method provided by Stafford-Smith and Carter (1969). The width, w, was shown as

$$w = \frac{\pi}{2\lambda} \qquad \textbf{[2-5]}$$

Mainstone (1971) performed tests of a series of 1/6 scaled infilled frames and proposed a set of equations to calculate the width of the diagonal strut for concrete as well as brickwork infilled frames. Expressed as the width-to-length ratio of the diagonal strut w/d, the equations were as shown.

(a) Brick infill

$$w/d = 0.175(\lambda H)^{-0.4} \quad 4 \le \lambda H \le 5$$
$$w/d = 0.16(\lambda H)^{-0.3} \quad \lambda H \ge 5 \qquad \textbf{[2-6]}$$

(b) Concrete infill

$$w/d = 0.115(\lambda H)^{-0.4} \quad 4 \le \lambda H \le 5$$
$$w/d = 0.11(\lambda H)^{-0.3} \quad \lambda H \ge 5 \qquad \textbf{[2-7]}$$

This method was later adopted by Federal Emergency Management Agency (FEMA 1998) and they recommended that the width of the diagonal strut be taken as in equation [2-23]

Saneinejad and Hobbs (1995) also provided equations for determining the respective contact lengths with the column and the beam of the frame, $\alpha_c H$ and $\alpha_b L$, as follows:

$$\alpha_c H = \sqrt{\frac{2M_{pj} + 2\beta_o M_{pc}}{\sigma_{co} t}} \leq 0.4h$$
$$\alpha_b L = \sqrt{\frac{2M_{pj} + 2\beta_o M_{pb}}{\sigma_{bo} t}} \leq 0.4\ell \qquad \textbf{[2-8]}$$

where α_c is the ratio of the column contact length to the height of the column, α_b is the beam contact length to the span of the beam, β_o is the nominal upper bound to a reduction factor to account for the non-ideal plasticity, taken as 0.2, M_{pj} is the least of the beam, the column, and their connection plastic resisting moment, M_{pc} and M_{pb} are the plastic resisting moment of the column and the beam, respectively. σ_{bo} and σ_{co} are the upper-bound normal contact stresses on the face of the beam and column.

Flanagan and Bennett (1999) performed experiments on large-scaled clay tile infilled steel frames under in-plane lateral load. They also proposed an equation to calculate the area of the diagonal strut.

$$A = \frac{\pi t}{C\lambda \cos\theta} \qquad \textbf{[2-9]}$$

where λ is the non-dimensional stiffness parameter provided by Stafford-smith and Carter (1969) shown in equation [2-4] and C was an empirical constant that varies with the in-plane displacement and was an indicator of the limit state of the infill. Flanagan and Bennett (1999) provided tables listing values of C for steel frames with structural clay tile infill, steel frames with concrete masonry infill, concrete frames with concrete masonry infill, and concrete frames with brick masonry infill.

El-Dakhakni et al. (2003) showed that the bending moment and shearing forces in the framed members cannot be simulated using a single diagonal strut and they in turn proposed a so-called three strut model where two additional off-diagonal struts located at the end points of maximum field moment in the beam and columns were suggested. Figure 2.2 shows the proposed method and the location of the struts.

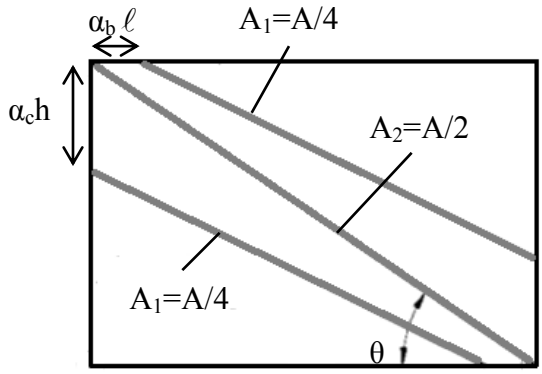

Figure 2.2 Proposed concrete masonry-infilled steel frame model
(Adapted from El-Dakhakni et al. 2003).

Adopting the contact length equations suggested by Saneinejad and Hobbs (1995) as shown in equation [2-8]. The total diagonal struts area, A, was then calculated as follows:

$$A = \frac{(1-\alpha_c)\alpha_c Ht}{\cos\theta} \qquad \textbf{[2-10]}$$

They adopted the upper value of 0.2 in place of β_o as well as $f'_{m\text{-}0}$ and $f'_{m\text{-}90}$ in places of σ_{co} and σ_{bo}. H is the height of the frame, and $f'_{m\text{-}0}$ and $f'_{m\text{-}90}$ were defined as the compressive strength of masonry panel parallel and normal to the bed joint, respectively.

Liauw and Kwan (1984) conducted a finite element analysis that neglected friction between the frame and the infill. They provided equations for the width of diagonal strut to be the smaller of

$$w = \frac{0.86h\cos\theta}{\sqrt{\lambda h}} \quad \text{or} \quad 0.45h\cos\theta \qquad \textbf{[2-11]}$$

Decanni and Fantin (1986) developed equations for uncracked and cracked infill in terms of the relative stiffness parameter λH. The equations were shown as follows:

$$w = \left(\frac{0.748}{\lambda H} + 0.085\right)d \quad \text{if} \quad \lambda H \le 7.85 \quad \text{uncracked}$$

$$w = \left(\frac{0.393}{\lambda H} + 0.130\right)d \quad \text{if} \quad \lambda H > 7.85 \quad \text{uncracked}$$

$$w = \left(\frac{0.707}{\lambda H} + 0.010\right)d \quad \text{if} \quad \lambda H \le 7.85 \quad \text{cracked} \qquad \textbf{[2-12]}$$

$$w = \left(\frac{0.470}{\lambda H} + 0.040\right)d \quad \text{if} \quad \lambda H > 7.85 \quad \text{cracked}$$

Moghaddam and Dowling (1988) performed an experimental study with scaled frames with brick infill and estimated the effective width of the diagonal strut based on the diagonal length of the frame, d, as follows:

$$w = \frac{d}{6} \qquad \textbf{[2-13]}$$

Stafford Smith and Coull (1991) extended the work done by Stafford-smith and Carter (1969) developed an equation for the area of the equivalent diagonal strut as

$$A = (1/10)dt \qquad \textbf{[2-14]}$$

Paulay and Priestley (1992) had suggested that the effective width of the equivalent diagonal strut be calculated as the following equation, provided that the in-plane force on the infill was equal to half of the ultimate load.

$$w = 0.25d \qquad \textbf{[2-15]}$$

Durrani and Luo (1994) analyzed the lateral load response of reinforced concrete infilled frames based on Mainstone's equations. He proposed an equation for effective width of the diagonal strut, w, as

$$w = \gamma d \sin(2\theta) \qquad \textbf{[2-16]}$$

where γ, the effective width factor is calculated as

$$\gamma = 0.32\sqrt{\sin 2\theta}\left(\frac{H^4 E_I t}{m E_c I_c h}\right)^{-0.1}$$

and where m is the dimensionless parameter relating the ratio of beam to column stiffness and can be calculated as

$$m = 6\left(1 + \frac{6\tan^{-1}\left(\frac{E_b I_b H}{E_c I_c h}\right)}{\pi}\right)$$

and where E and I are the modulus of elasticity and moment of inertia of the frame, subscripts b and c denotes the beam and column of the frame.

Al-Chaar (2002) proposed the following two equations to calculate the effective width of the equivalent diagonal strut for different aspect ratio of the frame based on the non-dimensional stiffness parameter λH.

$$w = 0.0835 C_{AC} d\left(1 + \frac{2.574}{\lambda H}\right) \quad \text{for} \quad \ell/h \geq 1.5$$
$$w = 0.1106 d\left(1 + \frac{6.027}{\lambda H}\right) \quad \text{for} \quad \ell/h = 1.0 \qquad \textbf{[2-17]}$$

where C_{AC} was the multiplication factor that accounts for aspect ratio and could be calculated as

$$C_{AC} = -0.3905\left(\frac{\ell}{h}\right) + 1.7829$$

Linear interpolation can be used for aspect ratios between 1.0 and 1.5.

Papia, Cavaleri, and Fossetti (2003) developed an empirical equation for the effective width of the diagonal strut as

$$\frac{w}{d} = \frac{c}{z}\frac{1}{(\lambda^*)^{\beta}} \qquad \textbf{[2-18]}$$

where

$$c = 0.249 - 0.0116\upsilon + 0.567\upsilon^2$$
$$\beta = 0.146 + 0.0073\upsilon + 0.126\upsilon^2$$
$$\lambda^* = \frac{E_I t h}{E_f A_c}\left(\frac{h^2}{\ell^2} + \frac{A_c \ell}{4 A_b h}\right)$$
$$z = 1 \qquad \text{if} \quad \ell/h = 1$$
$$z = 1.125 \qquad \text{if} \quad \ell/h = 1.5$$

And where z is an empirical constant, λ^* is the stiffness parameter, υ is the poison ratio for the infill, E_f was the Young's modulus of the frame, A_c was the cross sectional area of the column and A_b was the cross sectional area of the beam.

Tucker C. (2007) proposed nine empirical equations for calculating effective width of the diagonal strut either developed by modifying existing equations using regression analysis. He concluded that the following equation was the preferred in the calculation of the diagonal strut width.

$$w = 0.25d(\lambda h)^{-1.15} \quad \textbf{[2-19]}$$

2.3 CODE GUIDELINES FOR STIFFNESS CALCULATIONS

There were a significant number of code guidelines for masonry structures in general but only a few contain provisions designated to masonry infill walls. The following provides a brief summary of current design guidelines in this regard.

CSA S304.1 – 04 recognizes the frame-infill interaction and adopted the diagonal strut concept for the consideration of infill contribution of frame behavior. The determination of contact lengths, effective diagonal strut width, compression resistance of diagonal strut, and length of diagonal strut for slenderness effects was provided in various provisions.

The diagonal strut width was calculated as follows

$$w = \sqrt{\alpha_h^2 + \alpha_L^2} \quad \textbf{[2-20]}$$

where α_h and α_L were the vertical and horizontal contact length between the frame and the diagonal strut, they were calculated in the following equations.

$$\alpha_h = \frac{\pi}{2}\sqrt[4]{\frac{4E_f I_c h}{E_I t_e \sin 2\theta}}; \quad \alpha_L = \pi\sqrt[4]{\frac{4E_f I_b \ell}{E_I t_e \sin 2\theta}} \quad \textbf{[2-21]}$$

where E_I and E_f is the Modulus of Elasticity of the masonry infill and frame material, h and ℓ are the height and length of the infill, t_e is the effective thickness of the wall, I_c and I_b are the moments of inertia of the column and the beam, and θ is shown as follows. The effective diagonal strut width is taken as w/2 as suggested in Hendry, A. (1981). The design length of the diagonal strut is taken as the length of diagonal minus w/2.

Eurocode 8 only requires that masonry infilled frames to be designed in accordance with the provisions for zones with high seismicity. Section G.5.5.2.7 in Eurocode 8 provides a guideline for the infilling of frames based on diagonal strut concept. The equivalent diagonal strut width, w, was taken as

$$w = 0.5\ell_d \qquad \textbf{[2-22]}$$

where ℓ_d was the diagonal length of the infill panel.

Both Federal Emergency Management Agency (FEMA) 273 NEHRP Guidelines for the Seismic Rehabilitation of Buildings and FEMA 306 Evaluation of Earthquake Damaged Concrete and Wall Building guidelines uses the diagonal compression strut method provided by Mainstone (1971) and Mainstone and Weeks (1970). This method was based on infilled steel frame where the method by Stafford-Smith and Carter (1969) was mainly based on reinforced concrete infilled frames. The equation below was determined empirically from an extensive experimental program. The evaluation method in the guideline was shown as follows.

$$w = 0.175(\lambda H)^{-0.4}\ell_d \qquad \textbf{[2-23]}$$

where,

$$\lambda = \left[\frac{E_I t \sin 2\theta}{4E_f I_c h}\right]^{1/4}$$

and where H was the column height between centerlines of beams, h was the height of infill panel, E_f was the expected modulus of elasticity of frame material, E_I was the

expected modulus of elasticity of infill material, I_c was the moment of inertia of column, ℓ_d was the diagonal length of infill panel, t was the thickness of the infill panel and equivalent strut, and θ was the angle whose tangent was the infill height-to-length aspect ratio, calculated as follows.

$$\theta = \tan^{-1}\left(\frac{h}{\ell}\right)$$

The guidelines also require the designer to check the strength capacity of the infill panel against the Mohr-Coulomb failure criteria, compression failure of diagonal strut by Stafford-Smith and Carter (1969), the diagonal tension failure recommendation by Saneinejad and Hobbs (1995), general shear failure by FEMA 273 as well as the effect of infill panel reinforcement by the provisions provided in ACI 318-95 Building Code Requirements for Structural Concrete.

The 2011 Masonry Standards Joint Committee proposed a design method to compute the width of equivalent diagonal strut based on the research by Flanagan and Bennett (2001). The equation for the width of the diagonal strut, w, was as follows:

$$w_{inf} = \frac{0.3}{\lambda_{strut} \cos\theta} \qquad \textbf{[2-24]}$$

where the characteristic stiffness parameter, λ_{strut} was calculated as

$$\lambda_{strut} = \sqrt[4]{\frac{E_I t_{net\,inf} \sin 2\theta}{4 E_{bc} I_{bc} h}} \qquad \textbf{[2-25]}$$

and where E_I was the modulus of elasticity of the masonry infill, E_{bc} was the modulus of elasticity of the columns, I_{bc} was the moment of inertia of column for bending in the plane of the infill, h was the height of the infill, θ was the angle of infill diagonal with respect to the horizontal, and determination of $t_{net\,inf}$ was shown in Figure 2.3 below.

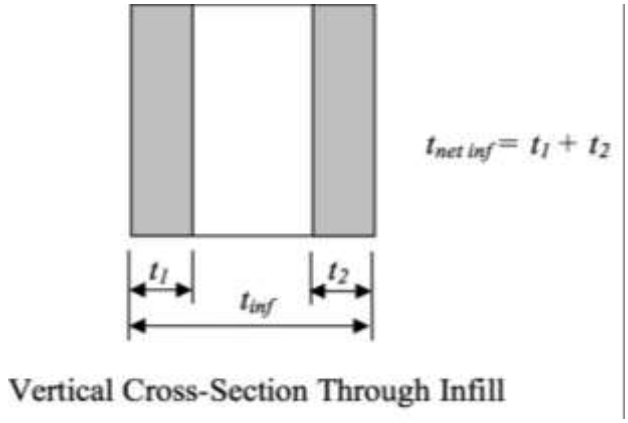

Figure 2.3 Determination of $t_{net\ inf}$

2.4 STRENGTH ANALYSIS

Ultimate and first crack strengths are usually calculated based on their respective failure modes. There are five different failure modes for laterally loaded infilled frames as reported by various researchers in the past six decades (Flanagan and Bennett 1999, Moghaddam 2004, etc.). These five failure modes can be categorized as follows.

Compression Strut (CS) – Crushing in the central region of the infill, which happens when the diagonal strut is too slender that causes the out-of-plane buckling of the infill.

Knee Brace or Sliding Shear (SS) – Sliding along the bed joints of the infill. This usually happens due to weak mortar joints and strong frame members.

Diagonal Tension Failure (DT) – Diagonal cracking along the two loaded corners of the infill. This occurs when the infill wall failed in shear due to the diagonal tension force acting in the direction towards the two non-loaded corners from the center of the infill.

Corner Crushing Failure (CC) – Crushing at the two loaded corners of the infill. This is the most common mode of failure.

Frame Failure (FF) – Columns of the frame yielding in flexure or failed in compression due to an exceptionally strong infill.

Mainstone (1971) proposed an equation for the corner-crushing load, H_{ult}, of the infill based on the equivalent strut method. This load must then be added to the strength of the frame in order to get the total ultimate load of the infilled frame.

$$H_{ult} = 0.56(\lambda H)^{-0.875} f'_m \, Ht \cot\theta \qquad \textbf{[2-26]}$$

where f'_m is the compressive strength of the masonry and all other terms were as defined before.

Wood (1978) considered the plastic action of infill wall panels in frames. The idealized plastic failure modes for wall frame panels includes the shear mode for strong frame and weak wall, the shear rotation mode for medium strength walls, the diagonal compression mode for strong wall and weak frame, and the corner crushing mode for very weak frame. Wood had also provided a design chart for racking loads based on the frame-infill strength ratio and aspect ratio of the infill.

Based on the findings with non-linear finite element analysis, a plastic theory of analysis for integral frame was proposed by Liauw and Kwan (1983). Integral frame takes into account of the shear strength at the infill and frame interface, the plastic moments of the surrounding beam and columns, and the stress redistribution towards collapse. They proposed several equations for calculating the collapse shear for cases of single storey and multistory infilled frames. However, the equations were complex to use in practical applications.

Stafford Smith and Coull (1991) recommended an empirical equation for the net cracking strength of the masonry infill,

$$H_{cr} = 1.72 \ell t f_t \qquad \textbf{[2-27]}$$

where f_t is the tensile strength of the masonry. They also developed a corner crushing load based on the equivalent strut method for the infill as follows with terms as defined before.

$$H_{ult} = f'_m \, t \frac{\pi}{2} \sqrt[4]{\frac{4E_f I_f H}{E_I t}} \qquad \textbf{[2-28]}$$

Saneinejad and Hobbs (1995) developed a method to consider the inelastic behavior of infilled masonry walls with steel frames. The method accounts for both plastic and elastic behavior of the infill frames assuming a plastic collapse mechanism with plastic hinges developed at the corners of the panel. They proposed equations for the cracking strength, H_{cr}, and corner crushing strengths, $H_{ult,}$ of the infill as follows:

$$H_{cr} = 2\sqrt{2th}\, f_t \cos^2\theta \qquad \textbf{[2-29]}$$

$$H_{ult} = \sigma_c t(1-\alpha_c)\alpha_c H + \tau_b t \alpha_b \ell \qquad \textbf{[2-30]}$$

where σ_c and σ_b is the normal contact stress along the column and the beam, and τ_b was the shear stress along the beam. The term τ_b can be determined as follows:

$$\tau_b = \mu\sigma_b$$

$$\sigma_b = \sigma_{bo} \quad \text{and} \quad \sigma_c = \sigma_{co}\left(\frac{A_b}{A_c}\right) \quad \text{if} \quad A_c > A_b$$

$$\sigma_b = \sigma_{bo}\left(\frac{A_c}{A_b}\right) \quad \text{and} \quad \sigma_c = \sigma_{co} \quad \text{if} \quad A_c \le A_b$$

Where,

$$A_c = r^2\sigma_{co}\alpha_c(1-\alpha_c-\mu r)$$

$$A_b = \sigma_{bo}\alpha_b(1-\alpha_b-\mu r)$$

And where,

$$\sigma_{co} = \frac{f'_m}{\sqrt{1+3\mu^2\left(\frac{h}{\ell}\right)^4}}$$

$$\sigma_{bo} = \frac{f'_m}{\sqrt{1+3\mu^2}}$$

and where μ was the coefficient of friction on the interface between the frame and infill, and A_b and A_c are the cross-sectional area of the beam and column.

Flanagan and Bennett (1999) also developed equations for cracking load, H_{cr}, and corner crushing strength, H_{ult}, as follows:

$$H_{cr} = K_{cr} \ell t \sqrt{f'_m} \quad \textbf{[2-31]}$$

$$H_{ult} = K_{ult} t f'_m \quad \textbf{[2-32]}$$

where K_{cr} and K_{ult} are empirical constants provided by Flanagan and Bennett (1999) determined through experimental results for calculating the cracking and corner crushing strengths, respectively.

2.5 CODE GUIDELINES FOR STRENGTH CALCULATIONS

CSA S304 provided ultimate load calculations according to the different failure modes. These failure modes include diagonal tension shear (DT), corner crushing (CC) and sliding shear (SS) as shown in equations [2-33], [2-34] and [2-35], respectively.

$$V_r = \phi_m (\nu_m b_w d_v + 0.25 P_d) \gamma_g \quad \textbf{[2-33]}$$

$$V_r = 0.16 \phi_m \sqrt{f'_m} A_{uc} + \phi_m \mu P_l \quad \textbf{[2-34]}$$

$$V_r = \frac{\ell}{\sqrt{h^2 / \ell^2}} P_r \quad \text{where} \quad P_r = \varphi_m \chi (0.85 f'_m) b (2t_f - r) \quad \textbf{[2-35]}$$

where ,

$$\nu_m = 0.16 \left(2 - \frac{M_f}{V_f d_v} \right) \sqrt{f'_m}$$

v_m = shear strength of contributed by the masonry,

and where,

$$r = \left(\frac{t}{2} + e\right) - \frac{1}{2}\sqrt{t^2 + 4t_e + 4e^2 - 16et_f}$$

r = the general solution of a quadratic equation of eccentricity for the case where the edge of the stress block is within the tension flange of hollow masonry.

$$e = \frac{r(t-r)}{2(2t_f - r)}$$

The 2011 Building Code Requirements and Specification for Masonry Structures Appendix A - Design of Masonry Infill provided by the Masonry Standards Joint Committee (MSJC 2011) stated three empirical equations for calculating the design forces (ie. ultimate strength) as shown in equation [2-36]. Note that the values used with the following equations provided by MSJC 2011 are to be in imperial format and the result can be converted in to metric system for comparisons purposes.

$$V_r = \text{smallest of} \begin{cases} (a)(6.0\text{in})t_{netinf}f'_m \\ (b)\text{The calculated horizontal component of the force in the equivalent strut at a horizontal racking displacement of 1.0in (25mm)} \\ (c)V_n/1.5 \end{cases} \quad \textbf{[2-36]}$$

where,

$$V_n = \min\begin{cases} 3.8A_{uc}\sqrt{f'_m} \\ 300A_{uc} \\ \text{or} \\ 56A_n + 0.45N_u \quad \text{if not full} \\ 90A_n + 0.45N_u \quad \text{if full} \end{cases}$$

and where,

$$A_{uc} = 0.8\,\ell\,t_e$$

2.6 OTHER EXPERIMENTAL AND ANALYTICAL STUDIES

Riddington (1984) studied the influence of initial gaps between the infill panel and the frame on the behavior of infilled frames. These gaps could result from poor workmanship or the shrinkage of the infill or be intentionally implemented to isolate the infills from the compressive loading on the frame. He conducted various tests including frames with no infill, infill with no initial gaps, infill with top gap, as well as infill with top and side gaps. He concluded that initial infill gaps affect the behavior of infilled frames undesirably and should therefore be avoided whenever possible.

Dhanasekar and Page (1986) used a nonlinear finite element method to simulate the behavior of infilled frames subjected to racking loads. The finite element model included a material model that had appropriate elastic properties, inelastic stress-strain relations, and an appropriate failure surface. The finite element model compared well with experimental results. They concluded that the modulus of elasticity of the infill as well as the tensile and bond strength of the masonry can significantly influence the load-deflection characteristics and the ultimate strength of the composite frame. Furthermore, the masonry compressive strength did not influence the racking capacity of the infilled frame when the panels failed by shearing down of the panel diagonal.

Dawe and Seah (1989) conducted a series of 28 large scale tests of concrete block masonry infilled steel frames subjected to horizontal shear load at the top of the structure. It was concluded that the masonry infill greatly increased in-plane shear resistance of steel frames and specimens where tensile cracking was confined to a narrow band along the compression diagonal exhibited the best overall load deflection behavior. Panel-to-column ties increased the initial stiffness but had no significant effects on either the initial major crack or on the ultimate capacity. An initial top gap between the roof beam and the panel resulted in detrimental effects to the cracking and ultimate capacity of the system, therefore, a top gap should be avoided as much as possible. Door openings in a panel (17.5% of the panel) reduce the initial major crack load but have no significant effect on the ultimate load. The ultimate load was less affected if the openings were placed closer

to the loaded side of the panel. Vertical reinforcement increased the initial stiffness but did not affect the major cracking load and the ultimate strength of the panel.

Mehrabi et al. (1996) conducted experiments with two types of monotonically loaded as well as cyclically loaded specimens. One frame was designed for moderate wind load (weak frame) and the other was designed for strong earthquake forces. Results showed that with weak frames and strong (solid) panels, columns exhibited a brittle shear failure but the system exhibited a good energy dissipation capability. This was more desirable than the weak frame, weak (hollow) panel specimen; however, brittle shear failure might jeopardize the stability of the structure, and was non-repairable. The study also indicated that for a frame properly designed for seismic loading, infill panels will also have a beneficial effect on the system.

Mehrabi and Shing (1997) established a model that simulates the behavior of mortar joints between masonry units plus the behavior of the interface between the frame and panel. The model takes into the account the compressive hardening behavior, the reversal of shear dilatancy, as well as the normal contraction of cementitious interface. They also determined that the model can capture the failure mechanisms of the infill frame specimens, as well; the infill panels could substantially improve the performance of the existing non-ductile frame.

Chiou et al. (1999) performed a full-scale wall test and a numerical modeling using a so-called discontinuous deformation analysis (DDA). This technique allows the modeling of masonry structure as either a continuum or discontinuous structure by considering the behavior of discrete masonry blocks. The experiment consists of three 320cm x 300cm walls. The comparison with the experimental results showed that the numerical model was capable of simulating the discontinuous behavior of the masonry infill subjected to in-plane monotonic loading and identifying the failure regions in the panel.

Dawe et al. (2001) also developed a finite element analysis used to predict the strength and stiffness of masonry infilled steel frames. The finite element technique was used to

develop a complete load-deformation response for a single panel infilled frame. They used an augmented spring to model the mortar bond so that the joint separation and closure as well as shear and friction along the mortar joints can be modeled. They considered various parameters such as panel aspect ratio, frame-to-panel connectors, frame-to-panel interface friction, gaps between panel and frame, mortar joint bond and friction, frame rigidity, masonry panel strength, and the effects of gravity loading in the parametric study. The conclusion of the study was summarized as follows. A panel with aspect ratio of 1.0 has a greater first peak load as well as ultimate load than other aspect ratio. Adjustable ties between frame and panel were capable of resisting tension and limited compression forces normal to the frame and panel interface, but they cannot resist any vertical shear forces. The value of friction between frame and infill has little impact on the behavior of the system until the first peak load. The presence of gaps decreases the first peak load and the system also deteriorates more rapidly than the other specimens without gaps. The influence of mortar joint bond increases as the ratio of H/L increases. Gravity loading may increase the lateral in plane strength of the panel but may cause a local crushing at the corner of the system.

Moghaddam (2004) performed an experiment with 5 brick infilled frame specimens subjected to cyclic loading. An analytical method was also developed to determine the crack patterns and the shear strength of the infill frames. It was shown that even though perforated bricks have higher initial shear rigidity than solid bricks, the type of masonry units was not a significant factor on the shear strength of the infill panel.

Kaltakci et al. (2006) performed a series of 30 partially and fully grouted infilled frames under lateral reversed cyclic loading exerted at the top of the frames and applied in the elastic range. The experimental results were compared with analytical results obtained using the equivalent strut tie method. For infilled panels, the diagonal strut method provided results in generally good agreement with test results. Three different modes of failure were observed including separation at the mortar joints, inclined diagonal tension crack, and compression crushing at compressive edges. Failure caused by separation at

the mortar joint often occurs in the infill walls when the walls were much weaker than the frame.

Mohebkhah et al. (2008) investigated the nonlinear in-plane behavior of masonry infilled frames with openings. Universal Distinct Element Code (UDEC 2004) was used to develop the discrete element for nonlinear inelastic static analysis of masonry infilled steel frames subjected to in-plane loading. These models were capable of considering both geometric and material nonlinearity. They verified the predictions of collapse mode and the evolution of deformation with experiments. It was also shown that this method was able to correctly simulate the failure mechanisms based on sliding and joint separation.

2.7 CONCLUDING REMARKS

The previous research has demonstrated that the presence of the masonry infills, if designed properly, can enhance the structural behavior of frame systems especially in the seismic zones. Several equations have been proposed by various researchers to account for the stiffness of the infills in the diagonal strut approach. However, they are either based on very limited experimental results conducted by the researcher for the purpose of developing the equation alone or numerical results of idealized finite element modeling. From the design standpoint, although some design guidelines are available in Canada and US, they are quite different in the expressions and their accuracy has not been thoroughly evaluated.

CHAPTER 3 EXPERIMENTAL PROGRAM

3.1 GENERAL

The experimental program for this research was designed to study the behaviour of concrete masonry infilled steel frames under in-plane lateral loading. While the problem involves both steel frame and the masonry infill, this study is focused on the behavior of masonry infills. The stiffness, strength and failure modes of infills are examined and compared with the predicted values obtained from various design codes and methods proposed by other researchers. The experimental program was separated into two parts; the testing of the infilled frame specimens and the auxiliary tests for masonry components such as unit blocks, grout and mortar cubes, reinforcement bars and prisms.

Although many experimental studies have been performed over the years, effects of several parameters have yet to be determined. These parameters include the use of partially grouted walls compared to the common fully grouted or hollow walls, as well as comparisons of different aspect ratios, and the difference in types of openings. More importantly, since the release of MSJC 2011 design guidelines, very few studies were performed and those equations are yet to be validated.

3.2 TEST SPECIMENS

Table 3.1 shows a summary of specimens with various testing parameters. A total of 10 specimens including nine infilled frame specimens and one bare frame specimen were tested under an in-plane lateral loading applied at the roof beam level. The bare frame was tested without the infill under the same loading condition for verification of calculation and comparison purposes. Parameters considered for the infilled frame specimens included the aspect ratio, grouting situation and opening of the fills, and the frame-to-infill stiffness. The infill walls were constructed using custom made one-third scale of standard 200 mm masonry blocks. Scaled blocks were used in this study to keep the size of the infills reasonable for transportation, storage, and testing. The use of scaled

concrete masonry units for the construction of infill frame model tests has been adopted and validated by several past researchers (Mehrabi et al. 1996, Mosalam et al. 1997, Maleki et al. 2007). Referring to Figure 3.1, three aspect ratios of 1.0, 1.3 and 1.6 were considered where the height of the infill was kept at approximately 1 meter while the length was changed accordingly.

Table 3.1 Specimen Table

Specimen ID	Specimen Designation	Aspect Ratio	Grouting	Opening	Frame Column Axis
1	Bare frame	1.0 : 1.0	N/A	None	Major
2	P1NA	1.0 : 1.0	Partial	None	Major
3	F1NA	1.0 : 1.0	Full	None	Major
4	P3NA	1.0 : 1.3	Partial	None	Major
5	P3WA	1.0 : 1.3	Partial	Window	Major
6	P3DA	1.0 : 1.3	Partial	Door	Major
7	P3NI	1.0 : 1.3	Partial	None	Minor
8	F3NA	1.0 : 1.3	Full	None	Major
9	F3NI	1.0 : 1.3	Full	None	Minor
10	P6NA	1.0 : 1.6	Partial	None	Major

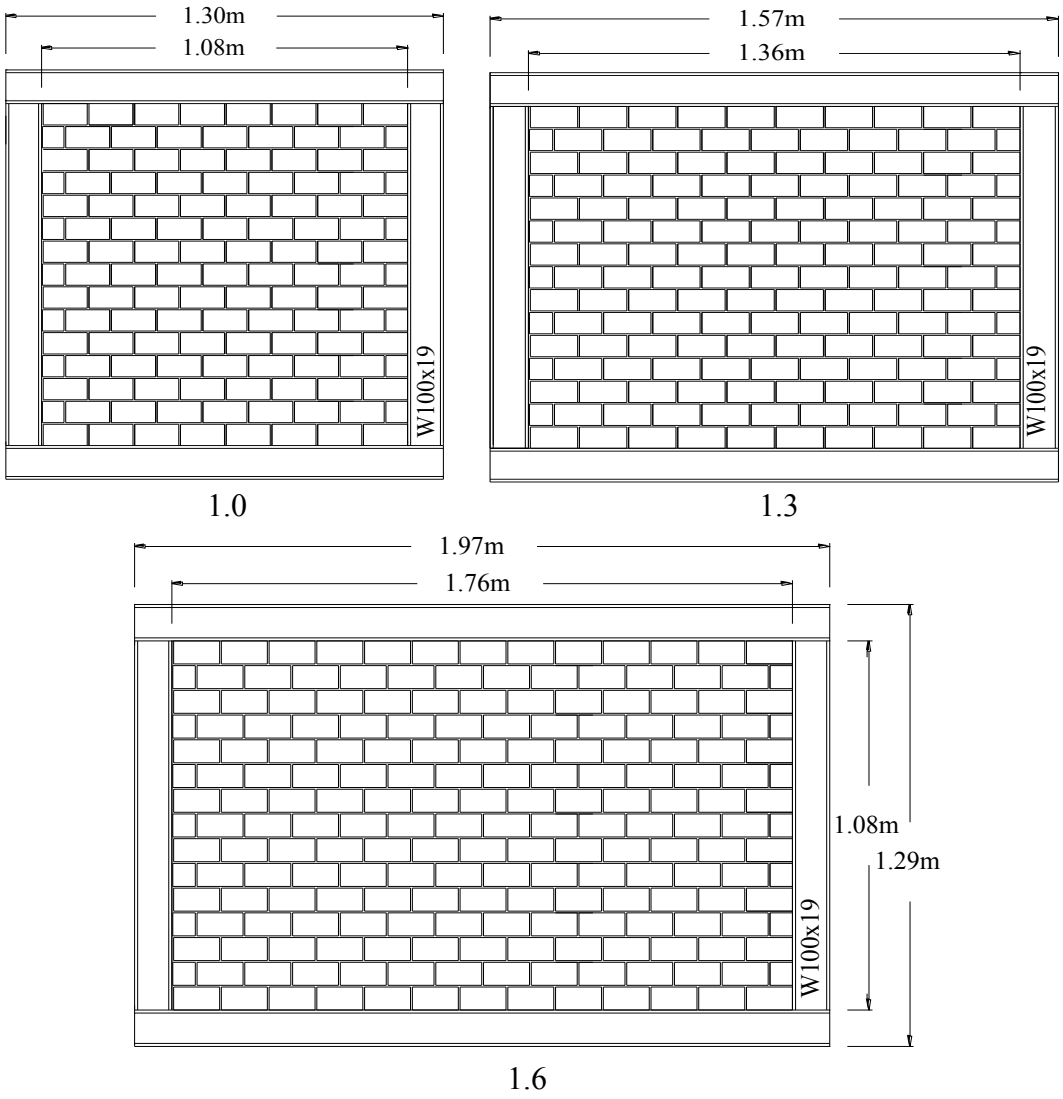

Figure 3.1 Infilled frame aspect ratios

The typical grouting configurations of the partially grouted infills are as shown in Figure 3.2. Six of the infill specimens were built to be partially grouted and the three remaining were fully grouted. Vertical steel rebar with a diameter of 6mm was placed in designated cells as indicated in the figure. A smaller size would be more desirable with the size of the block but this size rebar was the smallest available on the market at the time of testing. For fully grouted infills, the vertical reinforcement location remained the same as their partially grouted counterparts. No joint reinforcement was used for any specimens.

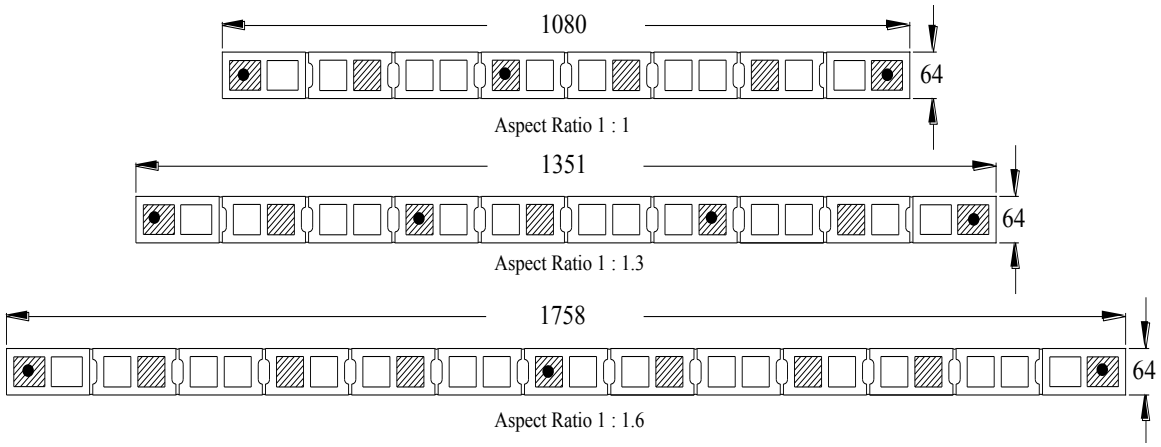

Figure 3.2 Infill grouting configuration

Two opening situations (window and door) were considered for partially grouted infills with a 1.3 aspect ratio as shown in Figure 3.3. Both openings were placed in the central region of the infill so the diagonal strut would be interrupted. The reductions in the area were 10.5% for the window opening and 18% for the door opening. For wall specimens with window openings, there was a slight difference for the grouting configuration due to the placement of the reinforcement bars. Figure 3.3 also shows the dimensions and position of the openings in the wall specimens as well as the reinforcement details around the window and door.

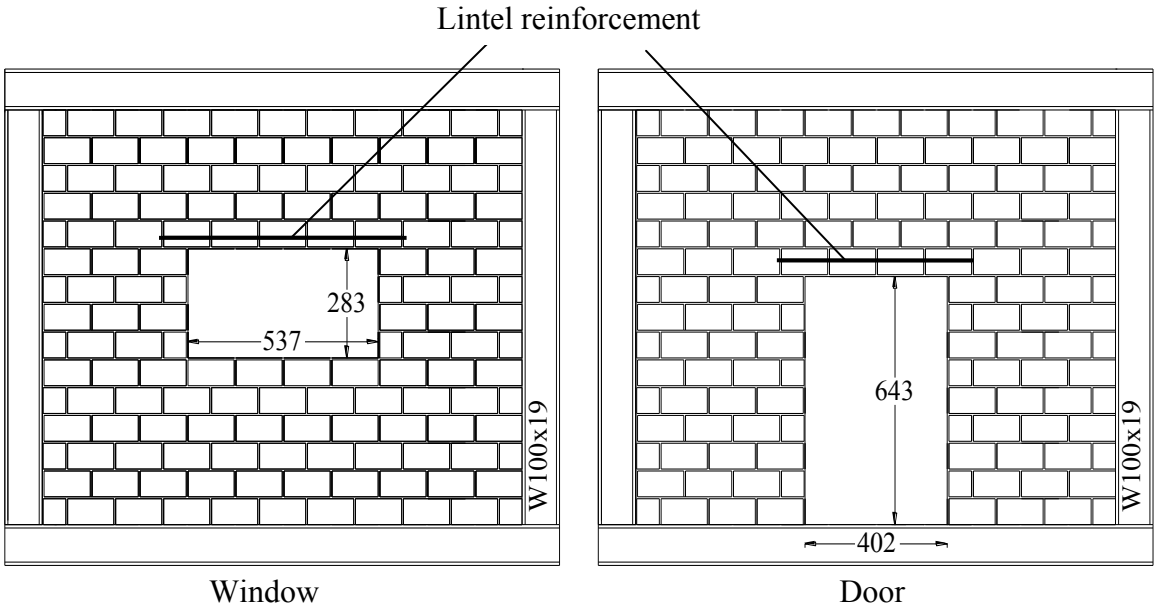

Figure 3.3 Window and door openings

Figure 3.4 shows the grout placement of the wall specimen with a window. The grouting arrangement for wall specimens with door opening remained the same. Above the opening, a one course lintel beam with a horizontal reinforcement as shown in Figure 3.4 was implemented to be consistent with the standard of practice.

Figure 3.4 Grouting arrangement for walls with window

The frame-to-infill stiffness ratio was varied by changing the orientation of frame columns. The major axis column orientation indicates that the web of the column is orientated in the plane of the wall whereas the minor axis orientation indicates that the web of the column is perpendicular to the plane of the wall. The labeling scheme of specimens is explained as follows. The first digit, a letter, indicates the grouted situation; the second digit, a number, represents the aspect ratio; the third digit, a letter, indicates the opening; and the last digit, a letter, identifies the orientation of the column web where A stands for major axis column orientation and I stands for minor axis column orientation. For example, specimen P1NA is a partially grouted specimen with an aspect ratio of 1.0 and no opening, having frame column web oriented in the plane of the infill.

3.2.1 Fabrication

All wall specimens were built to the standard of practice by an experienced mason in the Heavy Structures Laboratory at the Department of Civil and Resource Engineering of Dalhousie University. Two methods were used in the construction of the specimens. The first batch of four wall specimens were built directly on the laboratory floor and they were later positioned in a three-member frame to form the infilled frame specimens. During the curing, they were laterally braced with wood frames for stability. Figure 3.5 shows the walls supported by the wood frames.

Figure 3.5 Wood frame support

For the remaining five specimens, the bounding frames were fabricated first and the infill walls were built inside of the frame. As shown in Figure 3.6, each frame was fabricated excluding the top beam and the infill was contained inside the frame. After at least 7 days of curing, the top beam was welded to the frame and the whole assembly was later transported to the testing position.

Figure 3.6 Pre-welded infill frames

In order to ensure that the infill was built plumb and was as close to the mid-line of the frame as possible, two pieces of custom cut plywood were clamped to the sides of the frame as seen in the Figure 3.6 before the mason began to lay the blocks. The concrete masonry units were placed carefully and leveled after each course. Mortar was employed on both bed joints and head joints. The cells were grouted with high fluid grout and grout

was manually vibrated and compacted to reduce the air pockets to minimum. The vertical reinforcement bars were then placed. For wall specimens with openings, a lintel beam reinforced with horizontal rebar of 6 mm diameter was employed above the opening as shown in Figure 3.7. All wall specimens were moisture cured for 7 days and air cured for minimum of 21days before the commencement of the testing.

Figure 3.7 Bond beams and horizontal reinforcement

3.2.2 Infilled Frame Specimen Test Set-Up

3.2.2.1 Bounding frames

The infilled frame was constructed using W100x19 (W4x13) steel sections for both the beam and columns by qualified steel fitters. For the first four specimens, a three-member frame was used where the beam, framing on top of the column, was bolted through a 13 mm (½ inch) bearing plate which was in turn welded to the column as shown in Figure 3.8.

Figure 3.8 Initial Beam-to-column connection detail.

Columns were bolted with 4-19 mm A325 bolts on each side to the floor beam through a 13 mm (½ inch) thick bearing plate. The details of connections are shown in Figure 3.9.

Figure 3.9 Connection Details

For the remaining five specimens, a four-member frame was used to accelerate the construction process and improve the alignment of the infill walls. In this case, two columns were welded to the bottom beam which was in turn bolted to the floor beam as shown in Figure 3.10. The top beam was then welded to the two columns after the specimens were cured. This method of preparation also reduces the potential gap between the wall and the frame since the infill was directly built into the frame.

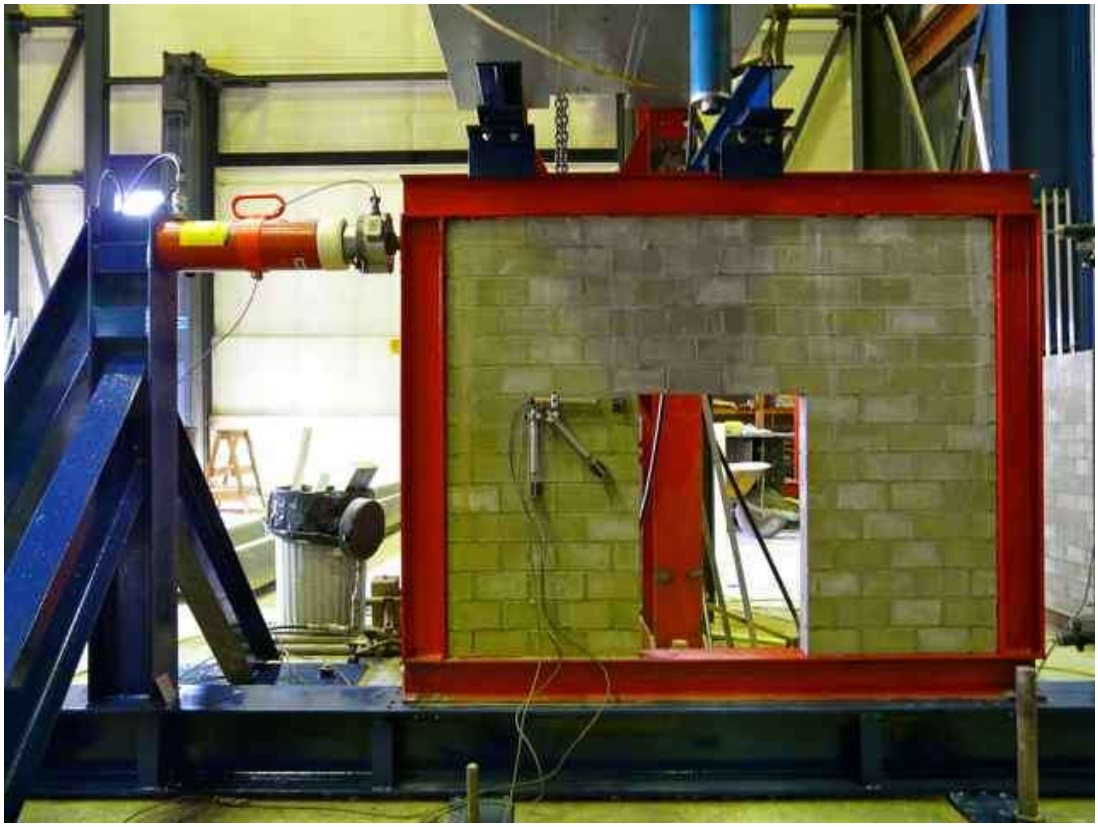

Figure 3.10 Bounding frame of infills

The detail of the welded connections between the top beam and the column is shown in Figure 3.11 and column to bottom beam as shown in Figure 3.9.

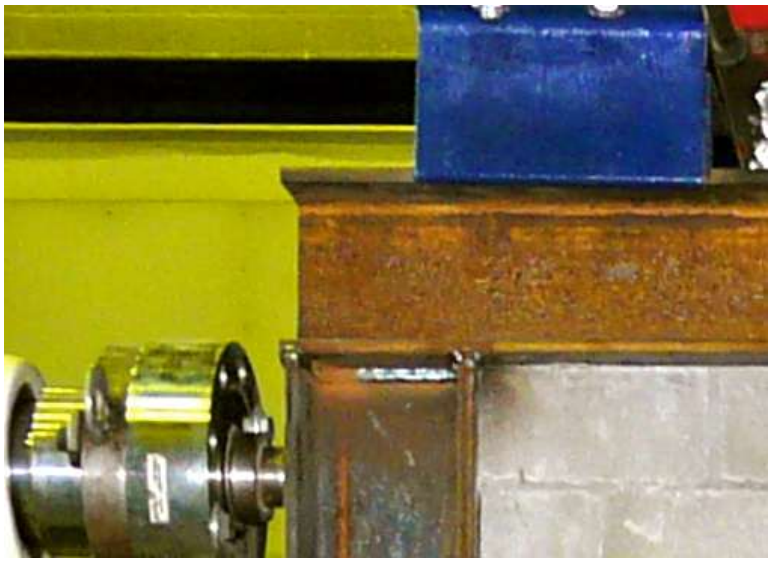

Figure 3.11 Top beam-to-column connection.

3.2.2.2 Loading and Reaction frames

As shown in Figure 3.12, lateral load was applied through a hydraulic actuator with a capacity of 250kN. The actuator was bolted to the column of the reaction frame and connected to a pressure-controlled pump. A load cell was attached to the actuator in order to obtain accurate load readings. The loading arrangement and specimens are supported on a W200x46 (W8x31) steel floor beam which was in turn connected to the strong floor through twelve 40 mm diameter threaded steel bars. The beam was stiffened using 6.5mm (¼ inch) thick web stiffeners on both sides of the web at 3 locations along its length. A skewed A-frame consisting of two W150x30 (W6x20) columns was provided as a reaction support for the load. The reaction frame was designed such that it was sufficient to withstand the reaction force 500kN exerted from the load cell to the infilled frame. This frame was also braced in the out-of-plane direction using two W200x15 (W8x10) section.

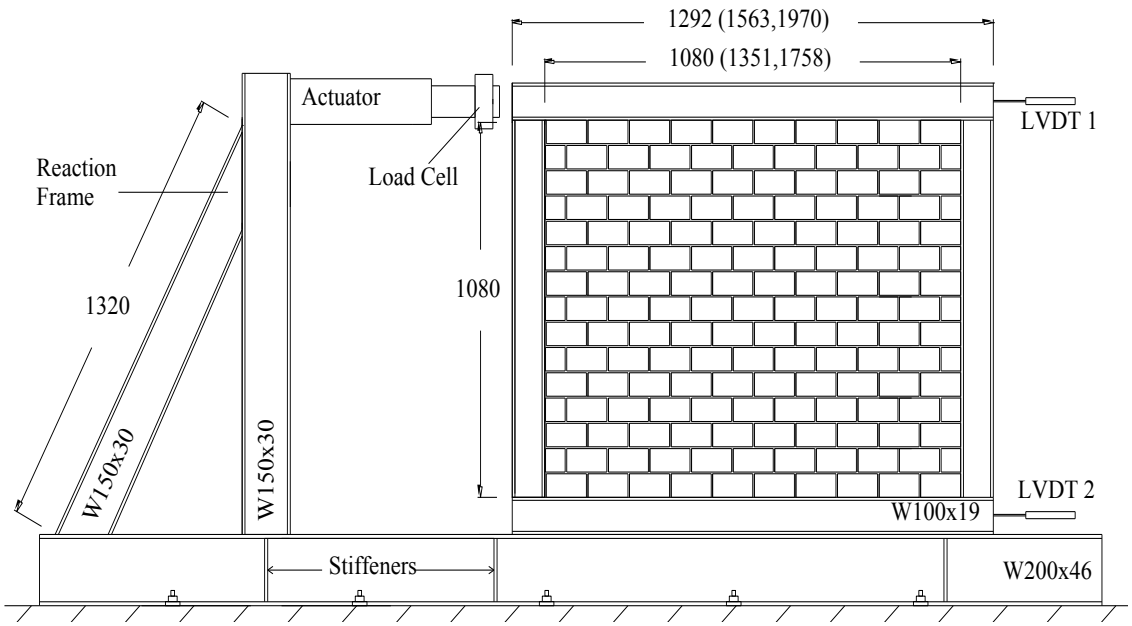

(a) Front View

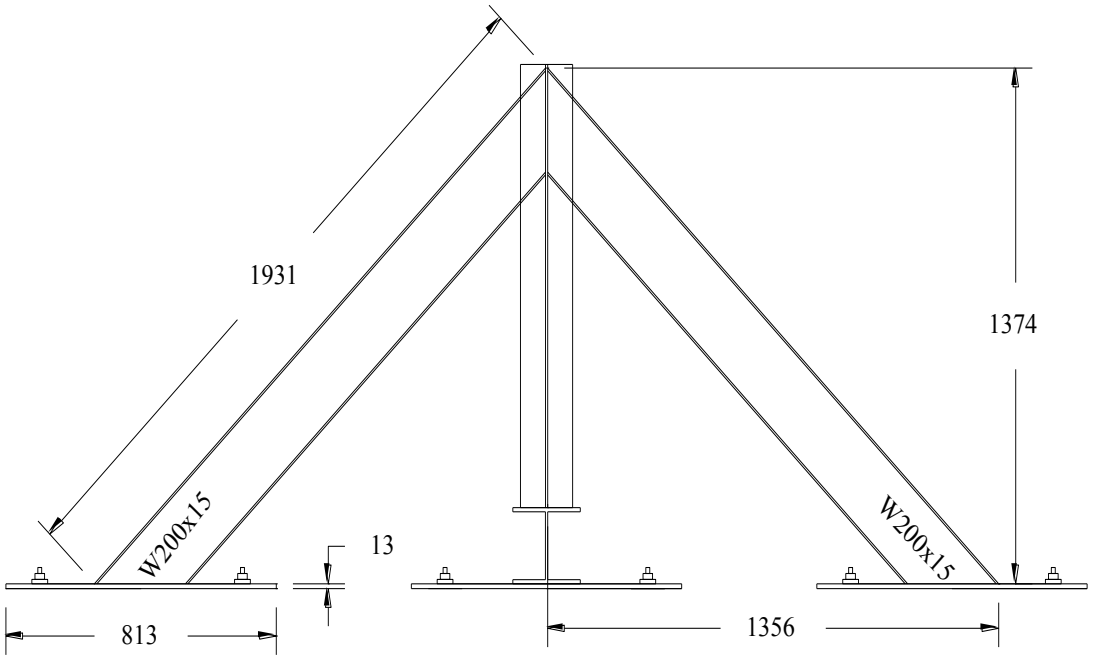

(b) Side View

Figure 3.12 (a) Front and (b) Side View of the Reaction Frame

3.2.2.3 Out-of-plane Restraints for Roof Beam

Typically, a building includes both gravity and lateral load, therefore, out of plane restraints are generally not required. However, for this experiment, angle sections were provided as lateral restraint to the flange tips of the roof beam at two locations along its length as shown in Figure 3.13 to prevent the potential out-of-plane twisting of the roof beam. The angle sections were bolted to the flange of a W100x19 section which was attached with bolts to an independent frame. The bolt connection was used for the angle section so that it can be removed easily when the wall was positioned in the test frame.

Figure 3.13 Out of plane support

3.2.2.4 Instrumentation and Data Acquisition

Six Linear Variable Differential Transducers (LVDTs) were used to measure the lateral, vertical as well as diagonal displacements of the infill frame system. LVDTs 1 and 2 were attached at the side of the infill frame at the roof and bottom beam level to measure the relative lateral displacement as shown in Figure 3.14. For the regular walls without openings, LVDTs 4, 5 and 6 were mounted at the mid-section of the infill to measure the lateral, vertical and diagonal deformation of the infill. For the walls with openings, LVDTs 4, 5 and 6 were mounted at the mid-section of the left zone besides the opening.

As an example, the configuration of the wall with door opening was shown in Figure 3.15. One LVDT was used to measure any out-of-plane movement at about the half height of the wall on the back side.

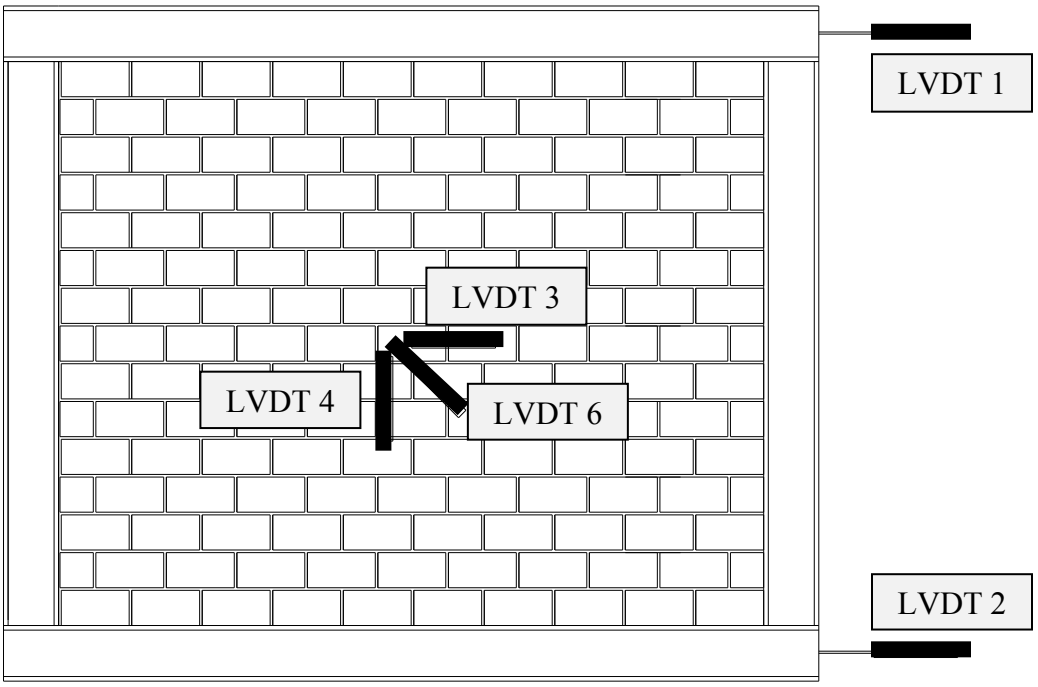

Figure 3.14 LVDTs position for walls without opening

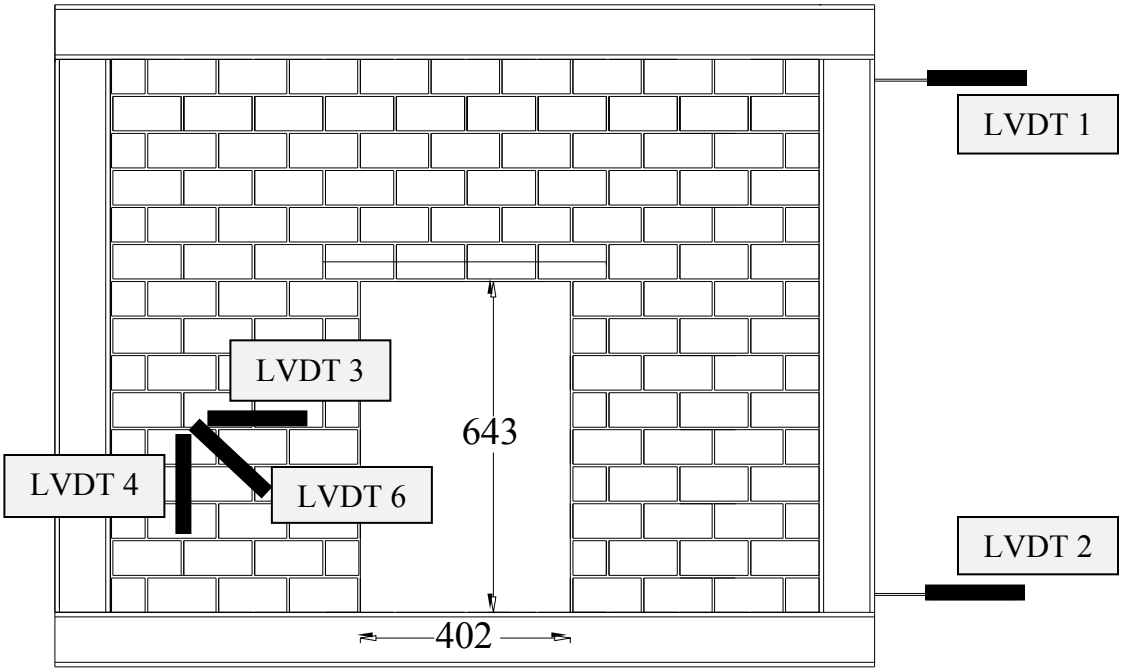

Figure 3.15 LVDTs position for walls with door opening

3.2.3 Wall Specimens Test Procedure

A 10 ton capacity ceiling crane was used to transport the infilled frame specimen to its test location after curing. The infilled frame was then positioned in the test frame as shown in Figure 3.16 and effort was taken to ensure that the frame was aligned properly in both in-plane and out-of-plane direction. The frame was then bolted to the floor beam and secured in place. Out-of-plane restraints were then mounted against the flange of the roof beam. The LVDTs were mounted and checked before each test. For the first four specimens, extra care was taken to ensure that the wall was plumb and square in the testing position while gaps, if any, between the wall and the surrounding frame members were reduced to a minimum. In some cases, cement and shims were used to reduce the gap between the infill and the frame as much as possible. Lateral load was applied gradually at a rate of 8kN per minute until failure occurred. Load and LVDT readings were monitored and recorded with an interval of 0.1 seconds throughout each test using an electronic data acquisition system. During each test, the cracking load, cracking pattern, failure mode, and ultimate load were noted.

Figure 3.16 Test Set-up

3.3 AUXILIARY TESTS

3.3.1 Concrete Masonry Units

Third scale concrete masonry units were used in the experimental program. They included regular, end and half blocks. Figure 3.17 shows the typical regular and end unit blocks used. The average dimensions for the units shown in the Figure 3.17 were approximately 1/3 of a standard 200mm concrete block. The weight of each regular unit block was approximately 580 grams. The concrete masonry units were tested for its compressive strength in accordance with ASTM C140-07a (2007). The physical properties including the percentage adsorption, density, as well as moisture content were also tested according to ASTM C140-07a.

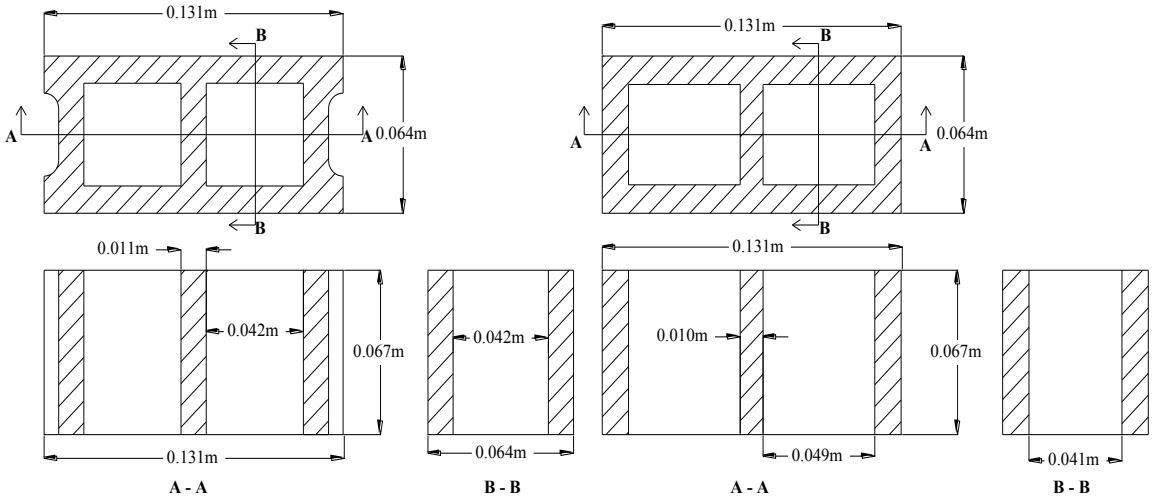

(a) Regular Block (b) End Block

Figure 3.17 Typical regular and end concrete masonry unit blocks dimensions.

3.3.2 Mortar and Grout

Type S mortar was used for the wall construction. The composition of mortar included Portland cement, type N masonry cement, and sand with a respective ratio of 1:2:8. Twenty-six 50 mm (2 inch) mortar cubes were prepared in molds as the mason mixed the mortar on site as shown in Figure 3.18.

Figure 3.18 Mortar cubes in mold

The mortar cubes were cured in a moisture room for 7 days and tested for compressive strengths at seven days as well as at twenty-eight days. The constructing and testing of mortar cubes was performed in accordance to CSA A179-04(R2009) Mortar and Grout for Unit Masonry. Grout was made out of five parts sand and one part masonry cement for the dry mix. A sufficient amount of water was mixed in as-needed manner by the mason to achieve the fluidity of the grout. To test the compressive strength of the grout, nine grout prisms were prepared in accordance with CSA A179-04. Grout mix was poured into a "mold" formed with four unit blocks as shown in Figure 3.19.

Figure 3.19 Grout cube molds

The grout prisms were air-cured for 48 hours and moist cured for another 25 days in the moist room. The grout prisms were then tested for compressive strength to ensure quality and consistency.

3.3.3 Masonry Prisms

Two types of masonry prisms were constructed and tested in this study. One type was three-course high with a height to thickness ratio of 3.3 as shown in Figure 3.20.

Figure 3.20 3-High Prisms testing arrangement

A total of 12 prisms of this type including 3 hollow, and 9 fully grouted were constructed. The prisms were tested for the compressive strength, the modulus of elasticity, and the stress-strain relationship of the masonry in accordance with ASTM C1314-07 – Standard test methods for compressive strength of masonry prisms.

The second type of masonry prisms, referred to as square prisms, was 4-course high, 2-course wide with a height to thickness ratio of 4.4. A total of 27 prisms of this type including 9 hollow, 9 partially grouted, and 9 fully grouted were prepared. The partially grouted prisms were grouted on the two outer cells of the prisms. They were tested for compressive strength under three loading conditions. Vertical compression refers to a loading direction which was perpendicular to the bed joint; horizontal compression indicates that the loading was applied in parallel to the bed joint; and the diagonal compression was to load the specimen in diagonal direction. The diagonal, vertical and horizontal loading conditions are shown in Figure 3.21. These prisms were tested to have

a better understanding of the effect of loading direction on the compressive strength of masonry assemblage. All prisms were cured together with the walls and tested at approximately the same time as the walls. LVDTs were mounted at the front and the back of all the square prisms to obtain deformation readings. The gauge lengths of the LVDTs were kept at approximately 200 mm. Horizontal and vertical specimens had a similar testing procedure to the three-high prisms. For testing in the diagonal direction, two custom-made supports were used for the loaded corners where each support was a V-shaped joint inside a rectangular box designed to encase the corners and provide a straight surface for testing as shown in Figure 3.22.

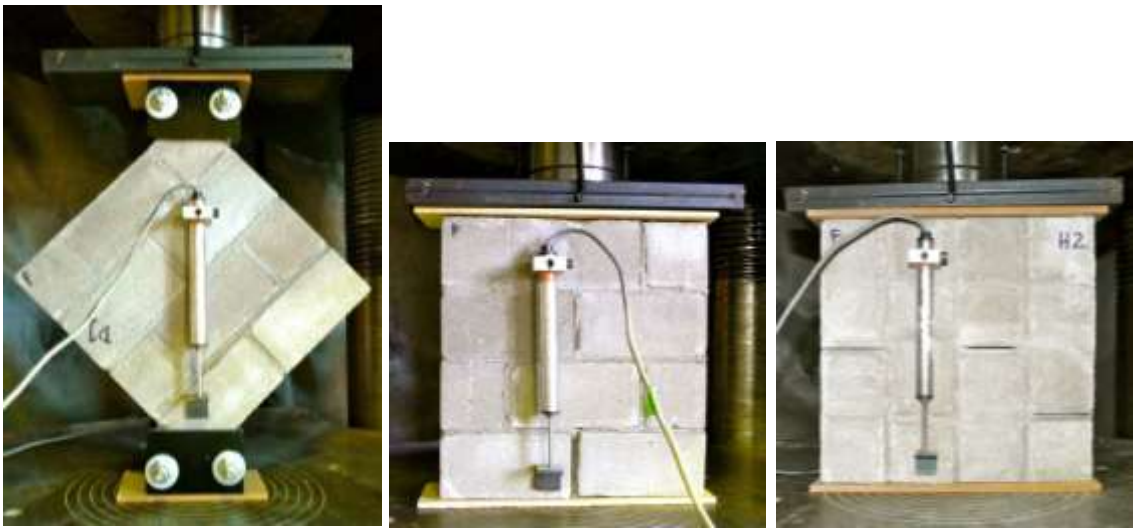

Diagonal **Vertical** **Horizontal**

Figure 3.21 Loading Conditions of Compression Test for Square Prisms.

Figure 3.22 Diagonal prism test loading shoe.

3.3.4 Reinforcing Bars

Due to the size of the scaled concrete blocks, 6mm threaded rods were used as both vertical and horizontal reinforcements in the infills. The tensile strength of the reinforcement bars was determined in accordance with ASTM E8-08 Standard Test Methods for Tension Testing of Metallic Materials as shown in Figure 3.23(a). In order to prevent slippage between the bars the grip of the Instron machine, a custom fit brackets with set-screws were made to hold the bar as shown in Figure 3.23(b).

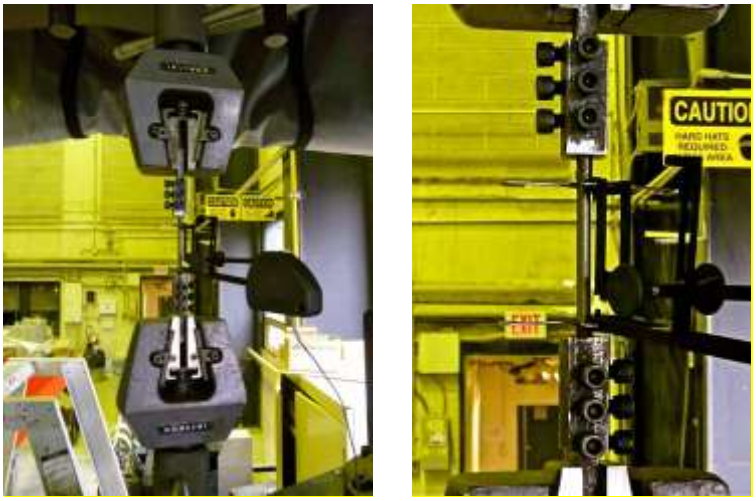

(a) (b)

Figure 3.23 (a) Reinforcing bars tension testing, (b) Custom fit brackets.

Three pieces of the 6mm threaded rods were randomly chosen for testing to obtain the tensile strength, the modulus of elasticity, as well as the stress-strain behavior of the material.

CHAPTER 4 EXPERIMENTAL RESULTS AND DISCUSSION

4.1 INTRODUCTION

In this chapter, results of both auxiliary and infilled frame specimen test are presented. Auxiliary test results include physical and mechanical properties of concrete masonry unit blocks, mortar, grout, reinforcement bars, and prisms whereas results of infilled frame specimens are focused on the behavior and capacity of infill systems as affected by parameters including aspect ratio, grouting, and opening of the infill as well as frame-to-infill stiffness ratio.

4.2 AUXILIARY TEST RESULTS

4.2.1 Physical Properties

One-third scale concrete masonry units with a nominal dimension of 130x65x65mm were used in this experimental program. To obtain the physical properties of these masonry units, three stretcher unit blocks were randomly selected and tested for absorption, moisture content and density in accordance with ASTM C140-07a Standard Test Methods for Sampling and Testing Concrete Masonry Units and Related Units (2007). Equations for calculating the moisture content and absorption rate were given in the ASTM C140-07a standard. The original received weight of the unit blocks were obtained first and then the blocks were immersed in water for 24 hours. They were then weighted in water to obtain the immersed weight. After removal from the water, the surface water was dried off and the blocks were measured for the saturated weight. The blocks were then dried in the oven at approximately 100°C for 24 hours wherein the oven-dry weights were then measured. Table 4.1 shows the absorption, moisture content and density obtained as well as their respective standard deviations and coefficient of variations. The average absorption obtained for the tested unit blocks was 174.2% with a coefficient of variation (COV) of 7.3%. The average moisture content was 8.6% with a COV of 10.7% and the average density for the unit blocks were 2058kg/m^3 with a COV of 0.9%. According to CAN/CSA-A165-04 (R2009) - CSA Standards on Concrete Masonry Units, a standard 200mm hollow block should have a density of greater than 2000kg/m^3,

absorption of less than 175% and maximum moisture content of 45% for a relative humidity higher than 75%. The averages of the test data for the scaled concrete masonry units demonstrated to be in compliance with these specifications.

Table 4.1 Physical properties of concrete masonry units

ID	Received Weight (g)	Saturated Weight (g)	Immersed Weight (g)	Dry Weight (g)	Absorption (%)	Moisture Content (%)	Density (kg/m^3)
1	576	621	341	572	175.8	7.5	2039.9
2	565	611	339	561	186.1	9.1	2058.4
3	585	626	346	581	160.7	9.1	2075.7
				Avg.	174.2	8.6	2058.0
				Std. Dev.	12.8	0.9	17.9
				COV(%)	7.3	10.7	0.9

4.2.2 Mechanical Properties

The compressive strengths of 1/3-scale unit blocks, mortar, grout and prisms as well as tensile strength of reinforcement bars were tested in accordance with respective ASTM standards.

4.2.2.1 Concrete Masonry Units

Compressive strength of the concrete masonry units was also obtained following ASTM C140-07a. Thirteen unit blocks were randomly selected and their surface dimensions were carefully measured using a digital caliper. Specimens were then tested in compression in the Instron Universal testing machine. Fiberboard capping was used to ensure a uniform loading. Compressive strength for the three types of concrete masonry units used in construction are listed in Table 4.2 where R denotes regular blocks, E for end blocks and H for half blocks. The compressive strength was calculated using the ultimate load divided by the net area of the unit block. The net area of the unit block ranges from 50 to 60% of the gross area for all the unit blocks. The average compressive strength obtained for all the units was 20.2MPa with COV values less than 15% for all three different types of blocks. The compressive strengths obtained were shown to be

comparable with standard full-scale unit blocks, which usually have compressive strengths in the range of 10 to 40MPa based on the net area.

Table 4.2 Mechanical properties of concrete masonry units

Unit ID	Area (mm^2)	Ultimate Load (N)	Compressive Strength (MPa)
R1	4115	102524	24.9
R2	4075	97863	24.0
R3	4112	118403	28.8
R4	4125	94214	22.8
R5	4113	79293	19.3
R6	4053	74200	18.3
R7	4106	100142	24.4
R8	4206	86186	20.5
		Avg. (MPa)	22.9
		Std. Dev.	3.4
		COV (%)	15.0
E1	4269	55149	12.9
E2	4181	72424	17.3
E3	4159	71196	17.1
E4	4209	54684	13.0
E5	4163	61296	14.7
		Avg. (MPa)	15.0
		Std. Dev.	2.1
		COV (%)	14.3
H1	2445	58457	23.9
H2	2451	53940	22.0
H3	2369	52169	22.0
		Avg. (MPa)	22.6
		Std. Dev.	1.1
		COV (%)	4.8

Figure 4.1 shows a typical load-displacement curve of a unit block tested in compression where the displacement was taken as the position of the loading table. The response was characteristic of a brittle material where the curve remained almost linear up to failure. Figure 4.2 shows typical failures of unit blocks under compressive testing, which included vertical splitting and conical shear failure.

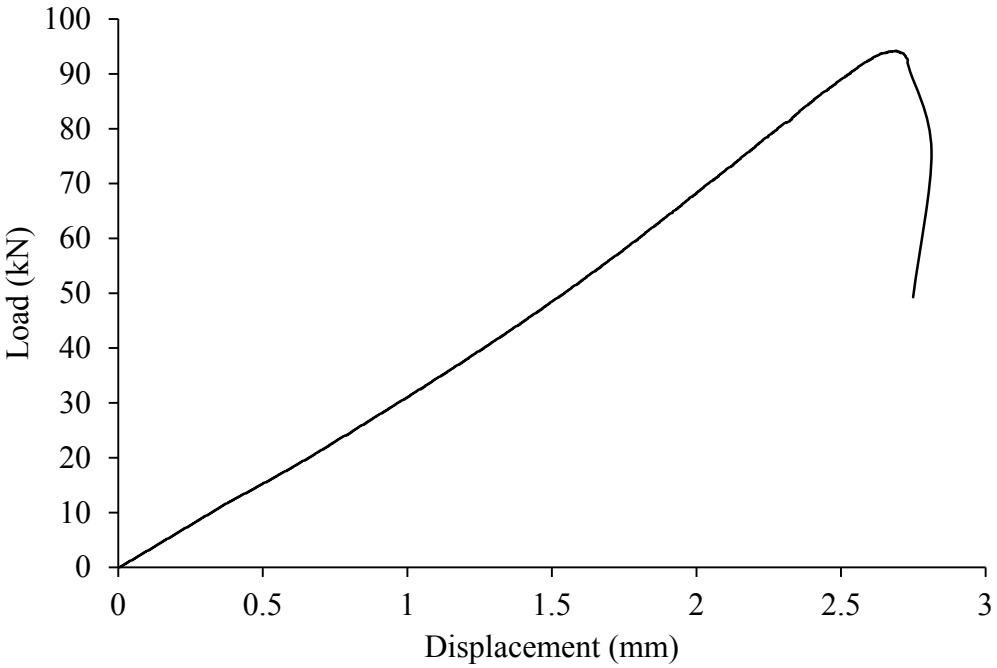

Figure 4.1 Load-displacement curve of a unit block in compression

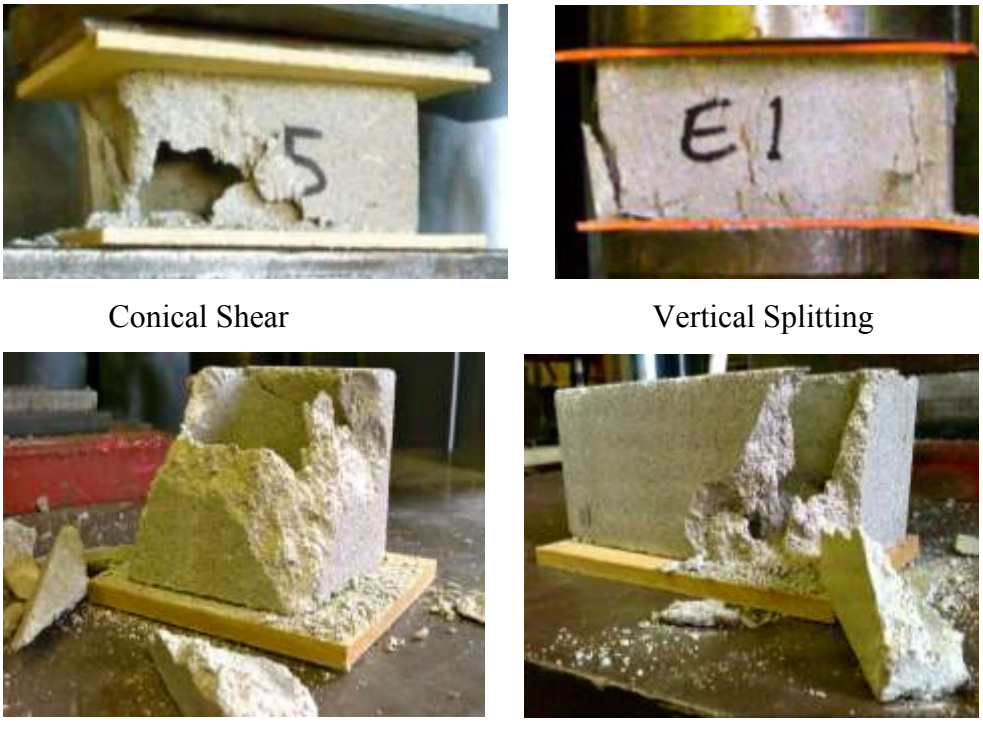

Conical Shear Vertical Splitting

Conical Shear Conical Shear

Figure 4.2 Failure of unit blocks under compression

4.2.2.2 Mortar

Type S mortar was used in the construction of wall infills. Three batches of mortar were used in the building of specimens and mortar cubes were made from each batch. A total of twenty-six 50mm mortar cubes were tested for their 28-day strength according to CSA A179-04 (2004) Mortar and grout for unit masonry. For batch 1 mortar, nine cubes were tested for 7-day strength as well for quality control purposes. Figure 4.3 shows an example of the failure of mortar cubes under compressive testing where most of the mortar cubes showed a conical shear or pyramidal shape failure. The compressive strength for mortar cubes are summarized in Table 4.3 where the mean 28-day compressive strength of all the mortar cubes tested was 13.6MPa. The average 28-day compressive strengths were 15.1MPa from batch 1 (BM1) and 9.6MPa for Batch 2 (BM2) mortar cubes. Mortar cubes from batch 3 (BM3) attained compressive strength of 19.6MPa. The COVs of all 3 batches mortar strength were well within the specified limit of 15%. It should be pointed out that BM2 mortar strength was lower than the minimum 28-day strength (12.5MPa) specified in CSA A179 - 04 (2004) for type S mortar under laboratory conditions.

Figure 4.3 Failure of mortar cubes under compressive testing

Table 4.3 Compressive strength of mortar cubes

Cubes	Sizes (mm)		Area (mm^2)	Test Age	Compressive Strength (MPa)
	Width	Length			
BM1 - 1	51.2	51.3	2628	7 days	9.4
BM1 - 2	51.3	51.2	2626		11.0
BM1 - 3	51.1	51.5	2634		8.9
BM1 - 4	51.2	51.2	2618		9.2
BM1 - 5	51.2	51.2	2621		10.6
BM1 - 6	51.0	51.2	2612		11.8
BM1 - 7	50.9	51.0	2596		10.8
BM1 - 8	51.0	51.1	2607		8.6
BM1 - 9	51.1	51.1	2612		9.9
			Avg. (MPa)		10.0
			Std. Dev.		1.1
			COV (%)		10.6
BM1 - 10	51.0	50.0	2550	28 Days	15.3
BM1 - 11	51.0	50.5	2576		12.5
BM1 - 12	50.5	50.0	2525		15.0
BM1 - 13	51.0	50.0	2550		16.3
BM1 - 14	50.0	51.5	2575		14.8
BM1 - 15	50.5	50.0	2525		16.6
			Avg. (MPa)		15.1
			Std. Dev.		1.5
			COV (%)		9.6
BM2 - 1	51.1	51.5	2632	28 Days	8.6
BM2 - 2	51.0	51.5	2627		8.7
BM2 - 3	51.2	51.3	2627		11.0
BM2 - 4	51.0	51.3	2616		10.5
BM2 - 5	51.0	51.4	2621		9.6
BM2 - 6	51.1	51.4	2627		9.3
			Avg. (MPa)		9.6
			Std. Dev.		1.0
			COV (%)		10.2
BM3 - 1	51.1	51.0	2606	28 Days	17.6
BM3 - 2	51.0	51.0	2601		19.9
BM3 - 3	51.4	51.0	2621		20.5
BM3 - 4	51.0	51.5	2627		18.6
BM3 - 5	51.0	51.5	2627		21.2
			Avg. (MPa)		19.6
			Std. Dev.		1.4
			COV (%)		7.4

4.2.2.3 Grout

Ten grout cubes were obtained from two batches of grout and they were tested in accordance with CSA A179-04 (2004) for their compressive strength. Table 4.4 shows the results where BG1 denotes batch 1 and BG2 represents batch 2 grout. Figure 4.4 shows typical failures of grout cubes under compressive loading and exhibited a vertical cracking failure. Figure 4.5 shows a load-displacement curve of a grout cube (BG1-5) under compressive, which demonstrates a brittle nature of failure. The overall average compressive strength of the grout cubes was 18MPa. The average compressive strengths of batch 1 (BG1) and batch 2 (BG2) grout cubes were 15.5MPa with a COV of 10.5% and 19.6MPa with a COV of 9.3%, respectively. BG1 and BG2 grout batches corresponded to the mortar of BM1 and BM2. Due to the limitation of supplies at the time of construction, no grout cubes were produced during the production of batch 3 specimens. The strengths of both batches of grout cubes were greater than the minimum compressive strength of 12MPa for coarse grout specified in CSA A179 – 04.

Table 4.4 Compressive strength of grout cubes

Cubes	Sizes (mm)			Compressive Strength
	Width	Length	Height	(MPa)
BG1 - 1	61	63	58	15.5
BG1 - 2	61	63	58	15.2
BG1 - 3	65	68	68	16.2
BG1 - 4	70	72	66	15.2
BG1 - 5	70	71	60	19.4
		Avg. (MPa)		15.5
		Std. Dev.		1.6
		COV (%)		10.5
BG2 - 1	66	67	68	22.1
BG2 - 2	67	68	68	19.0
BG2 - 3	69	65	67	18.5
BG2 - 4	67	68	66	17.6
BG2 - 5	68	69	65	20.9
		Avg. (MPa)		19.6
		Std. Dev.		1.8
		COV (%)		9.3

Figure 4.4 Failure of grout cubes under compressive testing

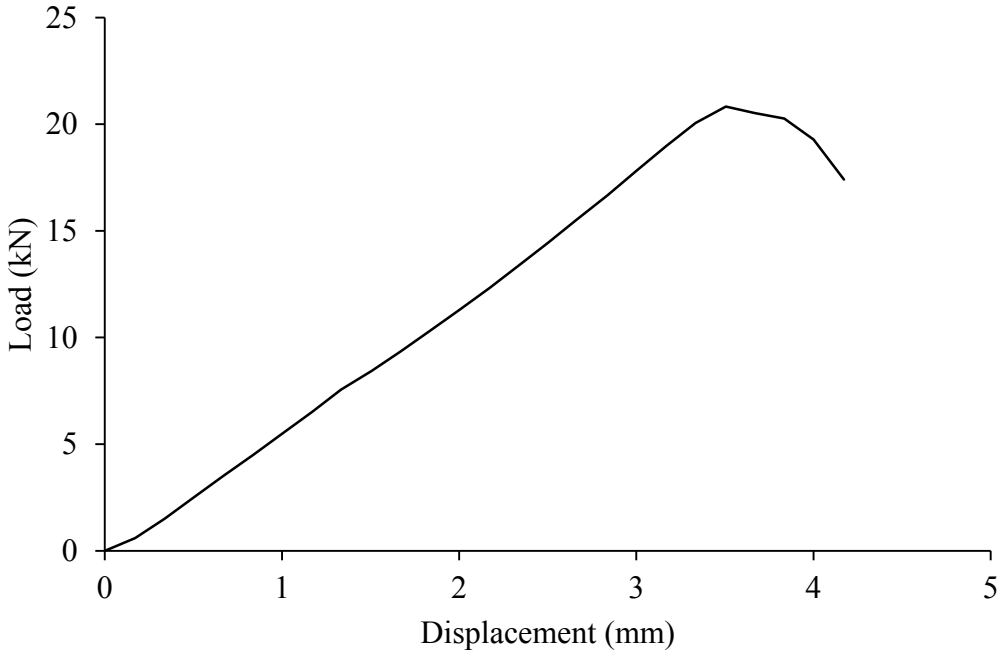

Figure 4.5 Load-displacement diagram of a grout cube in compressive

4.2.2.4 Prisms

A total of 39 prisms including 12 three-high and 27 square prisms were fabricated and tested in compression in accordance with ASTM C1314-07 (2007) standard test method for compressive strength of masonry prisms. Table 4.5 lists results of three-high prisms sampled from two batches. Both ungrouted and grouted prisms were tested for BP1 prisms while only grouted prisms were tested for BP2 prisms. For BP1 prisms, mortar batch BM1 and grout batch BG1 were used in the building of the prisms. For BP2 prisms, mortar BM2 and grout BG2 were used.

Table 4.5 Compressive strength of 3-high prisms

Sample	Grouting	Net Area (mm^2)	Height (mm)	Ultimate Load (N)	Stress (MPa)
BP1 - 1	No	4221	208	53346	12.6
BP1 - 2	No	4239	209	48035	11.3
BP1 - 3	No	4242	211	59470	14.0
				Avg.	12.7
				Std. Dev.	1.3
				COV (%)	0.1
BP1 - 4	Yes	8312	210	71435	8.6
BP1 - 5	Yes	8352	209	59649	7.1
BP1 - 6	Yes	8306	209	62057	7.5
BP1 - 7	Yes	8378	208	79042	9.4
BP1 - 8	Yes	8352	210	62777	7.5
				Avg.	8.0
				Std. Dev.	1.0
				COV (%)	0.1
BP2 - 1	Yes	8310	208	103897	12.5
BP2 - 2	Yes	8515	210	96359	11.3
BP2 - 3	Yes	8334	210	78616	9.4
BP2 - 4	Yes	8311	209	97833	11.8
				Avg.	11.3
				Std. Dev.	1.3
				COV (%)	0.1

The typical failure modes of 3-high prisms are shown in Figure 4.6. The most common failure mode was observed to be vertical cracking either through the face shell or the web. However, several specimens of the grouted 3-high prisms exhibited face-shell spalling

while the grouted column remained practically intact. These are common failure modes in prisms as reported by Drysdale and Hamid (2005).

Vertical crack (face-shell) Vertical crack (web) Face-shell spalling

Figure 4.6 Failure of 3-high prisms under compressive loading.

Net areas were used for the calculation of compressive strength of prisms. The net area for the 3-high ungrouted prisms is the outside shell-area of the prism as shown in Figure 4.7. The net area of the 3-high fully grouted prisms was the gross area less the web area of the unit block as shown in Figure 4.8.

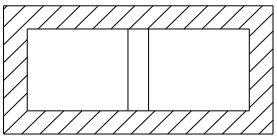

Figure 4.7 Net area for 3-high ungrouted prisms

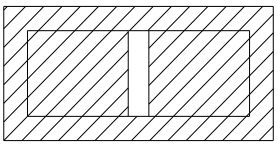

Figure 4.8 Net area for 3-high grouted prisms

The compressive stress of the BP1 ungrouted and grouted prisms were 12.7MPa and 8.0MPa, a difference of 37% with the difference in net areas of 49%. The higher

compressive strength of non-grouted prisms resulted from the fact that a smaller net area was used for the non-grouted prisms, which achieved similar ultimate load to the grouted prisms. For batch 2 prisms, only fully grouted prisms were produced. The average compressive strength of the BP2 prisms was obtained to be 11.3MPa, which was slightly lower than the BP1 prisms. The slightly lower compressive strength in this batch of prisms was attributed to the weaker mortar used in this batch of prisms.

As described in Chapter 3, twenty-seven square prisms were tested with loading applied in parallel, perpendicular and diagonal directions with respect to the bed joint in order to study the effect of loading direction on the prism compressive strength. For simplicity, these three loading conditions are referred to as vertical, horizontal and diagonal loading. These prisms are designated as batch 3 (BP3) prisms. In the case of the vertically loaded prisms, the net areas of the prisms used in the calculation of the ultimate stress are determined as follows. For partially grouted prisms, the net area as shown in Figure 4.9 equals the gross areas minus the areas of ungrouted cells and the webs. For fully grouted prisms, the net area equals the gross area.

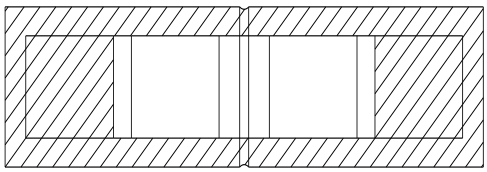

Figure 4.9 Net area for partially grouted prisms

For hollow prisms, the net area was the faceshell area as the webs of the prisms were not mortared as shown in Figure 4.10.

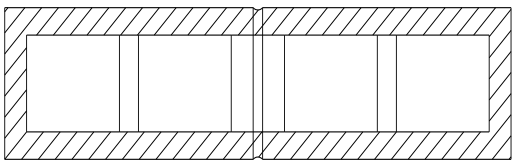

Figure 4.10 Net area for hollow prisms

For the horizontally loaded prisms, net area was calculated to be the same as the vertically loaded prisms with respect to the different grouting situations. For diagonally loaded prisms, the net area used for the fully grouted diagonally loaded prisms was the rectangular area where the prisms were in contact with the loading shoes as shown in Figure 4.11. The net area of the hollow prisms was taken as the faceshell area contained within the loading shoe. For partially grouted diagonal loaded prisms, the average areas between the fully grouted and hollow diagonally loaded prisms were used to calculate the net areas.

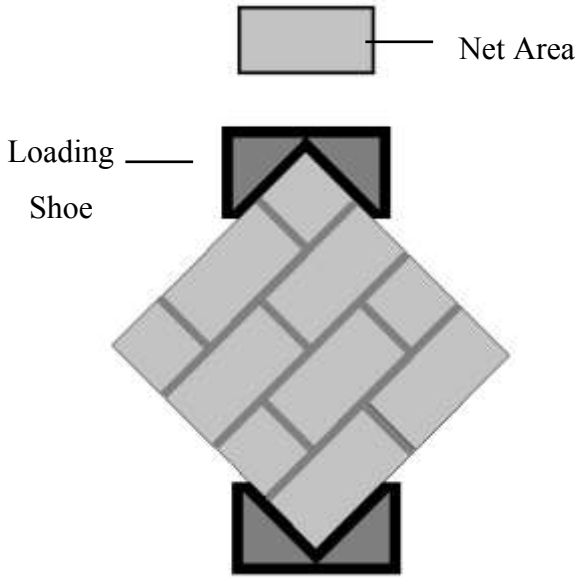

Figure 4.11 Diagonally loaded prisms net area

To study the behavior of the prisms in different loading directions, a stress-strain curve of each prism specimen was obtained and the Modulus of Elasticity, E_m, was also determined. It is a common practice to express E_m in terms of compressive strength, f'_m, obtained with loading applied perpendicular to the prism bed joint. In this study, this practice was followed and thus E_m in the following tables is expressed in terms of f'_{mV}, compressive strength of the vertically loaded prisms. Figure 4.12 shows the stress-strain curves of partially grouted prisms loaded in three directions. The full-set of stress-strain curves can be found in Appendix A. It can be seen that partially grouted prisms loaded in the horizontal direction displayed the lowest modulus of elasticity. However, diagonally loaded partially grouted prisms had the highest modulus of elasticity. As expected,

vertically loaded prisms had the highest compressive strength and horizontally loaded prisms had the lowest compressive strength for partially grouted prisms. It is also noted that vertically loaded prisms showed a greater strain at the maximum load than the other two specimens.

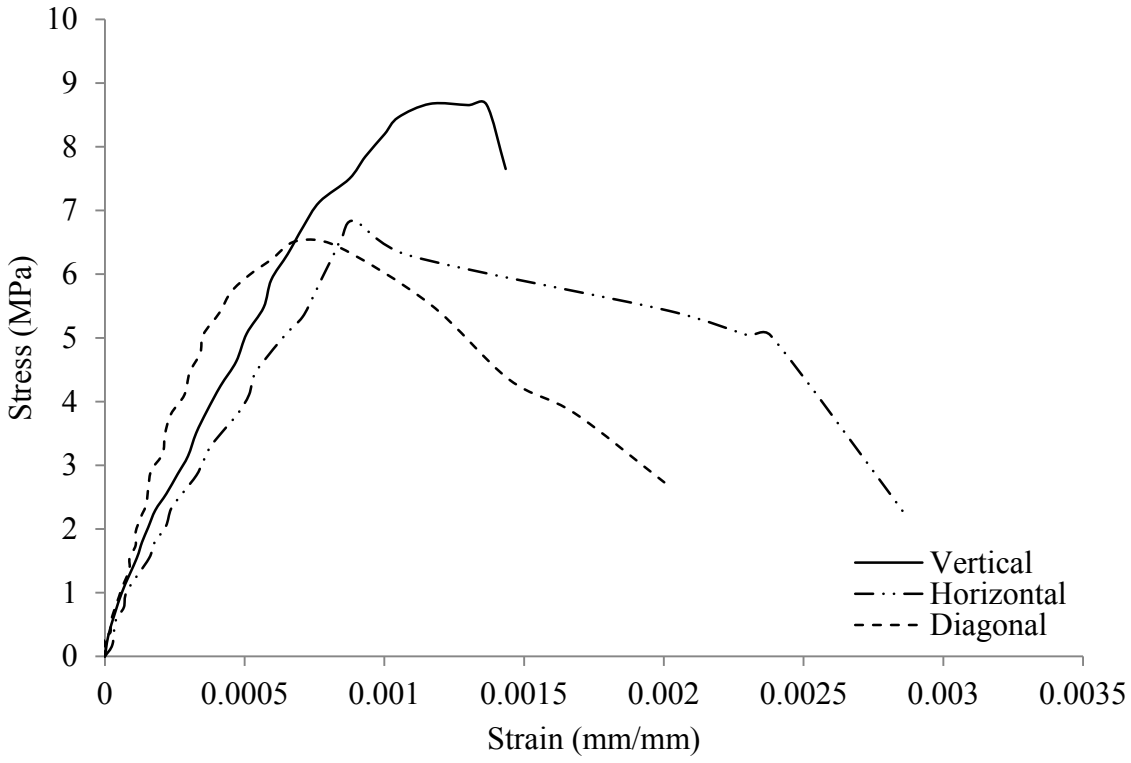

Figure 4.12 Stress-strain curves of typical partially grouted prisms

The average compressive strength, Modulus of Elasticity as well as their corresponding COVs for fully grouted, partially grouted and hollow square prisms loaded in the vertical direction are shown in Table 4.6.

Table 4.6 Compressive strength of vertically loaded square prisms

Fully Grouted						
Specimen	V1	V2	V3	Avg. (MPa)	Std. Dev.	COV (%)
f'_m (MPa)	11.5	9.3	8.8	9.9	1.5	14.7
E_m (x f'_m)	1224.5	1586.1	-	1405.3	-	-
Partially Grouted						
Specimen	V4	V5	V6	Avg. (MPa)	Std. Dev.	COV (%)
f'_m (MPa)	8.1	8.9	8.7	8.6	0.4	4.6
E_m (x f'_m)	1294.1	-	1202.0	1248.0	-	-
Hollow						
Specimen	V7	V8	V9	Avg. (MPa)	Std. Dev.	COV (%)
f'_m (MPa)	Not	12.5	10.7	11.6	-	-
E_m (x f'_m)	Usable	729.2	1255.6	992.4	-	-

The overall average compressive strength and modulus of elasticity for the vertical loaded prisms were 10.0MPa and 1215.2f'_{mV}, respectively. It can be seen that the fully grouted specimens showed 13.1% higher compressive strength than the partially grouted but 14.7% lower than the hollow prisms. The fully grouted prisms showed the highest modulus of elasticity (E_m) followed by partially grouted prisms with the hollow prisms showing the lowest modulus of elasticity. The E_m for prisms of all grouting configuration was greater than 850f'_{mV}, the value specified in the CSA S304.1 standard (2004). Failure of vertically loaded prisms involved vertical splitting and corner crushing as shown in Figure 4.13.

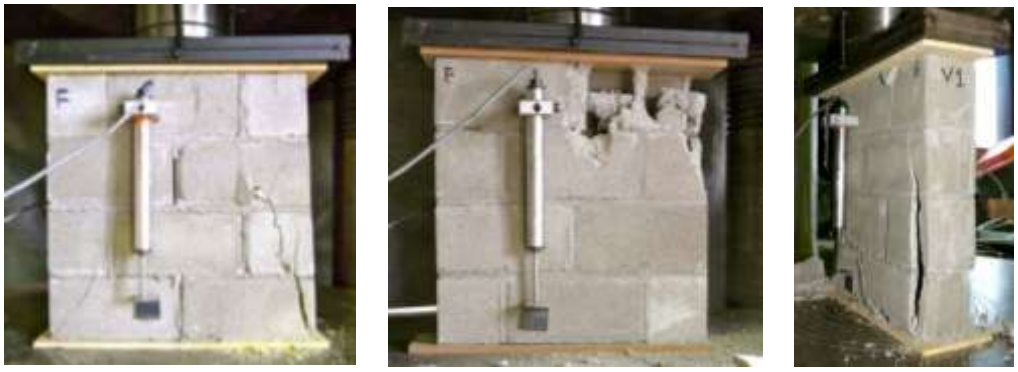

Figure 4.13 Vertically loaded square prisms

The average compressive strengths and modulus of elasticities for fully grouted, partially grouted and hollow square prisms loaded in the horizontal direction are shown in Table

4.7. Prisms of all three different grouting configurations attained strengths in the same order of magnitude.

Table 4.7 Compressive strength of horizontally loaded square prisms

Fully Grouted						
Specimen	H1	H2	H3	Avg. (MPa)	Std. Dev.	COV (%)
f'_m (MPa)	5.2	5.1	-	5.1	-	-
E_m (x f'_m)	1240.2	739.6	995.0	991.6	250.3	25.2
Partially Grouted						
Specimen	H4	H5	H6	Avg. (MPa)	Std. Dev.	COV (%)
f'_m (MPa)	4.8	6.9	Not	5.9	-	-
E_m (x f'_m)	982.5	850.8	Usable	916.6	-	-
Hollow						
Specimen	H7	H8	H9	Avg. (MPa)	Std. Dev.	COV (%)
f'_m (MPa)	4.7	Not	6.3	5.5	-	-
E_m (x f'_m)	581.8	Usable	840.8	711.3	-	-

The overall average compressive strength for the horizontally loaded prisms was 5.5MPa. Hollow prisms showed higher compressive strength than fully grouted prisms, which followed the same trend with the vertically loaded prisms as well as the 3-high prisms. The strength of horizontally loaded prisms was 55% of that of vertically loaded prisms. The average modulus of elasticity of prisms loaded in horizontal direction was $873.2f'_{mV}$ with fully grouted prisms showing the highest of the three grouting patterns. Two different failure modes were observed during the experiments, which were conical shear failure and web splitting as shown in Figure 4.14.

Figure 4.14 Horizontally loaded square prisms

Table 4.8 shows the values of compressive strength and modulus of elasticity for the square prisms loaded in the diagonal direction. The overall average compressive strength and modulus of elasticity for these prisms were 5.6MPa and $1355.9f'_{mV}$, respectively.

Table 4.8 Compressive strength of diagonally loaded square prisms

Fully Grouted						
Specimen	D1	D2	D3	Avg. (MPa)	Std. Dev.	COV (%)
f'_m (MPa)	5.1	5.2	5.4	5.2	0.1	2.3
E_m (x f'_m)	1139.9	1256.2	1559.2	1318.4	216.5	16.4
Partially Grouted						
Specimen	D4	D5	D6	Avg. (MPa)	Std. Dev.	COV (%)
f'_m (MPa)	5.2	6.6	6.0	5.9	0.7	11.7
E_m (x f'_m)	1414.3	1727.2	1730.8	1624.1	181.7	11.2
Hollow						
Specimen	D7	D8	D9	Avg. (MPa)	Std. Dev.	COV (%)
f'_m (MPa)	4.4	No	7.0	5.7	-	-
E_m (x f'_m)	907.5	LVDT	1342.7	1125.1	-	-

The overall average compressive strength for diagonally loaded prisms was slightly higher than that of the horizontally loaded prisms by about 1.8%. These diagonally loaded prisms had a Moduli of Elasticity higher than that of the vertically and horizontally loaded prisms in all three different grouting patterns. Partially grouted specimens had the highest compressive strength and modulus of elasticity for the diagonally loaded prisms. The failure pattern of diagonally loaded prisms usually involved either a vertical crack running through the units and mortar joints or a stepping-pattern crack along the mortar joints as shown in Figure 4.15.

Figure 4.15 Diagonally loaded square prisms

It can be seen that prisms loaded in the horizontal direction had compressive strengths of approximately 50% less than those of the vertically loaded prisms for fully grouted and hollow prisms. However, horizontally loaded partially grouted prisms exhibited a decrease of only 31% when compared to the vertically loaded prisms. Diagonally loaded prisms showed a slightly higher compressive strength when compared to the horizontally loaded prisms. The average Moduli of Elasticity of all three different grouting pattern for vertically, horizontally and diagonally loaded prisms were $1215.2f'_{mV}$, $873.2f'_{mV}$, and $1355.9f'_{mV}$.

The overall 3-high prisms showed higher compressive strengths for both hollow and fully grouted units when compared with the vertically loaded square prisms. The hollow 3-high prisms had an average compressive strength of 8.7% higher than the vertically loaded hollow square prisms. Fully grouted 3-high and square prisms showed compressive strength with a difference of 2.5% with square prisms showing to be the higher of the two. ASTM standard C1314 (2007) recognize this effect and provides conversion factors according to the height to thickness ratio for calculating the compressive strength of prisms tested with different height. In this case, the factors are 1.176 and 1.094 for the square prisms and 3-high prisms, respectively. Annex D of CSA S304.1 also provided conversion factors for prisms according to the height to thickness ratio, these factors for 3-high and square prisms are 0.915 and 0.969 for fully grouted prisms, and a factor of 1.0 applies to all prisms that are partially grouted or hollow. The compressive strengths before and after application of these conversion factors can be seen in Table 4.9.

Table 4.9 Compressive strength comparisons

	Grouting	3-High Prisms		Square Prisms (BP3)
		BP1	BP2	Vertically Loaded
Original	Full	8.0	11.3	9.9
f'_m	Partial	-	-	8.6
(MPa)	Hollow	12.7	-	11.6
Modified	Full	8.8	12.4	11.6
f'_{mASTM}	Partial	-	-	10.1
(MPa)	Hollow	13.9	-	13.6
Modified	Full	7.3	10.3	9.6
f'_{mCSA}	Partial	-	-	8.6
(MPa)	Hollow	12.7	-	11.6

The average original compressive strength as well as the compressive strengths modified with ASTM and CSA conversion factors for the fully grouted 3-high prisms was 9.7MPa, 10.6MPa and 8.8MPa, respectively. Since CSA had a modification factor of 1.0 for partially or hollow prisms, therefore there were no changes in the compressive strengths in those prisms mentioned. For square vertically loaded prisms, the overall average original compressive strength and the compressive strength modified with ASTM and CSA conversion factors were 10.0MPa, 11.8MPa, and 9.9MPa. The compressive strengths of the fully grouted and partially grouted vertically loaded prisms applied with the conversion factors were used in the later calculations for the strength and stiffnesses of the large-scale test specimens. For batch 1 and 2 of the wall specimens, 3-high fully grouted prisms compressive strengths were used, whereas for batch 3 wall specimens, square fully grouted and square partially grouted prisms were used for calculations.

4.2.2.5 Vertical Reinforcement

Three coupons of 6mm threaded rods were sampled and tested in tension following ASTM E8-08 Standard test methods for tension testing of metallic materials (2008) and the results are shown in Table 4.10. An average elastic modulus of 198,428 MPa, yield strength of 600MPa, and ultimate strength of 632MPa were obtained with an average COV of 7.5%, 6.7%, and 6.1%, respectively. According to ASTM, the yield strengths of the specimens were to be obtained using a 0.002mm/mm strain offset method. The ultimate strength was the largest value obtained on the stress-strain diagram of the tension loaded specimens. Figure 4.16 shows an example stress-strain curve of a tension tested reinforcement bar coupon with the 2% strain offset that was used to determine the yield strength of the specimen, as well as the ultimate strength of that particular specimen.

Table 4.10 Reinforcement bars properties

Specimen	Modulus of Elasticity E_s (MPa)	Yield Strength f_y (MPa)	Ultimate Strength f_u (MPa)
1	194104	620	657
2	186251	554	587
3	214930	626	656
Avg (MPa)	198428	600	632
St. Dev.	14821	40	39
COV (%)	7.5	6.7	6.1

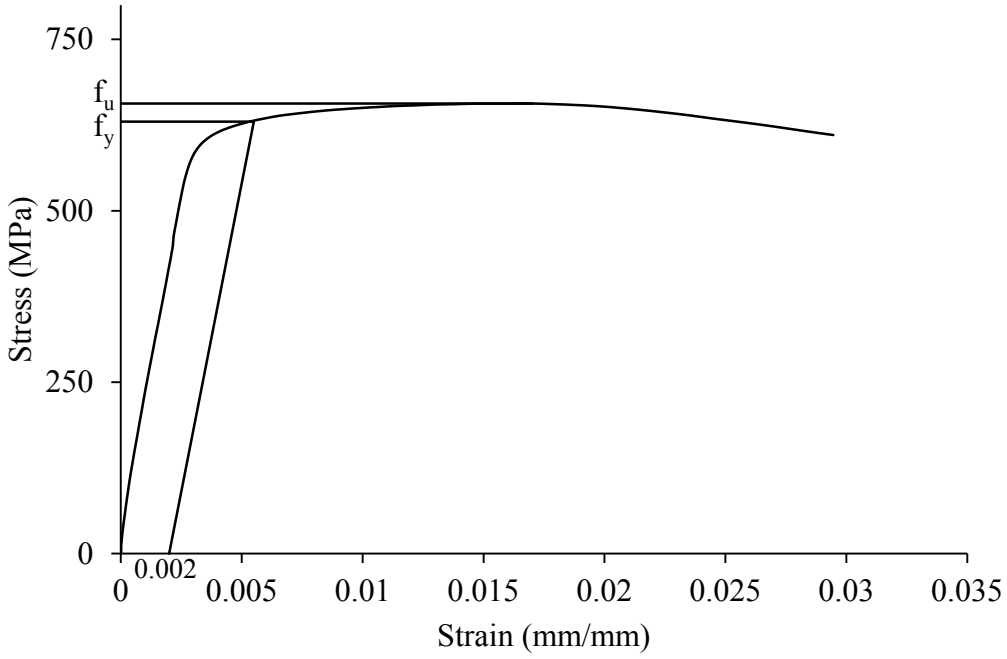

Figure 4.16 Stress strain diagram of reinforcement bar

4.2.3 Summary of Auxiliary Tests

Physical and mechanical tests were performed on the concrete masonry units. The unit blocks yielded absorption, moisture content, and density of 174.2 kg/m^3, 8.6%, and 2058kg/m^3, respectively. The overall average compressive strength of the concrete masonry unit was found to be 20.2MPa. Grout and mortar were casted into cubes and tested in compression. The 28-day compressive strength of the mortar and grout were determined to be 14.8MPa and 17.6MPa respectively. The overall average compressive strength of the hollow three-high prisms was tested to be 12.7MPa and the fully grouted three-high prisms had a compressive strength of 9.7MPa. Twenty-seven 4-high square prisms were tested to observe the effect of loading direction on the compressive strength of the prisms. It was shown that prisms with loading perpendicular to the bed joints achieved a higher compressive strength compared to prisms loaded in the direction parallel and diagonal to the bed joints. Tension coupon tests showed that the average modulus of elasticity of the reinforcement bars were very close to the standard of 200,000MPa, and the average yield strength and ultimate strength were tested to be 600MPa and 632MPa, respectively.

4.3 INFILLED FRAMES TEST RESULTS

The infilled frame test results are summarized in Table 4.11 including the ultimate load, first crack load, failure mode, initial stiffness, and secant stiffness. The batch designation of the wall specimen corresponding to the auxiliary tests as well as the converted prism compressive strengths according to the ASTM and CSA standards are also shown in the table. The definition of various terms used in Table 4.11 is illustrated in Figure 4.17 where a typical load versus lateral deflection curve (specimen P3NI for instance) is plotted. Note that the lateral deflection used in all following curves was calculated as the difference between readings of LVDT1 and LVDT2.

Table 4.11 Experimental test results of wall specimens

ID	Spec.	Batch	Orig. f'_m (MPa)	CSA f'_m (MPa)	ASTM f'_m (MPa)	P_{ult} (kN)	P_{cra} (kN)	K_{ini} (kN/mm)	K_{cra} (kN/mm)	K_{ult} (kN/mm)	Failure Mode
1	BF	-		-	-	-	-	3	-	-	-
2	P1NA	3	8.6	8.6	10.1	111.0	91.9	48.6	21.7	17.1	CC
3	F1NA	3	9.9	9.6	11.6	156.9	108.8	24.5	22.7	6.0	CC
4	P3NA	1	8.0	7.3	8.8	93.8	93.8	58.3	24.9	24.9	CC
5	P3WA	2	11.3	10.3	12.4	89.1	52.1	31.2	20.7	5.5	DT
6	P3DA	2	11.3	10.3	12.4	75.3	63.8	13.7	11.2	6.5	DT
7	P3NI	2	11.3	10.3	12.4	78.9	73.3	15.1	12.7	10.5	CC
8	F3NA	2	11.3	10.3	12.4	131.7	128.2	71.7	25.6	20.9	CC
9	F3NI	1	8.0	7.3	8.8	121.9	71.7	21.8	17.5	10.2	CC
10	P6NA	2	11.3	10.3	12.4	104.2	104.2	14.4	9.3	9.3	CC

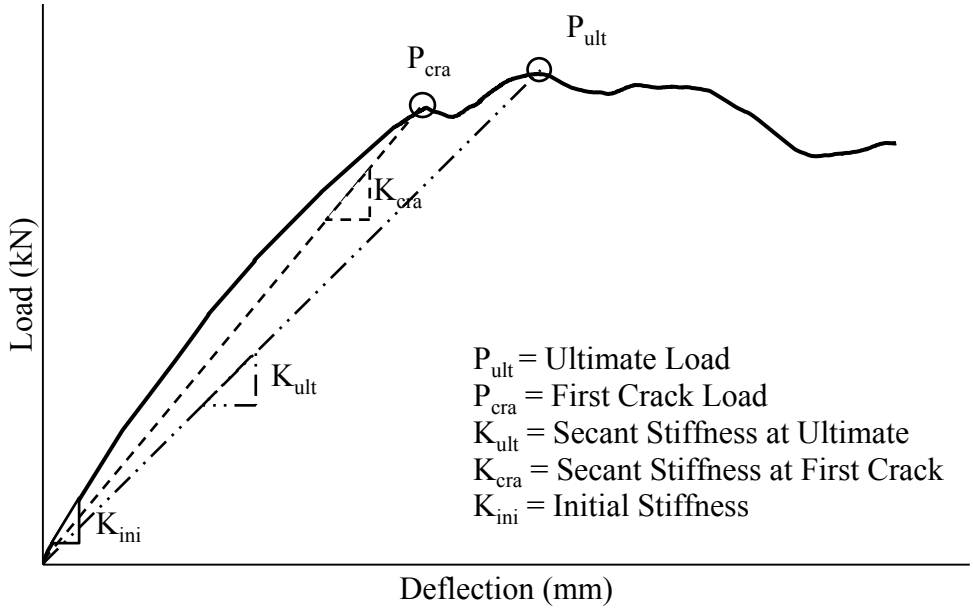

Figure 4.17 Definition of terms

The ultimate load is defined as the maximum load obtained by the specimen as shown on the load-deflection curve. The load at the appearance of the first visible crack is referred to as the first crack load and is determined from both experimental observation and the load-deflection curve. In most cases, the observed first visible crack corresponded to a point on the increasing branch of the load-deflection curve where a marked load drop occurred with a reduction in the stiffness from the initial stiffness and thereafter the load continued to increase. For several specimens such as P3NA and P6NA, however, visible cracks were only observed close to the failure of the infill and the corresponding load-deflection curve did not show a clear load drop in its rising branch. In this case, the observed crack load was indicated in the table. The initial stiffness was defined as the slope of the initial linear portion of the load-deflection diagram whereas the secant stiffnesses at ultimate and at the first crack load were calculated as the slope of the line connecting the origin and the ultimate load and the first crack load respectively.

Two types of failure modes observed in this study included diagonal tension cracking failure (DT) and corner crushing (CC). Except for specimens P3WA and P3DA with openings, the rest of the specimens failed predominately by corner crushing. Among these specimens, some developed diagonal cracks then failed by corner crushing while others started with corner crushing and diagonal cracks propagated from the crushed corners to the middle of the specimens. For specimens P3WA and P3DA, diagonal cracking formed and developed from the loaded corner to the edge of the opening but no evident crushing observed at the time of failure. A detailed discussion of failure modes of each specimen is provided in the following sections.

4.3.1 Parametric study

4.3.1.1 Aspect Ratio

Aspect ratios of 1.0, 1.3 and 1.6 were considered and their load-deflection curves are shown in Figure 4.18. For ease of reference, the portion of Table 4.11 related to these aspect ratios are reproduced in Table 4.12.

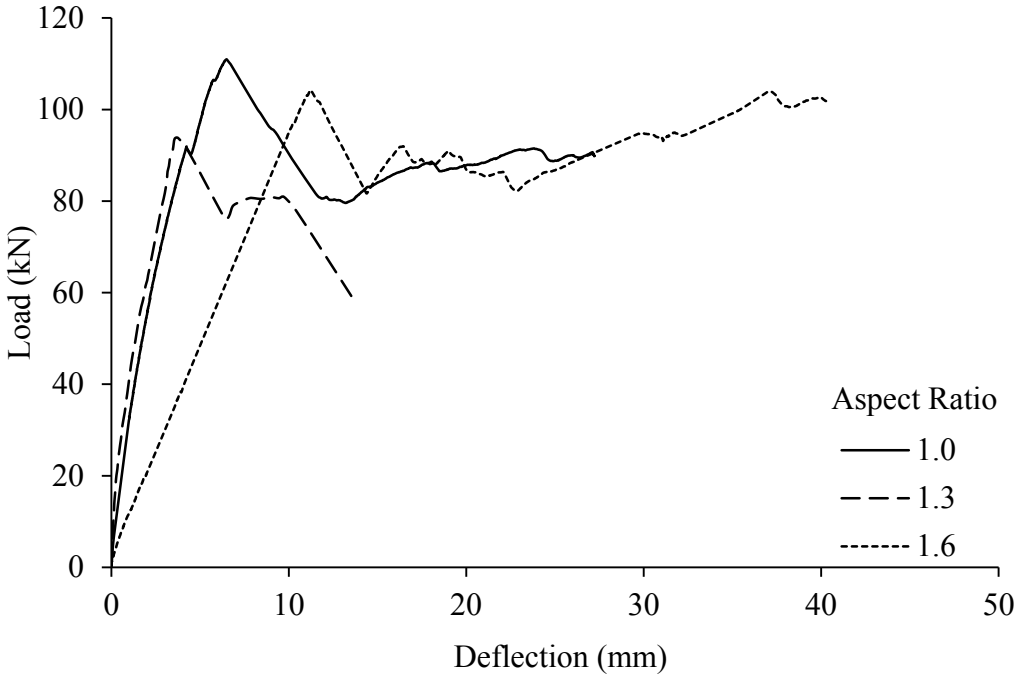

Figure 4.18 Load-deflection curves on the effect of aspect ratios

Table 4.12 Test results with respect to aspect ratios

ID	Specimen	Aspect Ratio	Strength (kN)		Stiffness (kN/mm)			Failure Mode
			P_{ult}	P_{cra}	K_{ini}	K_{cra}	K_{ult}	
2	P1NA	1.0	111.0	91.9	48.6	21.7	17.1	CC
4	P3NA	1.3	93.8	93.8	58.3	24.9	24.9	CC
10	P6NA	1.6	104.2	104.2	14.4	9.3	9.3	CC

It was noted that from Figure 4.18 and Table 4.12 that specimen with aspect ratio 1.0 attained the highest ultimate strength. Higher strength achieved by square infills than rectangular infills was also reported by Dawe et al. (2001) in a parametric study of infills based on finite element modeling. It was also noted that in this study, the specimen with 1.0 aspect ratio had virtually no gaps between the bounding frame and the infill while the other two specimens had gaps between the roof beam and the infill. It is believed that the intimate contact to the frame may also have attributed to the higher strength. Specimen with 1.3 aspect ratio had 16.6% higher initial stiffness, 12.9% higher in first crack secant stiffness, and 31.3% higher in ultimate load secant stiffness when compared to the specimen with 1.0 aspect ratio. Between specimens with aspect ratio of 1.3 and 1.6, the

latter showed higher strength in a magnitude of 10%. For specimen P6NA, a significant gap was present between the infill and the roof beam as seen in Figure 4.19 (P6NA). This gap may have prevented the full formation of diagonal strut and in turn resulted in a low value of the stiffness. At this point, more testing is required to make conclusive comment regarding the effect of aspect ratio. However, one recommendation can be made is that the presence of gap is critical to the stiffness and strength of the infill. All three specimens failed predominately by corner crushing. P1NA developed a single vertical crack close to the load-ward side of the infill as shown in Figure 4.15. P3NA developed diagonal tension cracks as the infill was being loaded but P6NA did not develop any cracks and failed only by corner crushing mode as seen in Figure 4.19.

Figure 4.19 Failure of wall specimens

4.3.1.2 Grouting

The effects of grouting are illustrated in Figure 4.20 and Figure 4.21 where load-deflection curves are plotted for partially and fully grouted specimens with aspect ratios of 1.0 and 1.3, respectively. The portion of Table 4.11 related to this parameter is reproduced in Table 4.13. In this study, the average net area of partially grouted infills is about 77% of the fully grouted infills for both aspect ratios of 1.0 and 1.3.

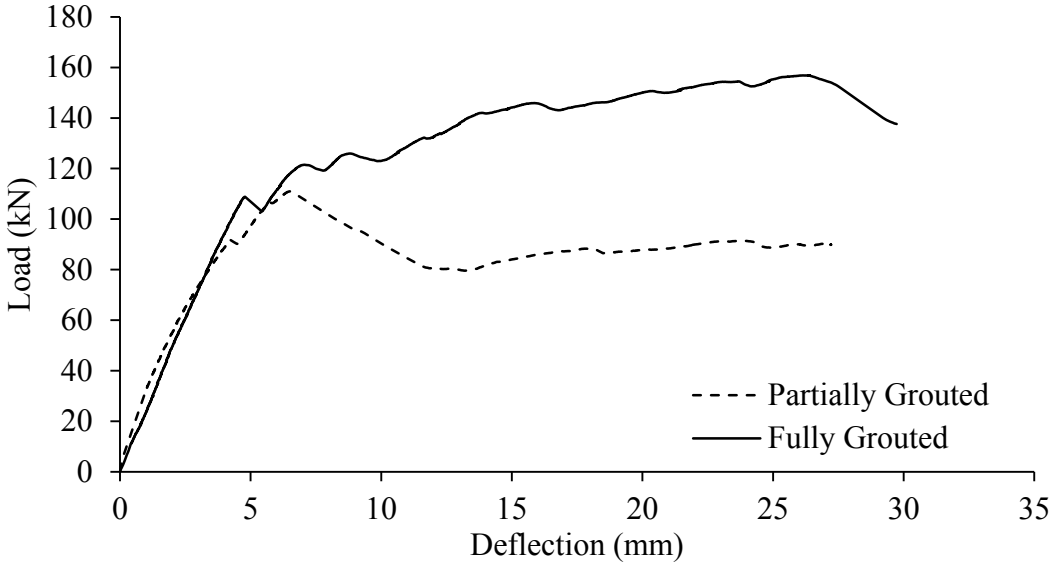

Figure 4.20 Load-deflection curves on the effect of grouting (1.0 aspect ratio)

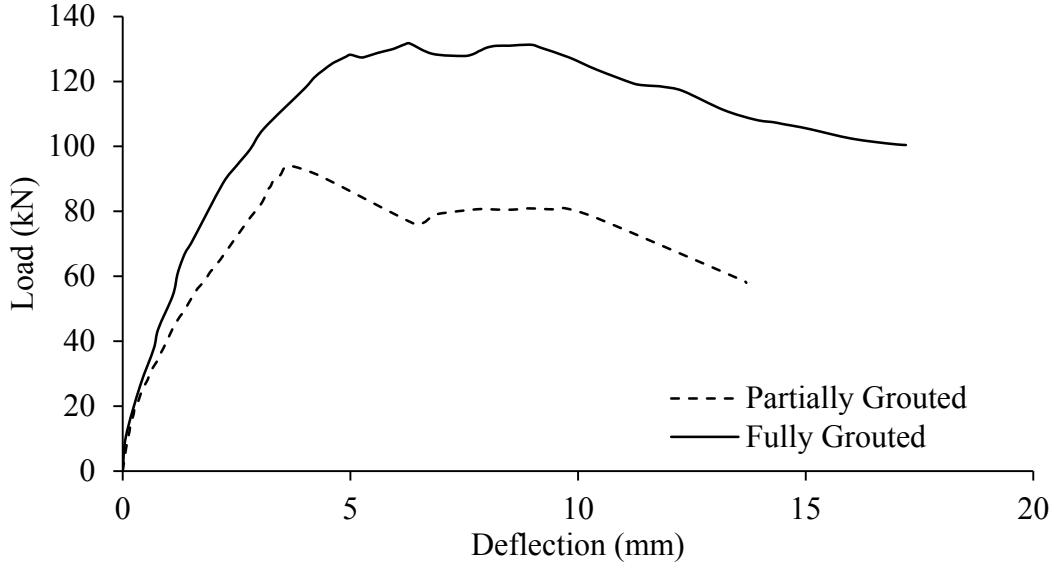

Figure 4.21 Load-deflection curves on the effect of grouting (1.3 aspect ratio)

Table 4.13 Test results with respect to grouting of the specimens

ID	Specimen	Grouting	Strength (kN)		Stiffness (kN/mm)			Failure Mode
			P_{ult}	P_{cra}	K_{ini}	K_{cra}	K_{ult}	
2	P1NA	Partial	111.0	91.9	48.6	21.7	17.1	CC
3	F1NA	Full	156.9	108.8	24.5	22.7	6.0	CC
4	P3NA	Partial	93.8	93.8	58.3	24.9	24.9	CC
8	F3NA	Full	131.7	128.2	71.7	25.6	20.9	CC

Table 4.13 shows that for specimens with aspect ratios of 1.0 and 1.3, as the grouting varied from partially grouted to fully grouted, the respective increases in the first crack load were 15.4% and 26.8% whereas the increases in the ultimate load were 29.3% and 28.8%, respectively. It was noted that there was a significant scatter in terms of the initial stiffness for all specimens. This was attributed to the "slack" in the test set-up and specimen system at the initial loading stage. On the other hand, the secant stiffness at the first crack appeared to be consistent and may be used as a more reliable indicator of system stiffness. For the specimens with a given aspect ratio, the first crack secant stiffness had no appreciable difference. However, the fully grouted specimens showed on average higher secant stiffness at first crack in an order of 3.6%. In the case of secant stiffness at ultimate, the fully grouted specimens showed lower values than the partially grouted ones. This can be clearly seen in Figure 4.20 where the ultimate load for the fully grouted specimen reached with a much higher deflection than the partially grouted specimen. This behavior showed that after the initial crack, fully grouted specimens fail with a much larger strain value than the partially grouted specimen. This showed that for all different types of walls tested in this experimental program, fully grouted specimens attained a greater ductility.

In Figures 4.20 and 4.21, the rising branch of the load-deflection curves shows a slightly "zig-zag" pattern where a drop of the load is accompanied by a load increase immediately thereafter and this pattern may be repeated before the reach of the ultimate load. This behavior is an indication of the initiation and the development of cracking in the infill. The first drop of the load often corresponded to the first visible crack observed in the testing. The following immediate increase in the load shows the ability of the infill to

realign itself and establish an alternate failure path to maintain some level of resistance even after the cracking and crushing. In this respect, the fully grouted specimen showed a better capability of maintaining the resistance without a significant loss of the capacity of the frame when compared with the partially grouted specimens. The failure modes of the 4 different specimens were shown in Figure 4.22, which include the corner crushing and the diagonal tension shear failure patterns.

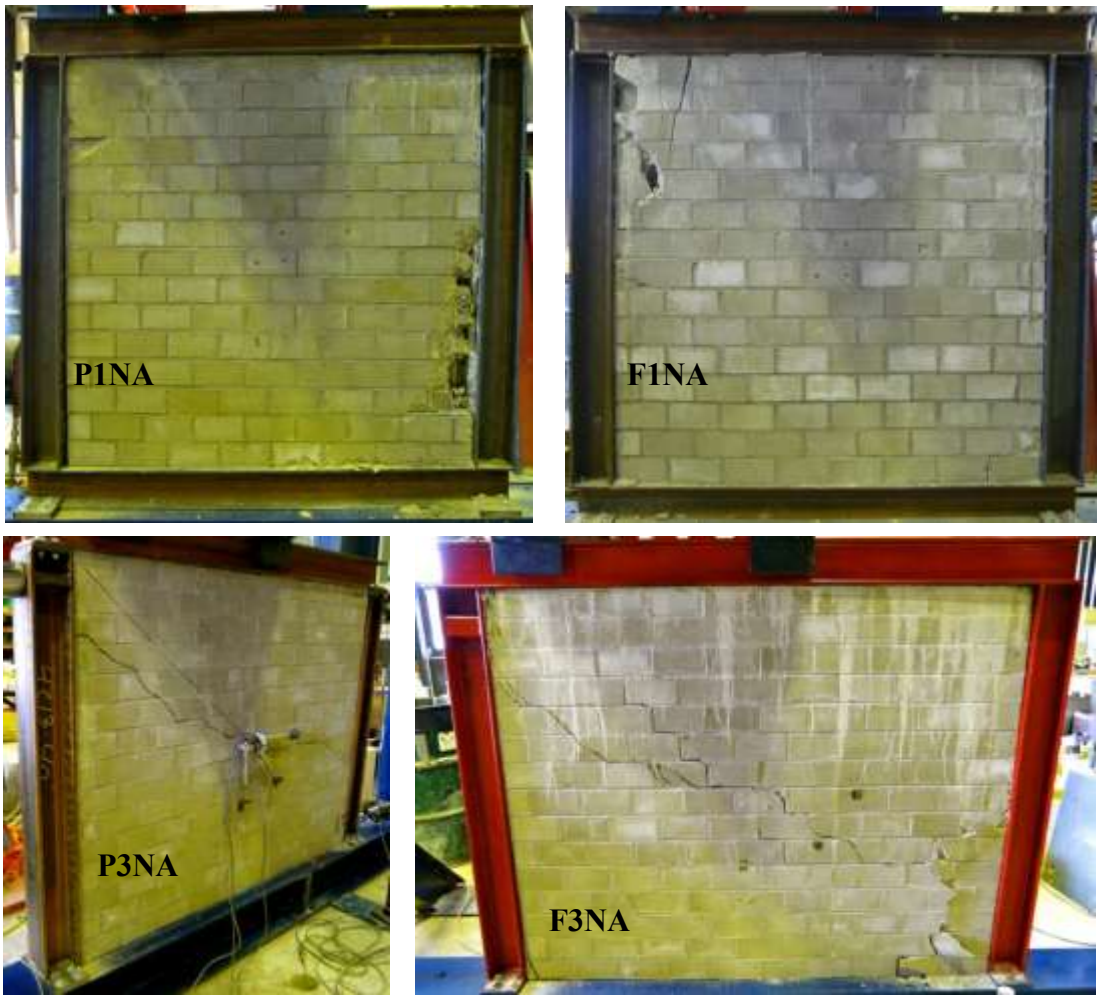

Figure 4.22 Failure modes of infill frame specimens of grouting situation

The specimens with 1.0 aspect ratio failed by corner crushing without the development of evident diagonal cracking compared with those with aspect ratio of 1.3. As noted before, none or very little gap was present between the frame and the infill for specimens with aspect ratio of 1.0. It is believed that the intimate contact of frame and infill enabled the corner crushing failure.

4.3.1.3 Openings

To assess the effect of openings on the behavior of infills, frames with and without openings were tested and compared. Figure 4.23 shows the load-deflection curves comparing specimens with no opening, window opening and door opening. The load response of the bare frame specimen was also included for comparison. Table 4.14 shows the portion of Table 4.11 with respect to this parameter. The area of the window opening for this experiment was about 11% of the infill surface area while the door opening accounted for 18% of the surface area. The failure patterns of the infills with openings are shown in Figure 4.24.

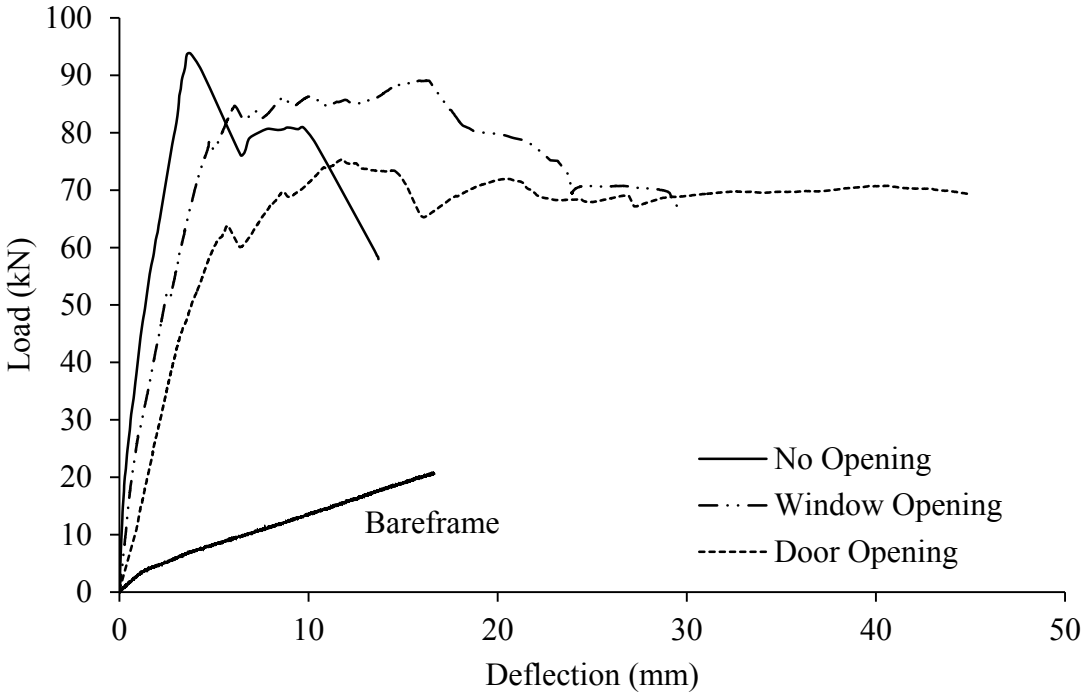

Figure 4.23 Load-deflection curves comparing walls with openings.

Table 4.14 Test results of specimens with openings.

ID	Specimen	Opening	Strength (kN)		Stiffness (kN/mm)			Failure Mode
			P_{ult}	P_{cra}	K_{ini}	K_{cra}	K_{ult}	
4	P3NA	None	93.8	93.8	58.3	24.9	24.9	CC
5	P3WA	Window	89.1	52.1	31.2	20.7	5.5	DT
6	P3DA	Door	75.3	63.8	13.7	11.2	6.5	DT

Figure 4.24 Failure of infilled frames with opening.

Of three specimens compared in this parameter, the infill without opening showed no cracking before failure and as shown in the load-deflection diagram, it showed a sudden drop in the load capacity occurred after the corner crushed. For the infill with a window opening, the failure started with multiple diagonal tension cracks on either side of the window and then extended to the corner next to the load-ward side of the window. The failure for the infill with a door opening consisted of very sudden vertical and diagonal tension cracks on either side of the door. As shown in Table 4.14, when compared with the specimens with no opening, the decrease in ultimate strength as a result of window and door opening were 5.0% and 19.7% and the decrease in the first cracking load were 44.5% and 32.0%, respectively. This suggests that the opening has more effect on the crack load than the ultimate load and even after cracking, the infill may still have considerable resistance left in the system. As shown in Figure 4.23, the drop in load at the first crack point for the window opening was very small, which represents a relatively small crack and the infill quickly realigned itself and upheld the resistance of the specimen. From the results, it was clearly shown that as the size of the openings increases, the initial stiffness and first crack secant stiffness all decreased with the exception of the ultimate secant stiffness, which showed a very close result for both window and door opening.

4.3.1.4 Column Axis Orientation

The frame-to-infill stiffness ratio is studied by changing the column axis orientation. Figure 4.25 and Figure 4.26 shows the comparison between infilled frames with either major or minor column axis orientation for fully grouted and partially grouted infills. Table 4.15 shows the portion of Table 4.11 with respect to this parameter. In this experimental study, the moment of inertias of columns with respect to its major and minor axis were 4.77×10^6 mm^4 and 1.61×10^6 mm^4, respectively, which represented a major/minor axis moment of inertia ratio of 3.0.

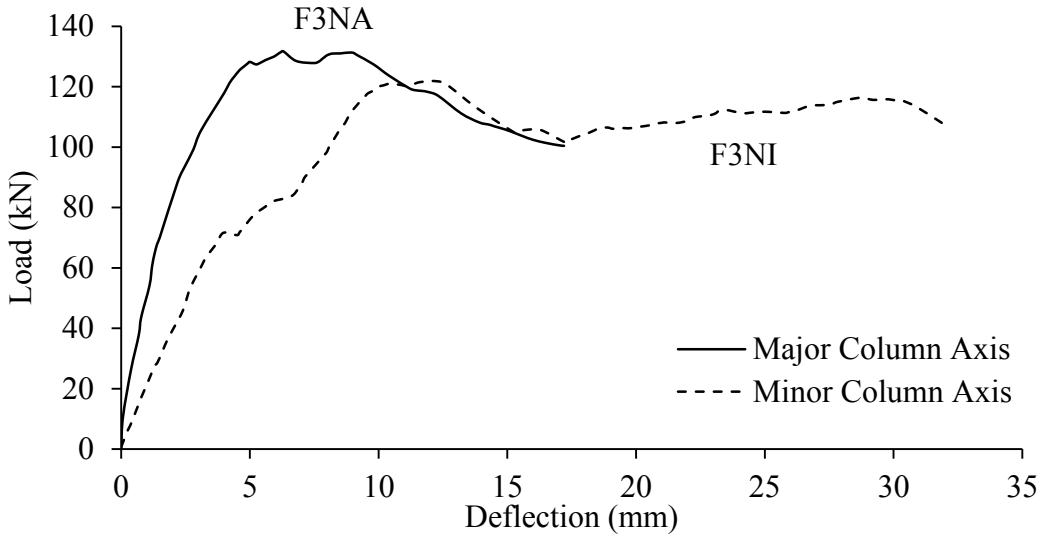

Figure 4.25 Effect of column axis orientation (fully grouted)

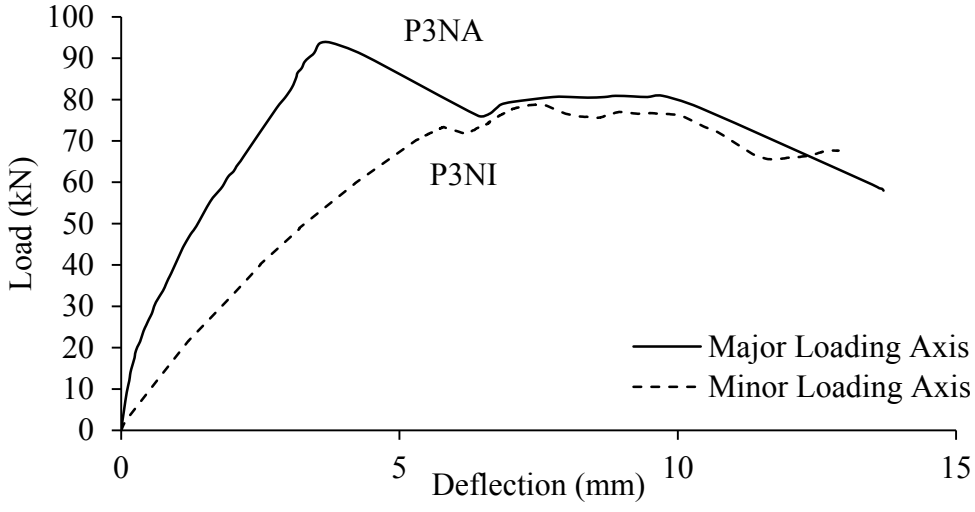

Figure 4.26 Effect of column axis orientation (partially grouted)

Table 4.15 Experimental results on the effect of different column axis orientation

ID	Specimen	Loaded Column Axis	Strength (kN)		Stiffness (kN/mm)			Failure Mode
			P_{ult}	P_{cra}	K_{ini}	K_{cra}	K_{ult}	
4	P3NA	Major	93.8	93.8	58.3	24.9	24.9	CC
7	P3NI	Minor	78.9	73.3	15.1	12.7	10.5	CC
8	F3NA	Major	131.7	128.2	71.7	25.6	20.9	CC
9	F3NI	Minor	121.9	71.7	21.8	17.5	10.2	CC

From Table 4.15, it can be seen that specimens with minor column axis orientation resulted in a reduction in strengths and stiffness on both the partially grouted and the fully grouted specimens when compared with those with major column axis orientation. The decreases in ultimate strength were 7.4% and 15.9% whereas the decreases in the load at first crack were 44.1% and 21.9% for the fully grouted and the partially grouted specimens, respectively. As the frame-to-infill stiffness decreases, stiffnesses including the initial stiffness, cracking secant stiffness and the ultimate secant stiffness decreased 74.1%, 49.0% and 57.8%, respectively, for partially grouted specimens. For fully grouted specimen, the corresponding decreases of the initial stiffness, cracking secant stiffness and ultimate secant stiffness were 69.3%, 31.6%, 51.2% respectively. Figures 4.25 and 4.26 further show that the specimen with major axis column orientation exhibited higher stiffness for all three stiffnesses investigated and the onset of non-linearity was much earlier but the ultimate deflection was greater for specimen with minor column axis orientation. It suggests that a weaker frame reduced the ultimate strength with compensation on a greater ductility of the frame system. For the partially grouted infills, specimen with both major and minor column axis orientations showed corner crushing followed by diagonal cracks propagating to the middle of the infill. However, for the fully grouted infills, both specimens failed by corner crushing but the specimen loaded in major column axis showed diagonal cracks before failure, and the specimen loaded in minor column axis failed by corner crushing mode, as shown in Figure 4.27.

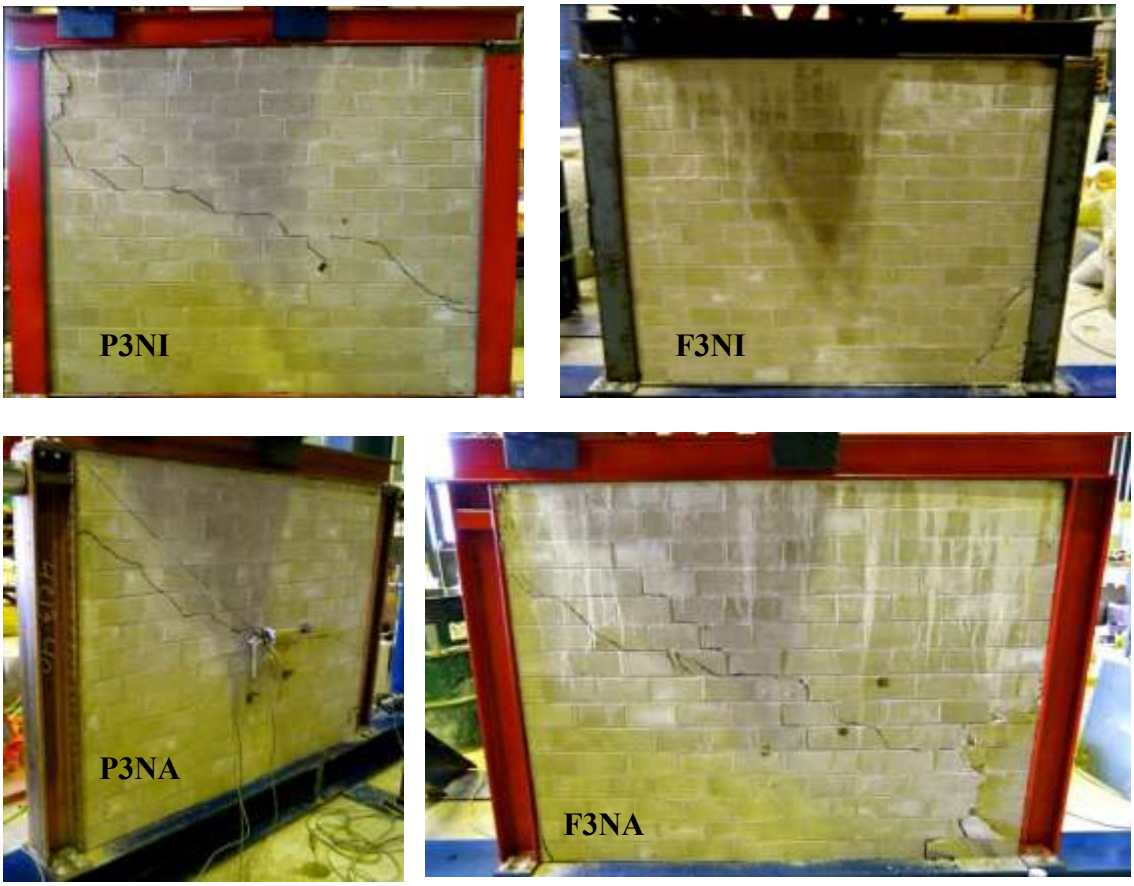

Figure 4.27 Infill frame failure (column axis orientation).

4.3.2 Load versus Strain Curves

Three LVDTs were used to measure the in-plane strain in the central region of the infill. Figure 4.28 shows the load versus strain curves for the horizontal, vertical, and diagonal strains for specimen F3NA. The trend of the load versus strain curves were plotted using a second order polynomial curve fitted along the median of the available data points. It was found that for these specimens, strain in all directions had the same behavior; but since positive strain values represent compression, the infill was in fact being compressed in the diagonal strut direction and expanding in the vertical and horizontal direction.

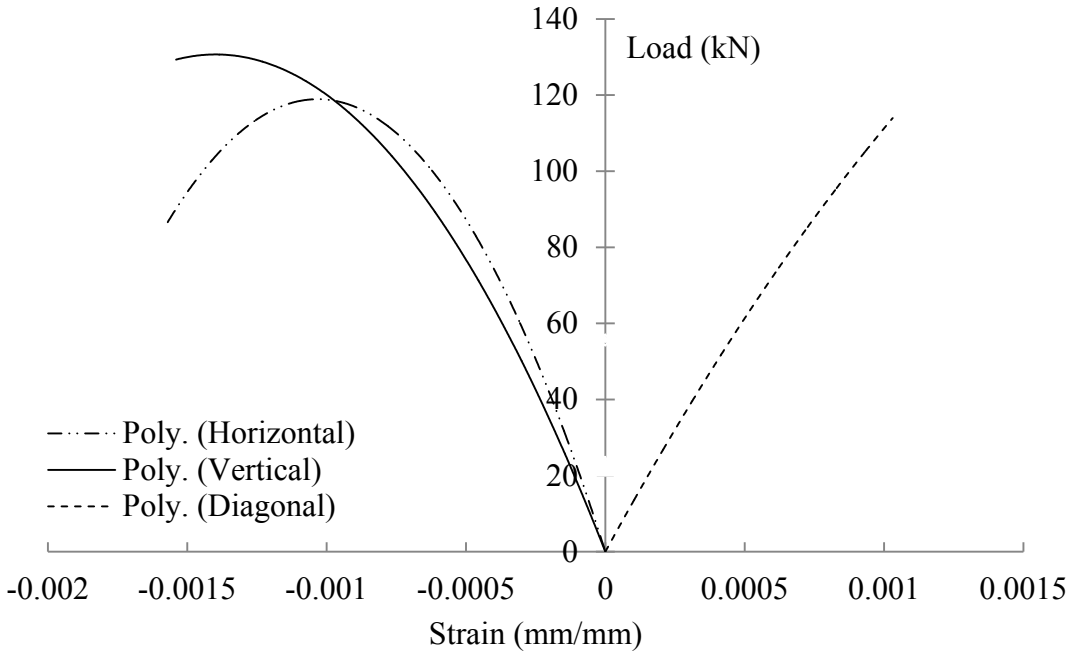

Figure 4.28 Load versus strain curves (F3NA)

Table 4.16 shows the recorded maximum in-plane strains for each specimen and the corresponding principal strains were calculated and listed. For specimen P3WA, the diagonal LVDT did not function properly, therefore, the full behavior of the diagonal strain was not captured and the principal strain was not calculated.

Table 4.16 Maximum in-plane and principal strain

ID	Spec.	P_{ult} (kN)	Maximum In-Plane Strain (mm/mm)			Principal Strain (mm/mm)		Angle (deg)
			Vertical	Horizontal	Diagonal	Major	Minor	
2	P1NA	111.0	0.0002	-0.0004	0.0005	0.0012	-0.0014	31.72
3	F1NA	156.9	-0.0026	0.0001	0.0002	0.0027	-0.0052	-23.52
4	P3NA	93.8	-0.0002	-0.0012	0.0006	0.0021	-0.0035	34.48
5	P3WA	89.1			N/A			
6	P3DA	75.3	0.0000	0.0000	0.0000	0.0000	0.0000	0.00
7	P3NI	78.9	0.0006	0.0001	0.0004	0.0001	0.0009	5.65
8	F3NA	131.7	-0.0005	-0.0015	0.0010	0.0031	-0.0051	37.98
9	F3NI	121.9	0.0000	-0.0005	0.0005	0.0013	-0.0018	35.78
10	P6NA	104.2	0.0001	0.0000	0.0002	0.0004	-0.0003	35.78

For the specimens with 1.0 aspect ratio, fully grouted specimen had a higher ultimate load as well as principle strains when compared to the partially grouted specimen. A similar trend was also present for specimens with a 1.3 aspect ratio. As the frame-to-infill stiffness value decreases, the ultimate strength decreased, as did the principal strains in both directions. Specimen P3DA showed no strains in any direction. Recalling that P3DA failed by diagonal cracking with no evident crushing and the cracking appeared outside region of the LVDTs, this may have attributed to little strain registered in LVDTs.

4.4 SUMMARY OF WALL TEST RESULTS

The results of nine infilled frame specimens were tested under four different parameters including the aspect ratios, grouting configuration, openings and column axis orientation. Two types of failure modes were observed in the specimens including corner crushing and diagonal tension cracking. Most specimens failed by corner crushing failure mode with some initial diagonal tension cracks. Results on grouting configuration showed that fully grouted infills provided higher ultimate strengths by about 28% when compared to partially grouted infills. A window opening, representing 11% of surface area, caused the ultimate strength to decrease by 5% and a door opening, representing 18% of surface area, caused the ultimate strength to decrease by 19.7%. It suggests that the reduction of surface area resulted in a decrease in ultimate strengths but the relationship is not linear. Changing of the column axis of the infilled frames caused both strength and stiffness to decrease but this decrease was more apparent in partially grouted specimens than fully grouted specimens.

CHAPTER 5 EVALUATION OF DESIGN METHODS

5.1 INTRODUCTION

In this chapter, the experimentally obtained strength and stiffness of the infill frame specimens are compared with the values obtained from the various analytical methods specified in the current design codes. Strength comparison included ultimate strength and the first crack strength whereas stiffness comparison considered the initial stiffness, secant stiffness at first crack load as well as secant stiffness at ultimate load. It is recognized that the parameters considered and number of repeated specimens tested in this research are limited. Test results obtained by other researchers in the available literature were also used to assess the efficacy of current design methods.

5.2 STIFFNESS COMPARISONS

The initial stiffness, K_{INI}, secant stiffness at first crack load, K_{CRA}, and secant stiffness at ultimate, K_{ULT} were obtained for all specimens. The definitions of these three stiffnesses were described in Chapter 4.

5.2.1 Comparison of Test Results with Design Methods

This section deals with the stiffness comparison of experimental results and values obtained from the current design standards. Three standards were considered including the current Canadian masonry design standard (CSA S304), the current American design code (TMS 402-08/ACI 530-08/ASCE 5-08) proposed by the Masonry Standards Joint Committee (MSJC 2011), and the Eurocode 8 (1996). All three design methods provided equations for calculating the width of the diagonal strut. A commercial software S-Frame® was used to perform the frame analysis for the infilled frame using the calculated strut width. The masonry infilled frame in the analysis is treated as a braced frame with the masonry infill replaced by equivalent diagonal strut acting in compression. The material and geometrical properties of test specimens as shown Table 5.1 were used in the analytical models. Since none of the design methods provide provisions on infills with openings, specimens P3DA and P3WA are omitted.

Table 5.1 Specimen material and geometrical properties

Spec.	h (mm)	ℓ (mm)	f'_m (MPa)			E_m (MPa)	I_b ($x10^6$ mm^4)	I_c ($x10^6$ mm^4)	t_e (mm)
			Orig.	CSA	ASTM				
P1NA	1080	1080	8.6	8.6	10.1	10496	4.77	4.77	43
F1NA	1080	1080	9.9	9.6	11.6	14430	4.77	4.77	64
P3NA	1080	1351	8.0	7.3	8.8	10496	4.77	4.77	43
P3NI	1080	1351	11.3	10.3	12.4	10496	4.77	1.61	43
F3NA	1080	1351	11.3	10.3	12.4	14430	4.77	4.77	64
F3NI	1080	1351	8.0	7.3	8.8	14430	4.77	1.61	64
P6NA	1080	1758	11.3	10.3	12.4	10496	4.77	4.77	43

It is noted that for partially grouted infills, the thickness, t_e, was taken as the average of full cross-section thickness and the faceshell thickness. However, CSA S304 suggests that partially grouted infills be treated as hollow infills whereas MSJC 2011 and Eurocode 8 (1996) are silent on the issue. The analytical stiffness was calculated as follows. In the S-Frame® linear analysis of the infill frame, a unit load (P) was placed at the roof level of the frame and the corresponding lateral displacement at the load point (Δ) was obtained. The stiffness of the infill was then calculated using equation [5-1].

$$K = \frac{P}{\Delta}\left[\frac{kN}{mm}\right] \qquad \textbf{[5-1]}$$

Table 5.2 shows the comparison of the experimental versus the calculated stiffness obtained from CSA S304, MSJC 2011 and Eurocode 8 (1996).

Table 5.2 Comparison of experimental and calculated stiffness

Specimen	Stiffness (kN/mm)					
	Test			Design		
	K_{INI}	K_{CRA}	K_{ULT}	K_{CSA}	K_{MSJC}	K_{EURO}
P1NA	48.6	21.7	17.1	54.7	26.2	38.2
F1NA	24.5	22.7	6.0	92.2	37.6	63.4
P3NA	58.3	24.9	24.9	65.9	25.8	44.5
P3NI	15.1	12.7	10.5	60.6	16.7	39.1
F3NA	71.7	25.6	20.9	115.2	38.4	76.8
F3NI	21.8	17.5	10.2	110.4	26.7	71.8
P6NA	14.4	9.3	9.3	77.7	24.4	51.2
Avg. K/K_{INI} (COV (%))				3.16 (58.4)	1.01(50.6)	2.09 (57.2)
Avg. K/K_{CRA} (COV (%))				4.74 (43.4)	1.55 (33.3)	3.15 (41.8)
Avg. K/K_{ULT} (COV (%))				7.38 (61.2)	2.50 (70.6)	4.93 (62.3)

It can be seen that on average, all three design methods provide design-to-test ratios higher than unity for all three stiffness, indicating the design stiffness is, in general, higher than the experimental results. Among the three methods, the design stiffness calculated using the equation provided by CSA S304 showed highest overestimation and values suggested by MSJC 2011 were in the best agreement with the test results. Values suggested by Eurocode 8 were somewhere in between. Taking the initial stiffness comparison for instance, the mean design-to-test ratios were obtained to be 3.16, 1.01 and 2.09 for CSA S304, MSJC 2011 and Eurocode 8, respectively. Although the mean of MSJC 2011 values was practically one, it is noted that the ratio showed a marked scatter with a COV of 50.6. In addition, several design values were less than experimental results, in some cases, to a large degree with the former being 44.3% to 53.9% of the latter. This high scatter of results is also evident for the other two methods. It is expected that the initial stiffness is sensitive and a little "slack" existent in the loading and set-up system would cause the results to fluctuate. On the other hand, when the K_{CRA} is considered, MSJC 2011 showed a mean design-to-test ratio of 1.55 with all ratios greater than one and a much improved COV of 33.3%. The improvement of COVs is also observed for other two methods. Note that the strut width equation in MSJC 2011

considers the damage sustained by the infill by incorporating a damage factor. It is therefore believed that K_{MSJC}/K_{CRA} is a more reliable indicator of the performance of infill stiffness equation for MSJC 2011. In the case of CSA S304 and Eurocode 8, no explicit information is available on the nature of the stiffness. But K/K_{CRA} ratios showed an improved COVs comparing with the other two design-to-test stiffness ratios. From this point on, the discussion on experimental results will be focused on the K_{CRA}.

The following discussion deals with the design stiffness as affected by those parameters investigated in this research. Figure 5.1 show that as the aspect ratio of the infill increases, the design stiffness by CSA S304 and Eurocode 8 (1996) also increases. However, the stiffness provided by MSJC 2011 showed an insignificant amount of change (differences of approximately 1%) between the specimens as the aspect ratio of the specimen increased. This insensitivity to the aspect ratio is resulted from the fact that the MSJC 2011 strut width equation does not have infill width as an explicit variable.

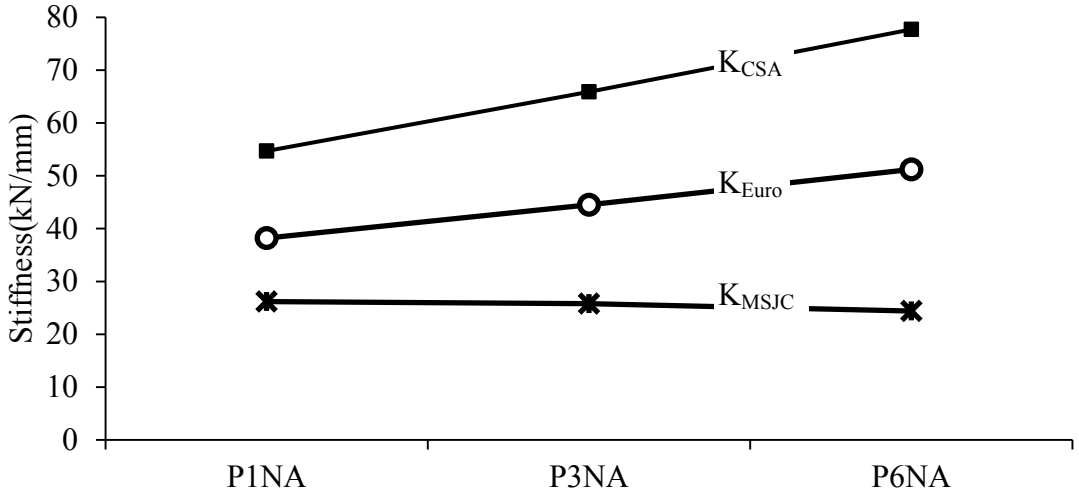

Figure 5.1 Aspect ratio effect on stiffness

The effect of grouting can be seen in Figure 5.2 for aspect ratios 1.0 and 1.3. As the specimens varied from partially grouted to fully grouted, the design stiffness increased for both aspect ratios. For instance, K_{CSA} increased 42.7% comparing specimen P3NA to F3NA whereas K_{MSJC} and K_{EURO} increased 32.8% and 42.1%. Experimental values of the K_{CRA} showed an increase as the infill changed from partially to fully grouted for both

aspect ratio. This suggests that partially grouting does contribute to the stiffness of the infill and by treating partially grouted infill as hollow; the design value gives a conservative estimate of the stiffness.

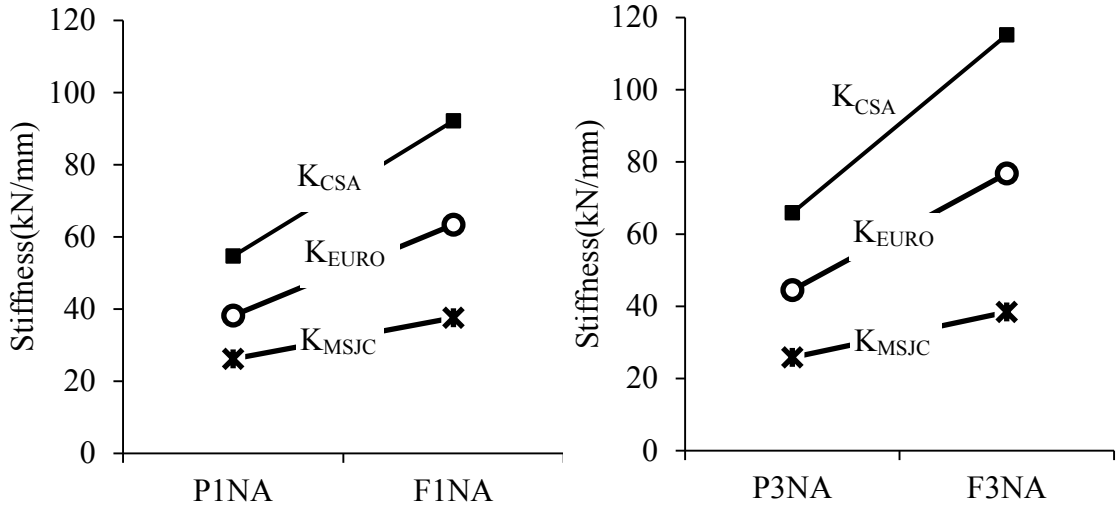

Figure 5.2 Grouting effect on stiffness

The effect of frame-to-infill stiffness ratio as reflected by changing the column orientation is illustrated in Figure 5.3. As the frame-to-infill stiffness decreased, i.e, the column rotates from major to minor axis orientation, both the design and experimental values of stiffnesses decreased. The degree of this reduction is comparable among all three design standards and they are in an agreement with the test results as well.

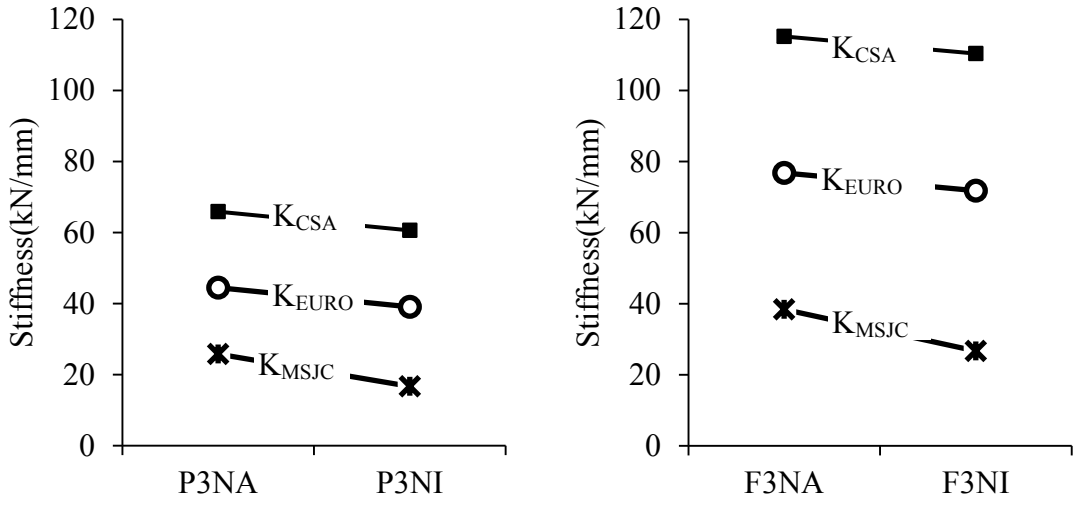

Figure 5.3 Column axis orientation effect on stiffness

5.2.2 Comparison of Test Results from Literature with Design Methods

In this section, stiffnesses obtained from the experiments performed by several researchers are compared with the design values using the equations of CSA S304.1-04 and MSJC 2011. The following sections provide a brief description of the various test set-ups and geometric and material characteristics of the infills in these experiments. The essential properties of the infill specimens are further summarized in Tables 5.3 and 5.4.

5.2.2.1 [MW] Mainstone, R.J. and Weeks, G.A. (1971)

The original full-scale tests performed by Mainstone and Weeks (1971) were made of concrete encased steel frames and solid brick infill. Infill specimens 1 to 4 listed in Table 5.5 had f'_m of 9MPa and an E_m of 6600MPa with height and length of 2770mm and 3360mm. All specimens had a nominal thickness of 110mm except for specimens 3 and 4 which had nominal thicknesses of 70mm and 340mm, respectively. The Modulus of Elasticity of the frame material was not reported in the article, therefore an E_f value of 30000MPa was assumed for the concrete frame.

5.2.2.2 [DS] Dawe, J.L. and Seah, C.K. (1989)

The standard specimen of WB3 provided by Dawe and Seah (1989) was to be compared. The standard specimen was a "panel with standard horizontal joint reinforcement, no openings, no gaps, or ties and is mortar-fitted snugly to the web of column but not mortared between column flanges". The frame of this standard specimen was made up of W200x46 for the columns and W250x58 for the beam. The infill for this specimen was made up of non-grouted 200mm concrete blocks 2800mm high and 3600mm long with a f'_m of 31.4MPa. The modulus of elasticity was not provided in the article and therefore the E_I was estimated to be 850 f'_m based on CSA S304.1-04 clause 6.5.2. This estimation was used for all the experimental calculations in which a modulus of elasticity of the infill was not provided.

5.2.2.3 [AN] Angel, R. (1994)

Specimen 4a in the experiment performed by Angel, R. (1994) consisted of a reinforced concrete frame with columns size of 254x305mm and beam size of 305x305mm. The moment of inertia provided in the article was $6.0x10^8mm^4$ for the columns and $7.21x10^8mm^4$ for the beam. The Modulus of Elasticity of the concrete was not reported in the literature, therefore an E_f value of 30000MPa was assumed in the calculation of this specimen. The infill was non-grouted concrete block infill with a reported compressive strength of 22.9MPa.

5.2.2.4 [MH] Mehrabi, A.B., Shing, P.B., Schuller, M.P., and Noland, J.L. (1996)

Three specimens were compared. These were reinforced concrete frame members with concrete masonry infill tested under monotonic in-plane loading. The properties of each specimen can be seen in Tables 5.3 and 5.4.

5.2.2.5 [AL] Al-Chaar, G., Issa, M. and Sweeney, S. (2002)

Specimen 2 and 3 from Al-chaar et. al. was concrete masonry and brick infill in reinforced concrete frames. The reinforced concrete frame was made up of 197x127mm sections for the columns and 203x127mm sections for the beam with concrete modulus of elasticity of 29992MPa. The height and length of the infill was 1327mm and 1769mm, respectively. The thickness of the infill for specimen 2 and 3 were 95mm and 58mm.

5.2.2.6 [EL] El-dakhakni, W. (2002)

Steel frame with standard hollow concrete masonry blocks were tested. The columns and beam of the frame was made up of W250x33 sections. The reported compressive strength of the hollow concrete masonry blocks was 13.4MPa. The height and length of the infill specimen was 2960mm and 3600mm with a thickness of 150mm.

Table 5.3 Frame properties of experimental set-ups

Author	ID	Material	E (MPa)	Beam		Column	
				Size (mm x mm)	I (x 10^7 mm^4)	Size (mm x mm)	I (x 10^7 mm^4)
MW (1971)	1	CS	30000**	305x203	108.8	305x305	65.2
MW (1971)	2	CS	30000**	305x203	108.8	305x305	65.2
MW (1971)	3	CS	30000**	305x203	108.8	305x305	65.2
MW (1971)	4	CS	30000**	305x203	108.8	305x305	65.2
DS (1989)	WB3	Steel	200000	W200x46	4.5	W250x58	8.4
AN (1994)	4a	RC	30000**	254 x 305	60.0	305 x 305	72.1
MH (1996)	SP 3	RC	21925	229 x 152	15.2	178 x 178	8.4
MH (1996)	SP 8	RC	17237	234 x 152	16.2	178 x 178	8.4
MH (1996)	SP 9	RC	17237	235 x 152	16.4	179 x 178	8.5
AL (2002)	2	RC	29992	197x128	8.1	203x128	8.9
AL (2002)	3	RC	29992	197x129	8.1	203x129	8.9
EL (2002)	SP2	Steel	200000	W250x33	4.9	W250x33	4.9

** - Assumed value due to incompletion of data provided in literature
CS – Concrete encased steel
RC – Reinforced concrete

Table 5.4 Infill properties of available literatures

Author	ID	Grout	Material	f'_m (MPa)	E_I (MPa)	h (mm)	l (mm)	t (mm)
MW (1971)	1	Solid	Bricks	9.0	6600	2770	3360	110
MW (1971)	2	Solid	Bricks	9.0	6600	2770	3360	110
MW (1971)	3	Solid	Bricks	9.0	6600	2770	3360	70
MW (1971)	4	Solid	Bricks	9.0	6600	2770	3360	340
DS (1989)	WB3	Hollow	CB	31.4	26690**	2800	3600	200
AN (1994)	4a	Hollow	CB	22.9	19465**	1626	2438	92
MH (1996)	SP 3	Solid	CMU	15.1	9522	1422	2032	100
MH (1996)	SP 8	Hollow	CMU	9.52	5102	1422	2032	100
MH (1996)	SP 9	Solid	CMU	14.2	8239	1422	2032	100
AL (2002)	2	Solid	CMU	18.2	15428**	1327	1769	95
AL (2002)	3	Solid	Bricks	26.7	22729**	1327	1769	58
EL (2002)	SP2	Hollow	CMU	13.4	11390**	2960	3600	150

** - Values not provided in literatures, an E_I value of $850f'_m$ was assumed
CMU – Concrete masonry unit
CB – Concrete blocks
DAB – Dense aggregate blocks
SCT – Structural clay tile

Table 5.5 summarizes the comparison of experimental and design stiffness of specimens from above mentioned experiments. Experimental stiffness listed in the table was obtained directly from the published work by those researchers. These stiffnesses were reported as either initial stiffness or secant stiffness at first crack load, which are indicated in the table below. Also those experiments where the modulus E_m was given are identified in the table.

Table 5.5 Average K/K_{EXP} values obtained from available literatures

Author	ID	Material	K_{EXP} (kN/mm)	CSA		MSJC	
				K_{CSA} (kN/mm)	K_{CSA}/K_{EXP}	K_{MSJC} (kN/mm)	K_{MSJC}/K_{EXP}
MW (1971)*	1	Brick	135.0 [IS]	116.0	0.86	79.3	0.59
MW (1971)*	2	Brick	75.0 [IS]	116.0	1.55	79.3	1.06
MW (1971)*	3	Brick	50.0 [IS]	81.3	1.63	61.8	1.24
MW (1971)*	4	Brick	315.0 [IS]	279.5	0.89	155.8	0.49
			Avg.		1.23		0.84
			COV (%)		33.6		42.6
DS (1989)	WB3	CMU	67.0 [IS]	171.2	2.56	53.3	0.80
AN (1994)	4a	DAB	152.4 [SS]	352.1	2.31	149.3	0.98
MH (1996)*	SP 3	CMU	129.6 [SS]	147.3	1.14	40.5	0.27
MH (1996)*	SP 8	CMU	57.8 [SS]	41.1	0.71	17.6	0.43
MH (1996)*	SP 9	CMU	103.4 [SS]	85.2	0.82	24.5	0.29
			Avg.		0.89		0.33
			COV (%)		24.8		25.8
AL (2002)	2	CMU	95.8 [SS]	205.8	2.15	64.3	0.67
AL (2002)	3	Brick	71.8 [SS]	190.1	2.65	60.8	0.85
EL (2002)	SP2	CMU	30.4 [SS]	102.2	3.36	30.6	1.01
			Overall Avg.		1.72		0.72
			COV (%)		50.9		43.6

* - E_I provided
[IS] – Initial stiffness
[SS] – Secant stiffness to first crack

The table shows that overall, the stiffness calculated with CSA S304 equations shows an average overestimation of 72% whereas stiffness calculated using MSJC 2011 equations showed an average underestimation of 28%. Due to the large scatter of results, the results were separated into two categories, which were specimens with steel frames and

specimens with concrete frames. The specimens with steel frames had an average K_{CSA}/ K_{EXP} value of 2.96 and an average K_{MSJC}/ K_{EXP} value of 0.91. However, the specimens with concrete frames had an average K_{CSA}/ K_{EXP} value of 1.47 and an average K_{MSJC}/ K_{EXP} value of 0.69, with COV values of 47.6% and 48.4%, respectively. The table shows that other than experimental specimens by Mehrabi et al. (1996), MSJC 2011 provided a better agreement with test results.

5.3 ULTIMATE STRENGTH COMPARISONS

In the calculation of design strength values, the experimentally determined compressive strength of masonry prisms was used and the resistance factors in equations were assumed to be unity to facilitate the comparison with the raw test data. As discussed in the previous chapter, three different f'_m were obtained, one of which was the original f'_m obtained through experiment and the other two were corrected using factors provided by CSA and ASTM standards according to the height-to-thickness ratio of the prisms. The design strengths based on all three f'_m values were calculated. One consideration given in the calculation of design strengths is described as follows. Since the infill frame members in the test were essentially rigidly connected and as such, the lateral load is shared between the frame and the infill with the latter taking a large portion. On the other hand, the strength calculated using the design methods is intended as the infill strength only and thus a coefficient needs to be applied to the design strength in order for it to be compared with the test ultimate load of the infilled frame. The coefficient was obtained as follows. The infill frame specimen was analyzed with a 1kN horizontal force applied at the roof level. The force resulted in the diagonal strut was then obtained. The value of the horizontal component of this diagonal force is the share taken by the infill and therefore it is the coefficient. The coefficients obtained using two design methods are shown in Table 5.6 for test specimens. The design strengths presented in the following sections are those obtained using analytical equations divided by the coefficient as appropriate.

Table 5.6 Horizontal coefficient of specimens

	P1NA	F1NA	P3NA	P3NI	F3NA	F3NI	P6NA
CSA S304.1	0.8108	0.8917	0.8480	0.9240	0.9155	0.9578	0.8769
MSJC 2011	0.5939	0.7269	0.6021	0.7153	0.7345	0.8149	0.6023

5.3.1 Comparison of Test Results with Design Methods

CSA S304 provides ultimate load calculations according to different failure modes. These failure modes include diagonal tension shear (DT), diagonal strut compression (CC) and sliding shear (SS) as shown in equations [2-33], [2-34], and [2-35]. Similarly, MSJC 2011 proposed three empirical equations for calculating the ultimate strength as presented in equation [2-36]. The failure modes identified in the provision include corner crushing, in-plane lateral displacement and sliding shear. Since corner crushing was the predominant failure mode, the design values listed were determined using equations for strut compression for CSA S304 and corner crushing for MSJC 2011 although in a design process the lowest load of all three failure modes identified in the standards would govern the design. It was found by varying the properties of the specimens, sliding shear failure mode would only govern when the infill has a very low compressive strength, as present in a material such as structural clay tiles or hollow clay units. Table 5.7 shows the comparisons of the design ultimate strengths with the experimental results of each specimen. In the case of CSA S304, it can be seen that the mean calculated ultimate load was 48% of the ultimate load from the experimental results with an average COV of 22.4%. In the case of MSJC 2011, the mean design-to-test strength ratio was 1.03 for original f'_m and 0.92 for design f'_m. The corresponding COVs were around 18% which is considered reasonable for masonry. Clearly, the design strength calculated using MSJC 2011 is closer to the test results. However, it should be cautioned that in several cases, the design strength values were greater than the test results, especially when design f'_m was used.

Table 5.7 Comparison of ultimate strength

ID	Test	Calculated			
	P_{EXP} (kN)	$P_{ULT - CSA S304}$ (kN)		$P_{ULT - MSJC 2011}$ (kN)	
		($f'_{mORIG.}$)	(f'_{mCSA})	($f'_{mORIG.}$)	(f'_{mASTM})
P1NA	111.0	39.1	39.1	95.0	111.5
F1NA	156.9	57.9	56.4	132.9	155.7
P3NA	93.8	42.2	38.9	87.0	95.8
P3WA	89.1	-	-	-	-
P3DA	75.3	-	-	-	-
P3NI	78.9	48.7	45.0	103.6	113.7
F3NA	131.7	74.1	69.1	150.0	164.7
F3NI	121.9	54.1	50.0	95.7	105.3
P6NA	104.2	65.2	61.2	123.0	135.0
Avg. P_{ULT}/P_{EXP}		0.49	0.46	1.03	0.92
COV (%)		23.2	21.5	19.2	17.9

The design strength as affected by parameters investigated in this research is presented in the following. Figure 5.4 shows the design ultimate load values normalized by dividing f'_m for three aspect ratios. While the CSA S304 shows an increase in design strength with an increase in the infill aspect ratio, MSJC 2011 values of design strength showed a slight decrease with the increase of the aspect ratio. This is not surprising since the MSJC 2011 values are calculated based on the corner crushing failure mode, in which the only variable is the compressive strength of masonry. The slight difference on the values provided by MSJC 2011 was due to the difference in the horizontal coefficients used when modifying the ultimate strengths. Although test results are not conclusive in the exact relationship between the aspect ratio and the infill strength, they suggest that aspect ratio does have an effect on the infill strength even when the failure mode is corner crushing. The accuracy of the MSJC 2011 design strength equation needs to be verified more thoroughly with more test data.

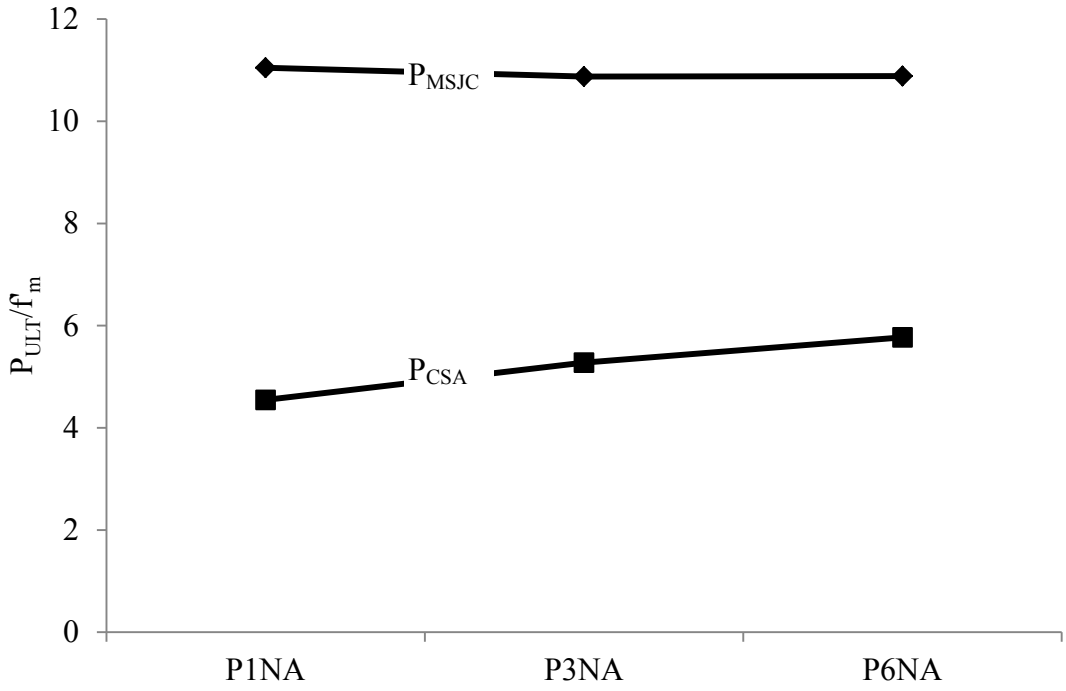

Figure 5.4 Aspect ratio effect on ultimate strength

Figure 5.5 shows the design P_{ult}/f'_m using the MSJC 2011 and CSA S304 equations for grouting effect. Both design methods show similar trend of design strength as affected by grouting. The fully grouted specimens of both aspect ratios had a higher experimental and calculated ultimate strength when compared to the partially grouted specimens.

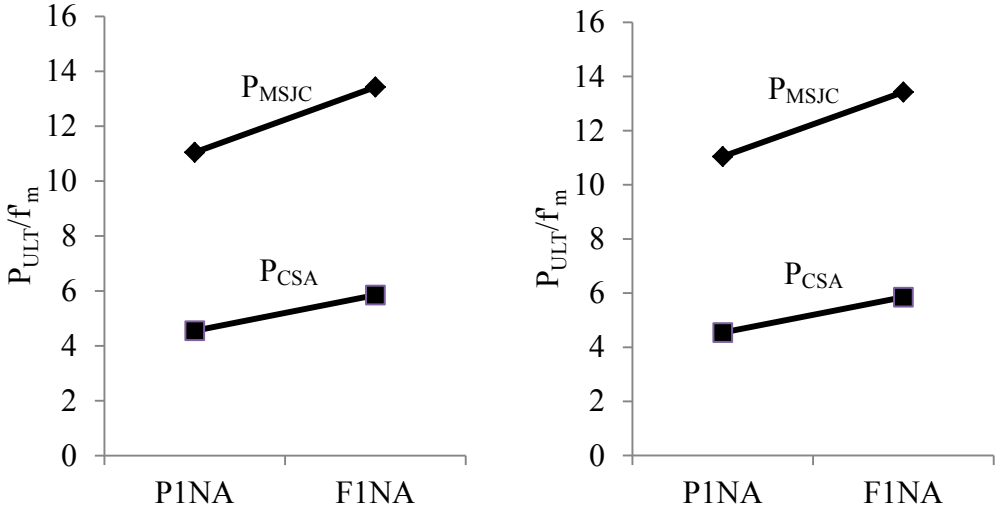

Figure 5.5 Grouting effect on ultimate strength

Figure 5.6 shows the effect of frame column orientation on the design strength for both partially and fully grouted specimens. The experimental ultimate strengths decreased as the columns were rotated from major loading axis to minor loading axis. However, the calculated ultimate strengths decreased as the moment of the inertia of the columns decreased. Figure 5.6 showed that P_{ULT}/f'_m increased slightly when the moment of inertia of the columns decreased due to the relatively large difference in compressive strength used during calculations, however, the ultimate strengths values decreases as the moment of inertia of the columns decreases.

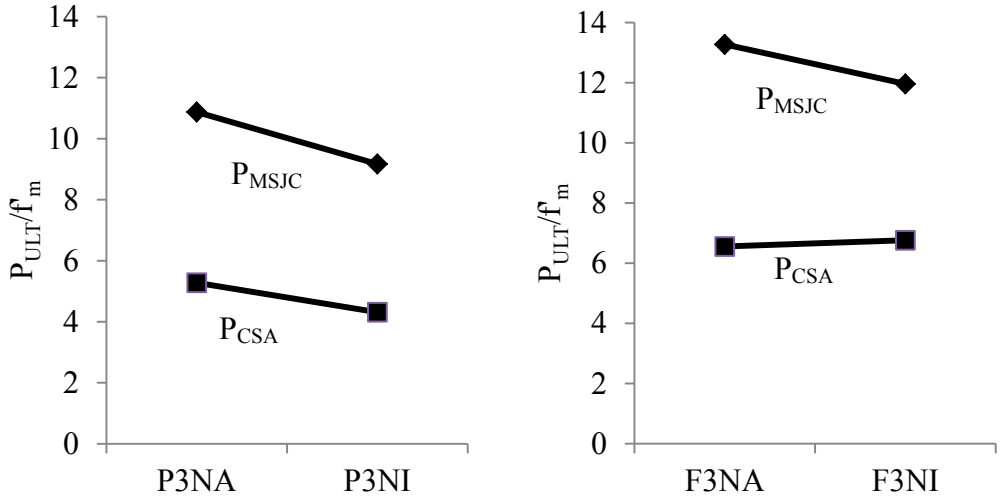

Figure 5.6 Column axis orientation effect on ultimate strength

5.3.2 Comparison of Test Results from Literature with Design Methods

As in the case of stiffness comparison, other experimental results available in the reported literature are also used to assess the strength equations in both the CSA S304 and MSJC 2011. The comparison results are as shown in Table 5.8. It can be seen from the table that the strength calculated by CSA S304 overestimates the ultimate strengths by 9% whereas strengths calculated by MSJC 2011 underestimates the strengths by 40%. Although the overall average design-to-test ratios for both methods are close to unity, both COVs are markedly high. The high COVs make any conclusions in terms of the efficacy of both design methods premature. It is believed that the random nature of masonry construction and some uncertainties associated with the test set-up and material properties have

resulted in the large scatter. Specimens by Mainstone and Weeks (1971) had the best correlation with the CSA S304.

Table 5.8 Ultimate strength comparison with results from available literature

Author	ID	Material	P_{EXP} (kN)	CSA		MSJC	
				P_{CSA} (kN)	P_{CSA}/P_{EXP}	P_{MSJC} (kN)	P_{MSJC}/P_{EXP}
MW (1971)*	1	Brick	339.5	410.0	1.21	150.9	0.44
MW (1971)*	2	Brick	370.4	410.0	1.11	150.9	0.41
MW (1971)*	3	Brick	239.2	236.1	0.99	96.0	0.40
MW (1971)*	4	Brick	1250	804.7	0.64	466.4	0.37
			Avg.		0.99		0.41
			COV (%)		24.9		7.2
DS (1989)	WB3	CMU	538.0	439.2	0.82	267.3	0.50
AN (1994)	4a	DAB	209.0	106.8	0.51	321.1	1.54
MH (1996)*	SP3	CMU	277.7	214.1	0.77	230.2	0.83
MH (1996)*	SP8	CMU	190.0	62.1	0.33	58.0	0.31
MH (1996)*	SP9	CMU	292.8	172.9	0.59	216.6	0.74
			Avg.		0.56		0.62
			COV (%)		39.7		44.9
AL (2002)	2	CMU	84.0	231.7	2.76	49.7	0.59
AL (2002)	3	Brick	89.0	179.9	2.02	30.4	0.34
EL (2002)	SP2	CMU	450.0	99.4	0.22	306.4	0.68
		Overall Avg.			0.997		0.60
		COV (%)			73.3		57.1

* - E_I provided

Similarly to the comparisons of stiffnesses, the specimens with steel frames had an average P_{CSA}/ P_{EXP} value of 0.52 and an average P_{MSJC}/ P_{EXP} value of 0.59. However, the specimens with concrete frames had an average P_{CSA}/ P_{EXP} value of 1.09 and an average P_{MSJC}/ P_{EXP} value of 0.60, with COV values of 69.2% and 62.5%, respectively.

5.4 FIRST CRACK STRENGTH COMPARISONS

As explained in the previous section, CSA S304 provided equation for calculating the diagonal tension shear strength as shown on equation [5-2].

$$P_{cr} = \phi_m (\upsilon_m b_w d_v + 0.25 P_d) \gamma_g \quad \textbf{[5-2]}$$

This calculated diagonal tension shear strength was used to compare with the first crack strength described in chapter 4 as shown in Table 5.9. Specimens P3NA and P6NA were omitted in this calculation as no significant diagonal cracking was observed prior to the corner crushing failure during the experiment and specimens P3WA and P3DA were also omitted since CSA S304 does not deal with infills with openings. It can be seen in the table that the average design-to-test first crack strength ratio was 0.52, suggesting the CSA S304 gives conservative estimate of the diagonal crack strength. This underestimate is in the same order as that in the ultimate strength.

Table 5.9 First crack strength comparison (CSA)

Specimens	P_{EXP} (kN)	P_{CSA} (kN) ($f'_{mORIGINAL}$)	P_{CSA}(kN) (f'_{mCSA})
P1NA	91.9	30.5	30.5
F1NA	108.8	48.7	48.0
P3NA	-	-	-
P3NI	73.3	43.7	41.8
F3NA	128.2	65.1	62.2
F3NI	71.7	54.8	52.3
P6NA	-	-	-
	P_{ULT}/P_{EXP}	0.53	0.51
	COV(%)	30.7	29.1

5.5 EFFECTIVE WIDTH SENSITIVITY STUDY

As discussed before, the stiffness calculated based on equations provided by CSA S304.1 overestimated the secant stiffness to first crack by 4.74 times. Through a sensitivity study of the effective diagonal width, which was taken as w/2 as explained in Section 2.3 of this document, a linear relationship was obtained between the effective diagonal width and the stiffness through elastic analysis. The linear relationship between the two shows that as the effective width increases, the stiffness of the infilled frame also increases. Therefore, a preliminary recommendation for an effective width of w/9 may lead to closer comparisons between the analytical and experimental stiffness values. By using the effective width as w/9, the stiffnesses for the various walls were obtained as shown in Table 5.10. Note that due to the properties and geometry of the experimental set-up, the stiffness of the various specimen from this experimental study were calculated with the effective width of $l_d/4$ as suppose to w/2 as CSA S304 specified a maximum l_d to w/2 ratio of 0.25.

Table 5.10 Stiffness comparisons with effective width of w/9

Specimen	K_{CSA}	K_{EXP}		
		K_{INI}	K_{CRA}	K_{ULT}
P1NA	17.3	48.6	21.7	17.1
F1NA	24.4	24.5	22.7	6.0
P3NA	19.2	58.3	24.9	24.9
P3NI	17.0	15.1	12.7	10.5
F3NA	28.1	71.7	25.6	20.9
F3NI	25.9	21.8	17.5	10.2
P6NA	20.5	14.4	9.3	9.3
Avg.	K_{CSA}/K_{EXP}	0.8	1.3	1.9
	COV (%)	55.3	39.5	58.3

Using the effective width of w/9 for the specimens however, causes the ratio of calculated to experimental ultimate strength to be 0.1, which could lead to an extremely uneconomical design. Therefore, a sensitivity study purely based on optimizing the stiffness cannot be performed. However, in order to optimize the effective width in relation to both stiffness and strength, it was found that by using an effective width of

w/3, a closer prediction for stiffness was achieved. The comparisons of calculated versus experimental strength did not however decrease as drastically as using the effective width as w/9 as shown in Table 5.11.

Table 5.11 Stiffness comparisons with effective width of w/3

Specimen	Stiffness		Strength	
	K_{CRA}	K_{CSA}	P_{ULT}	P_{CSA}
P1NA	21.7	51.8	111.0	30.1
F1NA	22.7	73.1	156.9	41.5
P3NA	24.9	57.6	93.8	30.8
P3NI	12.7	50.9	78.9	40.8
F3NA	25.6	84.3	131.7	51.4
F3NI	17.5	77.6	121.9	37.3
P6NA	9.3	61.6	104.2	46.8
Avg. K_{CSA}/K_{EXP}		3.75	Avg. P_{CSA}/P_{EXP}	0.36
COV (%)		39.5	COV (%)	26.4

As shown in Table 5.11, it was found that by using the effective width as w/3, the stiffness comparisons between the calculated and experimental value was 3.75 as compared with 4.74 when the effective width of w/2 was used. However, the ratio between calculated and experimental values of ultimate strength was 0.36 when an effective width of w/3 was used, as compared to 0.49 when the effective width of w/2 was used. To better compare the strength and stiffness values, another iteration of effective width was used. The stiffness and strength was calculated using an effective width of w/6 and the results are as shown in Table 5.12.

Table 5.12 Stiffness comparisons with effective width of w/6

Specimen	Stiffness		Strength	
	K_{CRA}	K_{CSA}	P_{ULT}	P_{CSA}
P1NA	21.7	25.9	111.0	15.5
F1NA	22.7	36.5	156.9	21.7
P3NA	24.9	28.8	93.8	16.0
P3NI	12.7	25.5	78.9	20.1
F3NA	25.6	42.1	131.7	27.8
F3NI	17.5	38.8	121.9	19.5
P6NA	9.3	30.8	104.2	25.9
Avg. K_{CSA}/K_{EXP}		1.88	Avg. P_{CSA}/P_{EXP}	0.19
COV (%)		39.5	COV (%)	26.1

It was found that by using the effective width as w/6, the stiffness comparisons between the calculated and experimental value was 1.88 as compared with 4.74 when the effective width of w/2 was used as shown in Table 5.12. However, the ratio between calculated and experimental values of ultimate strength was 0.19 when an effective width of w/6 was used, as compared to 0.49 when the effective width of w/2 was used.

Using the effective width of w/6, stiffness and strengths were also calculated and compared for specimens by other researchers as shown in Table 5.13 and 5.14.

Table 5.13 Stiffness comparisons with effective width of w/6 with results from available literature.

Author	ID	Material	K_{EXP}	CSA	
				K_{CSA}	K_{CSA}/K_{EXP}
MW (1971)*	1	Brick	135.0	53.6	0.40
MW (1971)*	2	Brick	75.0	53.6	0.71
MW (1971)*	3	Brick	50.0	42.0	0.84
MW (1971)*	4	Brick	315.0	97.4	0.31
			Avg.		0.56
			C.O.V. (%)		44.8
DS (1989)	WB3	CMU	67.0	48.0	0.72
AN (1994)	4a	DAB	152.4	184.7	1.21
MH (1996)*	SP 3	CMU	129.6	55.8	0.43
MH (1996)*	SP 8	CMU	57.8	21.8	0.38
MH (1996)*	SP 9	CMU	103.4	31.1	0.30
			Avg.		0.37
			C.O.V. (%)		17.6
AL (2002)	2	CMU	95.8	71.8	0.75
AL (2002)	3	Brick	71.8	68.1	0.95
EL (2002)	SP2	CMU	30.4	43.3	1.43
			Avg. K_{CSA}/K_{EXP}		0.70
			COV (%)		51.8

It can be seen from Table 5.13 that the overall average ratio of calculated versus experimental stiffness was 0.70 with the effective width of w/6 as compared to 1.72 with

an effective width of w/2, which represented a safer prediction of the experimental values through the results of available literature.

Table 5.14 Strength comparisons with effective width of w/6 with results from available literature.

Author	ID	Material	P_{EXP} (kN)	CSA	
				P_{CSA} (kN)	P_{CSA}/P_{EXP}
MW (1971)*	1	Brick	339.5	214.8	0.63
MW (1971)*	2	Brick	370.4	214.8	0.58
MW (1971)*	3	Brick	239.2	125.3	0.52
MW (1971)*	4	Brick	1250	297.8	0.24
				Avg.	0.49
				C.O.V. (%)	35.6
DS (1989)	WB3	CMU	538	384	0.71
AN (1994)	4a	DAB	209	63.7	0.30
MH (1996)*	SP3	CMU	277.7	85.9	0.31
MH (1996)*	SP8	CMU	190	33.8	0.18
MH (1996)*	SP9	CMU	292.8	57.3	0.20
				Avg.	0.23
				C.O.V. (%)	31.3
AL (2002)	2	CMU	84	84.2	1.00
AL (2002)	3	Brick	89	63.1	0.71
EL (2002)	SP2	CMU	450	42.4	0.09
			Avg. P_{CSA}/P_{EXP}		0.46
			COV (%)		60.8

However, from Table 5.14, it can be seen that with an effective width of w/6, the calculated results using equations provided by CSA S304 underestimated the strength by an overall average of 54% as compared to overestimation of 9% when using an effective width of w/2.

5.6 SAMPLE CALCULATIONS

The following section presents a step-by-step calculation using specimen P1NA as an example for design stiffness and strength according to both CSA S304 and MSJC 2011 standards. Figure 5.7 shows the actual specimen P1NA and the equivalent diagonal strut model. The properties of the frame and infill are also shown below.

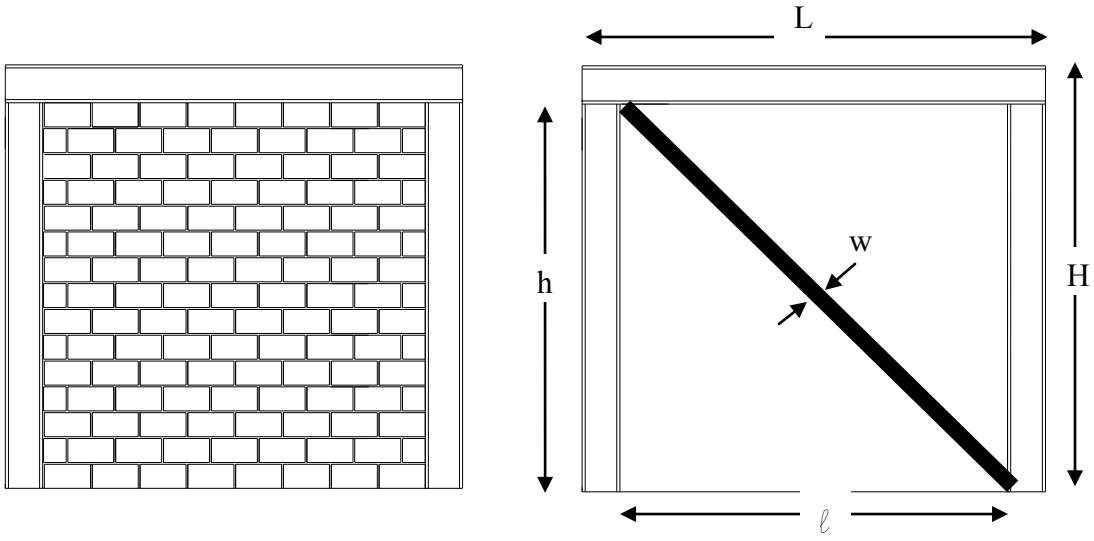

(a) **(b)**

Figure 0.1 (a) Specimen P1NA (b) Idealized diagonal strut model

Frame Properties	Infill Properties	
E_b and E_c = 200000MPa	f'_m = 8.6MPa	h = 1080mm
I_b and I_c = 4.77x10^{7}mm^4	E_I = 10496MPa	ℓ = 1080mm
H = 1186mm	t = 64mm	
L = 1186mm	t_e = 43mm	

5.6.1 CSA S304.1-04

5.6.1.1 Stiffness Calculations

CSA S304 specifies an "effective width" that were used to obtain the stiffness as follows,

$$\frac{w}{2} = \frac{1}{2}\sqrt{\alpha_h^2 + \alpha_L^2}$$

$$= \frac{1}{2}\sqrt{(485.6)^2 + (971.1)^2} = 542.9\text{mm}$$

where,

$$\alpha_h = \frac{\pi}{2}\sqrt[4]{\frac{4E_f I_c h}{E_I t_e \sin 2\theta}}; \quad \alpha_L = \pi\sqrt[4]{\frac{4E_f I_b \ell}{E_I t_e \sin 2\theta}}$$

$$\alpha_h = \frac{\pi}{2}\sqrt[4]{\frac{4(200000)(4.77\text{x}10^6)(1080)}{(10496)(43)\sin 2(0.7854)}} = 485.6\text{mm}$$

$$\alpha_L = \pi\sqrt[4]{\frac{4(200000)(4.77\text{x}10^6)(1080)}{(10496)(43)\sin 2(0.7854)}} = 971.1\text{mm}$$

And where ,

$$\theta = \tan^{-1}\left(\frac{h}{\ell}\right) = \tan^{-1}\left(\frac{1080}{1080}\right) = 0.7854$$

$$\text{ratio} \quad \frac{w}{2}\Big/_{\ell_d} = 542.9/1527.4 = 0.355 > 0.25$$

CSA S304.1-04 cl. 7.13.3.3 states that the effective width shall not exceed 0.25 of the diagonal length, which resulted an effective strut width of

$$\frac{w}{2} = \frac{\ell_d}{4} = \frac{1527.4}{4} = 381.8\text{mm}$$

Using the calculated effective width of the strut, an SFrame® model was created with a 100kN load placed at the roof level of the frame. A linear static analysis was performed and the displacement at the top of the frame was obtained to be 1.828mm. The idealized SFrame® model and the resulting displacements at the top of the frame due to the 100kN monotonic load can be seen below in Figure 5.8.

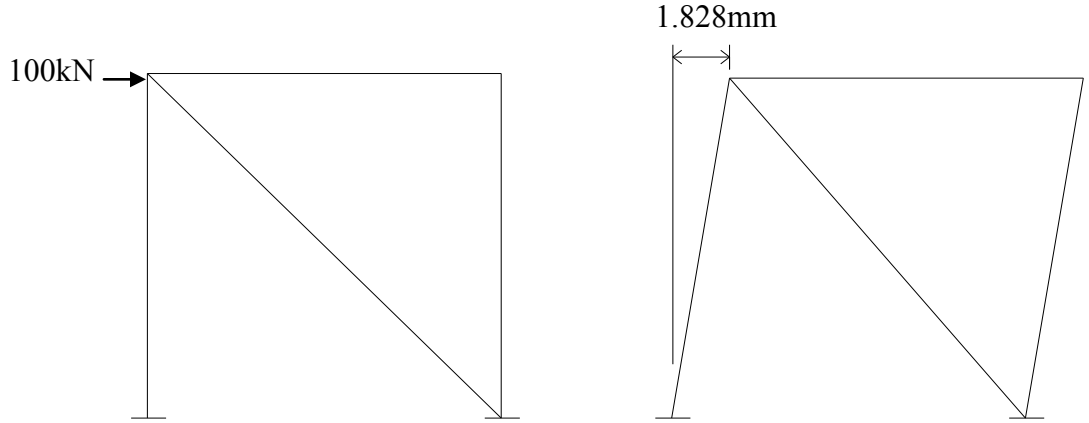

Figure 0.2 (a) SFrame® model; (b) Resulted diagonal strut frame displacement

Therefore, the stiffness, $K = \frac{P}{\Delta} = \frac{100kN}{1.828mm} = 54.7kN/mm$

5.6.1.2 Strength Calculations

CSA S304 provided equations for calculating the capacity of the infill based on the various failure modes. For the comparison with experimental ultimate load, the diagonal compression failure mode was used and for the comparisons with experimental first crack load, the diagonal tension failure mode equation was used. The equation for sliding shear failure mode was also shown but was not used as no sliding shear was evident in any of the specimens tested.

Diagonal Compression Failure Mode

Slenderness factor,

$$\frac{k\ell_d}{t} = \frac{0.9x[1527.4 - 0.25(1527.4)]}{64} = 16.1 < 30, ok$$

$$P_{r-Hollow} = \phi_m \chi (0.85f'_m) b(2t_f - r) = 1.0(0.5)(0.85x8.6)(381.84)[(2x11) - 3.86] = 25.3kN$$

$$P_{r-Full} = \phi_m \chi (0.85f'_m) b(t - 2e) = 1.0(0.5)(0.85x8.6)(381.84)[64 - 2(0.1x64)] = 71.5kN$$

Where,

χ = 0.5 (CSA S304.1 cl 10.2.6),

b = w/2 = 381.84mm,

t_f = 11mm (thickness of the flange) and,

e is taken as minimum eccentricity = 0.1t = 0.1(64) = 6.4mm,

As shown in Equation 7.27 from Drysdale and Hamid (2005), the equation for eccentricity for the case where the edge of the stress block is within the tension flange of hollow masonry is as shown.

$$e = \frac{r(t-r)}{2(2t_f - r)}$$

The value for r can be found by using the general solution for solving a quadratic equation, as described in Drysdale and Hamid (2005) section 7.4.4 .

Therefore, for this example with e taken as the minimum eccentricity,

$$r = \left(\frac{t}{2} + e\right) - \frac{1}{2}\sqrt{t^2 + 4t_e + 4e^2 - 16et_f}$$

$$= \left(\frac{64}{2} + 6.4\right) - \frac{1}{2}\sqrt{64^2 + 4(43) + 4(6.4)^2 - 16(6.4)(11)} = 3.86\text{mm}$$

The factored load, which equals to the resistance

$$P_{r-Partial} = \frac{P_{r-Holllow} + P_{r-Full}}{2} = 48.4\text{kN} = P_f$$

Taken slenderness into account,

$$P_{cr} = \frac{\pi^2 \phi_e (EI)_{eff}}{(kh)^2(1 + 0.5\beta_d)} = \frac{\pi^2 0.65(7304139)}{(0.9x1080)^2[1 + 0.5(0)]} = 185.1\text{kN}$$

where,

$\phi_e = 0.65$ for unreinforced masonry,

$\beta_d = 0$ for temporary loading,

$(EI)_{eff} = 0.4E_mI_o = 30.7x10^9 \text{Nmm}^2$

$$I_o = \frac{\left[\frac{1}{4}\sqrt{(1080)^2 + (1080)^2}\, t_f^3\right] - \left[4(t - 2t_f)(t - 2t_f)^3\right]}{12} = 7.3x10^6\,\text{mm}^4$$

And by using the moment magnifier method as outlined in CSA S304.1-04 cl. 7.7.6.3, the magnification eccentricity e′ is determined as follows. An iteration process is carried out between e and e′ until they converge.

For the first iteration of e',

$$e' = \frac{1}{1-\left(\frac{P_r}{P_{cr}}\right)} e = \frac{1}{1-\left(\frac{48.4}{185.1}\right)} e = 1.354e = 1.354(0.1x64) = 8.67mm$$

Once the first iteration e′ is obtained, it can replace the previous e to reiterate the results and the final P_r and P_{cr} results are 44.8kN and 185.1kN. Using these values,

$$Capacity, P_{ult} = \frac{1}{\ell_d} P_r = \frac{1080}{1527.4}(44.8) = 31.7kN$$

By having the frame with a diagonal strut undergo a linear static analysis, the member force for the strut can be found. For example, if specimen P1NA was modeled with a 1kN force placed at the top of the frame, the horizontal component of the member force obtained from the analysis was 0.8108kN. Therefore, to obtain the actual capacity of the frame, the original ultimate strength must be divided by this horizontal coefficient as follows.

$$P_{ult-mod.} = \frac{P_{ult-orig.}}{0.8108} = \frac{31.7kN}{0.8108} = 39.1kN$$

Diagonal Tension Failure Mode (First Crack Load)

$$P_{cra} = \phi_m(\upsilon_m b_w d_v + 0.25P_d)\gamma_g = 1.0(0.82x64x864 + 0.25x0)(0.672) = 30.5kN$$

where

$$\nu_m = 0.16\left(2 - \frac{M_f}{V_f d_v}\right)\sqrt{f'_m}$$

And since $M_f = 0$,

$\nu_m = 0.16(2)\sqrt{8.6MPa} = 0.82$

$b_w = t = 64mm$

$d_v = 0.8\ell = 0.8(1080mm) = 864mm$

$\gamma_g = t_e/t = 43mm/64mm = 0.672$

Sliding Shear Failure Mode

$$V_r = 0.16\phi_m\sqrt{f'_m}A_{uc} + \phi_m\mu P_l$$

Where $P_1 = V_r/2$ due to the vertical component of the diagonal compression force.

By rearranging the above equation yields,

$$V_r = \frac{0.16\varphi_m\sqrt{f'_m}A_{uc}}{1-\frac{\varphi_m\mu}{2}} = \frac{0.16(1.0)\sqrt{8.6}(0.8x1080x43)}{1-\frac{1.0x1.0}{2}} = 34.9kN$$

As described, since the failure mode of the experimental specimen was corner crushing, an ultimate strength of 39.1kN was used to compare with the experimental value of 111kN.

5.6.2 MSJC 2011

5.6.2.1 Stiffness Calculations

The width of the diagonal strut based on the MSJC 2011 code is determined as follows. The procedure of finding the stiffness using the width of the diagonal strut is as outlined in section 5.5.1.1.

$$w = \frac{0.3}{\lambda_{strut}\cos\theta} = \frac{0.3}{0.00323x\cos(0.7854)} = 131mm$$

where

$$\lambda_{strut} = \sqrt[4]{\frac{E_l t_e \sin 2\theta}{4E_c I_c h}} = \sqrt[4]{\frac{(10496)(43)\sin 2(0.7854)}{4(200000)(4.77x10^6)(1080)}} = 0.00323$$

By performing the linear static analysis as described above, the displacement obtained was 3.82mm, which resulted stiffness, K, of 26.2kN/mm.

5.6.2.2 Strength Calculations

The design forces in the equivalent strut can be determined as follows.

$$V_{inf} = \text{smallest of} \begin{cases} \text{(a)}(6.0\text{in})t_{netinf}f'_m \\ \text{(b) The calculated horizontal component of the force in the equivalent strut at a horizontal racking displacement of 1.0in (25mm)} \\ \text{(c)}V_n/1.5 \end{cases}$$

$$\text{(a) } P_{ult} = (6.0\text{in})t_{netinf}f'_m = 6\left(\frac{43\text{mm}}{25.4\text{mm/in}}\right)(1247\text{psi})\text{x}4.45 = 56.4\text{kN}$$

(b) With a horizontal force of 725kN, a horizontal displacement of 25mm was achieved using the same linear static analysis with SFrame® analysis software as described in the stiffness calculation section.

$$\text{(c) } P_{ult} = \frac{V_n}{1.5} = \frac{6373.6\text{lb}}{1.5} = 4247.7\text{lb} = 18.9\text{kN}$$

where

$$V_n = \min\begin{cases} 3.8A_{uc}\sqrt{f'_m} \\ 300A_{uc} \\ \text{or} \\ 56A_n + 0.45N_u \quad \text{if not full} \\ 90A_n + 0.45N_u \quad \text{if full} \end{cases} = \min\begin{cases} 3.8(57.6\text{in}^2)\sqrt{1247\text{psi}} = 7729\text{lb} \\ 300(57.6\text{in}^2) = 17280\text{lb} \\ 56(72.0\text{in}^2) + 0.45(3920\text{lb}) = 5794\text{lb} \end{cases}$$

and where,

$A_n = \ell t_e$ = (1080mm)(43mm) = 46440mm^2 = 72.0in^2

$A_{uc} = 0.8\ell t_e$=0.8 x 1080mm x 43mm = 37152mm^2 = 57.6in^2

$N_u = V_r/2$ = 34.9kN/2 = 17.5kN = 3920lb

Since the failure mode of this specimen was corner crushing, P_{ult} of 56.4kN was used to compare with the results of test specimen.

5.7 SUMMARY

From the comparison of the calculated and experimental results for various specimens, the following observations can be made.

- Among all three experimentally obtained stiffnesses, the secant stiffness at the crack load seemed to have the lowest COV and may be a more reliable indicator of the system stiffness.
- The comparison with test results obtained from this study showed that CSA S304, in general, overestimate the stiffness by 3 to 5 times and underestimate the strength by about 2 times. The resulting design would be conservative. On the other hand, the MSJC 2011 provides relatively better estimate for both stiffness and strength. However, in several cases, the MSJC 2011 design strength values were greater than the experimental results, indicating an overestimation of the design strength.
- Neither CSA S304 nor MSJC 2011 had provided equations for calculating strengths and stiffnesses with partially grouted infill panels. Treating partially grouted infills as hollow infills leads to underestimation of stiffness and strength.
- It can be seen from the previous chapter that even with an opening in the wall for the infill, it was still able to retain a large portion of the strength and stiffness. However, neither CSA S304 nor MSJC 2011 provided equations to calculate the strength and stiffness for infilled frames with openings.
- The comparison with test results obtained from other studies showed a much scattered results. It should be pointed out that the scatter might be a result of having key material property information missing from the reported literature.
- A sensitivity study was performed in relation to the effective width for the calculations of stiffness and strength using equations provided by CSA S304.1. It was found through the study that an effective width of w/6 rather than the specified w/2 better predicts the stiffness.

CHAPTER 6 SUMMARY AND CONCLUSIONS

6.1 SUMMARY

This study was undertaken to investigate the strength and behaviour of concrete masonry infilled frames with the focus on the masonry infills. The motivation of this research is to augment the limited experimental database on the subject, to provide insights in the behaviour of such infills under in-plane lateral loading, and to evaluate the efficacy of the design methods in current design standards for such infills.

The experimental program involved the testing of nine infilled frame specimens and one bare frame. Test specimens were subjected to one in-plane lateral load applied at the top beam level monotonically increased to failure. Four parameters including aspect ratio, grouting, opening and orientation of frame column were considered in the specimens. One-third scale of standard 200mm concrete masonry blocks were used in the construction of the infills. During testing the load and lateral deflections were measured and recorded. The behavior, ultimate load, and failure mode were presented and discussed.

The test results were then used to assess the efficacy of current methods for infill design including CSA S304 and MSJC 2011. Due to the recentness of the equations provided by MSJC 2011 for the design of masonry infills, the validity of those equations has not been thoroughly examined. One of the purposes of this study was to add to the very limited experimental results used to evaluate the equations provided. As well, experimental results of infilled frames obtained by other researchers were also used to aid in the assessment.

6.2 CONCLUSIONS

The following conclusions obtained from this research are separated into experimental results and analytical results as follows:

6.2.1 Experimental Results

1. The two most common failure modes on the specimens tested include corner crushing and diagonal tension failure mode. However, most specimens failed by corner crushing mode with some initial diagonal tension cracks.
2. Fully grouted specimens showed 28% higher ultimate strengths and higher secant stiffness when compared with partially grouted specimens.
3. Openings in infill cause the ultimate strength and stiffness to decrease, however, the decrease does not vary linearly with the size of the openings.
4. Decreasing the frame-to-infill stiffness causes both strength and stiffness to decrease.
5. When gaps are present between the infill and the bounding frame, the estimate of strength and stiffness will be compromised.

6.2.2 Analytical Results

1. Secant stiffness at first crack is more consistent stiffness with the lowest COV value when compared with the intial stiffness or secant stiffness at ultimate.
2. When compared to the experimental results of this study, design stiffness calculated using CSA S304 showed to be, on average, 4.74 times the experimental secant stiffness at first crack while calculated results provided by MSJC 2011 overestimates the secant stiffness at first crack by approximately 55%. On the other hand, CSA S304 underestimates the ultimate strength by approximately 2 times whereas MSJC 2011 overestimates the ultimate strength by approximately 3%.
3. When compared to the experimental results obtained by other researchers that provided a complete list of properties, a general trend remains the same where CSA S304 overestimates the stiffness and underestimates the ultimate strength whereas MSJC 2011 underestimates both the stiffness and strength. Although the average design-to-test ratios for both stiffness and strength were acceptable, large scatters of results are observed.

6.3 RECOMMENDATIONS FOR FURTHER RESEARCH

More experiments and research are required to have a thorough examination of the performance of both design methods in the standards. Parameters that were not listed in the scope of this study such as the variation of horizontal joint reinforcement, hollow infill specimens and the variation of materials for the infill and frame should be studied and compared with the results from this experimental study as well as experiments by other researchers to further validate the current design guidelines.

REFERENCES

ACI 318-95 Building Code Requirements for Structural Concrete. USA: Masonry Standards Joint Committee.

ACI 530-11/ASCE 5-11/TMS 402-11, (2011). Building Code Requirements for Masonry Structures. USA: Masonry Standards Joint Committee.

Al-Chaar, G. (2002). Evaluating strength and stiffness of unreinforced masonry infill structures. Journal of Structural Engineering, ASCE, **128**(8):1055-1063.

Al-Chaar,G., Issa, M., and Sweeney, S. (2002). Behavior of Masonry-Infilled Nonductile Reinforced Concrete Frames. Journal of Structural Engineering **128**(8):1055-1063.

ASTM C1314-07 (2007). "Standard Test Methods for Compressive Strength of Masonry Prisms," ASTM International, West Conshohocken, PA.

ASTM C140-07a (2007). "Standard Test Methods for Sampling and Testing Concrete Masonry Units and Related Units," ASTM International, West Conshohocken, PA.

ASTM E8-08 (2008). "Standard Test Methods for Tension testing of Metallic Materials," ASTM International, West Conshohocken, PA.

Angel, R. (1994). Behavior of Reinforced Concrete Frames with Masonry infill walls. Ph.D. Dissertation, The University of Illinois at Urbana-Champaign.

ANSI A41.4 (1953) American Standards Association Building Code Requirement for Masonry. American National Standards Institute, New York.

CAN/CSA A165 -04 (2009) - CSA Standards on Concrete Masonry Units. Mississauga, ON, Canada: Canadian Standard Association.

CAN/CSA A179-04 (2009) - Mortar and Grout for Unit Masonry. Mississauga, ON, Canada: Canadian Standard Association.

CAN/CSA S304.1-04 (2004) Design of masonry structures. Mississauga, ON, Canada: Canadian Standard Association.

Chiou, Y.J., Tzeng, J.C., and Liou, Y.W. (1999). Experimental and analytical study of masonry infilled frames. Journal of Structural Engineering, ASCE, **125**(10):1109-1117.

Dawe, J.L., and Seah, C.K. (1989). Behavior of masonry infilled steel frames. Canadian Journal of Civil Engineering, **16**(6):865-876.

Dawe, J.L., Liu, Y., and Seah, C.K. (2001). A parametric study of masonry infilled steel frames. Canadian Journal of Civil Engineering, **28**(1):149-157.

Dawe, J.L., Schriver, A.B., and Sofocleaus, C. (1989). Masonry infilled steel frames subjected to dynamic load. Canadian Journal of Civil Engineer, **16**(6):877-885.

Dawe, J.L., Seah, C.K., and Liu, Y. (2001). A computer model for predicting infilled frame behaviour. Canadian Journal of Civil Engineering, **28**(1):133-148.

Decanini, L. and Fantin, G. (1986). Modelos simplificados de la mamposteria incluida en porticos, caracteristicas de rigides y resistencia lateral en estado limite. (in Spanish), Jornadas Argentinas de Ingenieria Estuctural, Buenos Aires, Argentina (2):817-836.

Dhanasekar, M., and Page, A.W. (1986). The influence of brick masonry infill properties on the behavior of infilled frames. Proceedings of the Institution of Civil Engineers, Part 2, **81**(1):593-605.

Drysdale, R.G., and Hamid, A.A. (2005). Masonry structures: Behavior and design. Mississauga, Ontario: Canadian Masonry Design Centre.

Durrani, A.J., and Luo, Y.H. (1994). Seismic retrofit of flat-slab buildings with masonry infills. Proceedings of the 5th US national conference on earthquake engineering, **3**:627–36

El-Dakhakhni, W., Elgaaly, M., & Hamid, A.A. (2003). Three-strut model for concrete masonry-infilled steel frames. Journal of Structural Engineering, ASCE, **129**(2):177-185.

El-Dakhakni, W. (2002). Experimental and Analytical Seismic Evaluation of Concrete Masonry-Infill Steel Frames Retrofitted using GFRP Laminates. Ph.D. Dissertation, Drexel University, 1-165.

Eurocode 8 (1996) Design provisions for earthquake resistance of structures - Part 1-3: General rules - Specific rules for various materials and elements. Brussels: European Committee for Standardization

Federal Emergency Management Agency (FEMA) 273 NEHRP Guidelines for the Seismic Rehabilitation of buildings. Washington, D.C.: Building Seismic Safety Council (BSSC)

Federal Emergency Management Agency (FEMA) 306 Evaluation of earthquake damaged concrete and masonry wall buildings. Redwood, California: Applied Technology Council (ATC)

Flanagan, R. D., & Bennett, R. M. (1999). In-plane behavior of structural clay tile infilled frames. Journal of Structural Engineering, ASCE, **125**(6):590-599.

Flanagan, R. D., and Bennett, R. M. (2001). In-plane analysis of masonry infill materials. Practice Periodical on Structural Design and Construction, **6**(4):176-182.

Hendry, A. (1981). Structural Brickwork. Macmillan, London.

Holmes M. (1961). Steel frames with brickwork and concrete infilling. Proceedings of the Institution of Civil Engineers, **19**: 473-478.

Jamal, B.D., Bennett, R.M., Flanagan, R.D. (1992). Numerical Analysis for In-Plane Behavior of Infilled Frames. 6th Canadian Masonry Symposium, pp.1-12.

Kaltakci, M., Koken, A., and Korkmas, H.H. (2006). Analytical solutions using the equivalent strut tie method of infilled steel frames and experimental verification. Canadian Journal of Civil Engineering, **33**:632-638.

Liauw, T.C. and Kwan, K.H. (1983). Plastic theory of non-integral infilled frames. Proceedings of the Institute of Civil Engineers, **2**(75): 379-396.

Liauw, T.C. and Kwan, K.H. (1984). Plastic theory of infilled frames with finite interface shear strength. Proceedings of the Institute of Civil Engineers, **75**(4):707-723.

Mainstone, R. J. (1970). On the stiffness and strengths of infilled frames. Proceedings of the Institute of Civil Engineers, **Suppl.**(4):57–90.

Mainstone, R.J. and Weeks, G.A. (1971). The influence of a bounding frame on the racking stiffnesses and strengths of brick walls. Proceedings of the Second International Brick Masonry Conference, SIBMAC, pp. 165-171.

Maleki, M., Hamid, A.A., El-Damatty, A.A. and Drysdale, R.G. (2007) Behavior of partially grouted reinforced concrete masonry panels under in-plane diagonal loading. Proceedings of the 10th North American Masonry Conference. pp. 1039-1050.

Mehrabi, A. B., Shing, P. B., Schuller, M. P., and Noland, J. L. (1996). Experimental evaluation of masonry-infilled RC frames. Journal of Structural Engineering, ASCE, **122**(3):228-237.

Mehrabi, A.B., and Shing, P.B. (1997). Finite element modeling of masonry-infilled RC frames. Journal of Structural Engineering, ASCE, **123**(5):604-613.

Moghaddam, H. A. (2004). Lateral load behavior of masonry infilled steel frames with repair and retrofit. Journal of Structural Engineering, ASCE, **130**(1):56-63.

Moghaddam, H., & Dowling, P. (1988). Earthquake resistant design of brick infilled frames. Brick and Block Masonry(8th IBMAC) London, Elsevier Applied Science, **2**:774-784.

Mohebkhah, A., Tasnimi, A.A., and Moghaddam, H.A. (2008). Nonlinear analysisof masonry-infilled steel frames with opeinings using discrete element method. Journal of Constructional Steel Research, **64**(2008):1463-1472.

Mosalam, K. H., White, R. N., and Gergely, P. (1997). Static response of infilled frames using quasi-static experimentation. Journal of Structural Engineering, ASCE, **123**(11)1462-1469..

Papia, M., Cavaleri, L., and Fossetti, M. (2003). Infilled frames: Developments in the evaluation of the stiffening effect of infills. Structural Engineering and Mechanics, **16**(6):675-694.

Paulay, T., & Priestley, M. J. N. (1992). Seismic design of reinforced concrete and masonry buildings, Wiley New York.

Polyakov, S. V. (1956). Masonry in Framed Buildings (An investigation into the strength and stiffness of masonry infilling). Gosudarstvennoe izdatel'stvo Literatury po stroitel'stvu iarkhitekture, Moscow. (English translation by G. L. Cairns, National Lending Library for Science and Technology, Boston, Yorkshire, England, 1963).

Riddington, J. R. (1984). The influence of initial gaps on infilled frame behavior. Proceedings of the Institute of Civil Engineers, **77**(3):295-310.

Saneinejad, A., and Hobbs, B. (1995). Inelastic design of infilled frames. Journal of Structural Engineering, ASCE, **121**(4):634-650.

Shing, P.B. and Mehrabi, A.B. (2002). Behavior and analysis of masonry infilled frames. Proceedings of Structural Engineering Materials, **4**:320-331.

Smith, B. S. (1966). Behavior of square infilled frames. ASCE, Journal of the Structural Engineering, ASCE, **92**(1):381-403.

Smith, B.S., & Coull, A. (1991). Tall building structures: Analysis and design, Wiley-Interscience.

Stafford-Smith, B., & Carter, C. (1969). A method of analysis for infilled frames. Proceedings of the Institution of Civil Engineers, **44**(1):31-48.

Tucker, C. (2007). Predicting the in-plane capacity of masonry infilled frames. Ph.D. dissertation, Tennessee Technological University, United States.

Wood, R.H. (1978). Plasticity, composite action and collapse design of unreinforced shear wall panels in frames. Proceedings of the Institution of Civil Engineers, **65**(2):381-411.

APPENDIX A - STRESS-STRAIN CURVES FROM PRISM TESTS

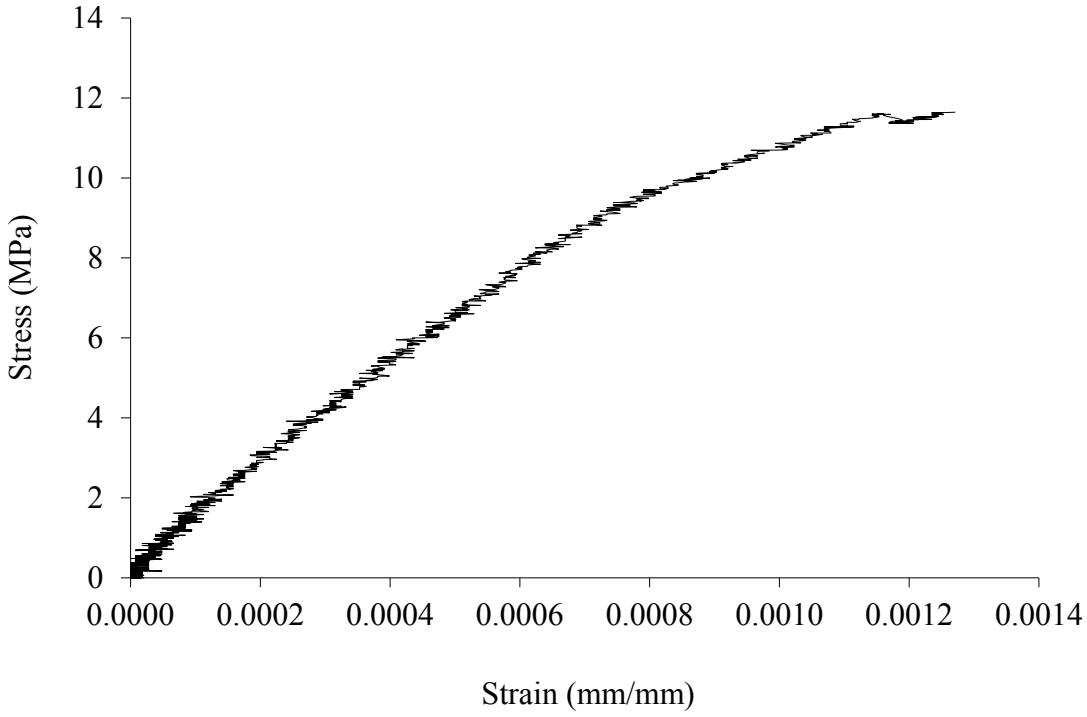

Figure A. 1 Stress-strain curve for prism V1

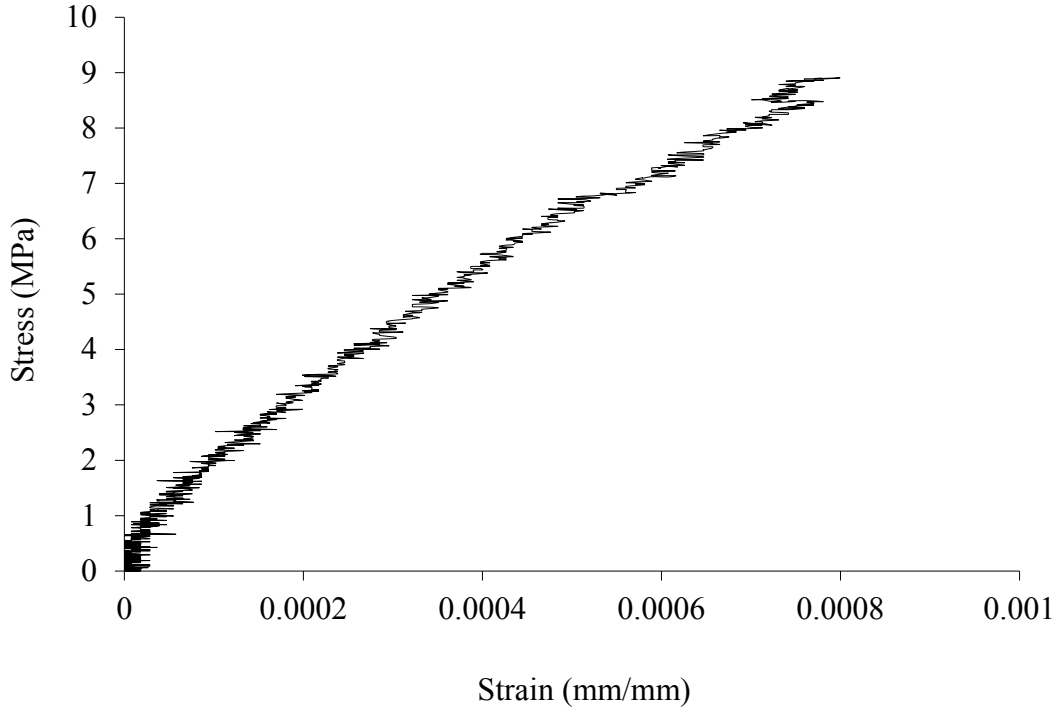

Figure A. 2 Stress-strain curve for prism V2

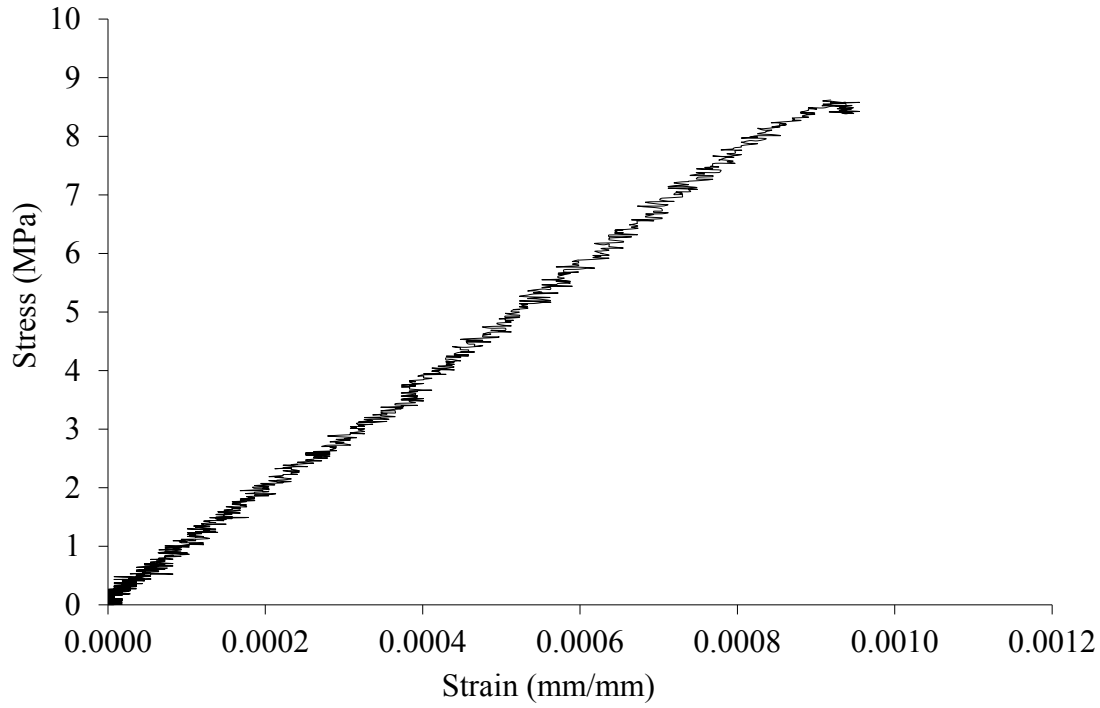

Figure A. 3 Stress-strain curve for prism V3

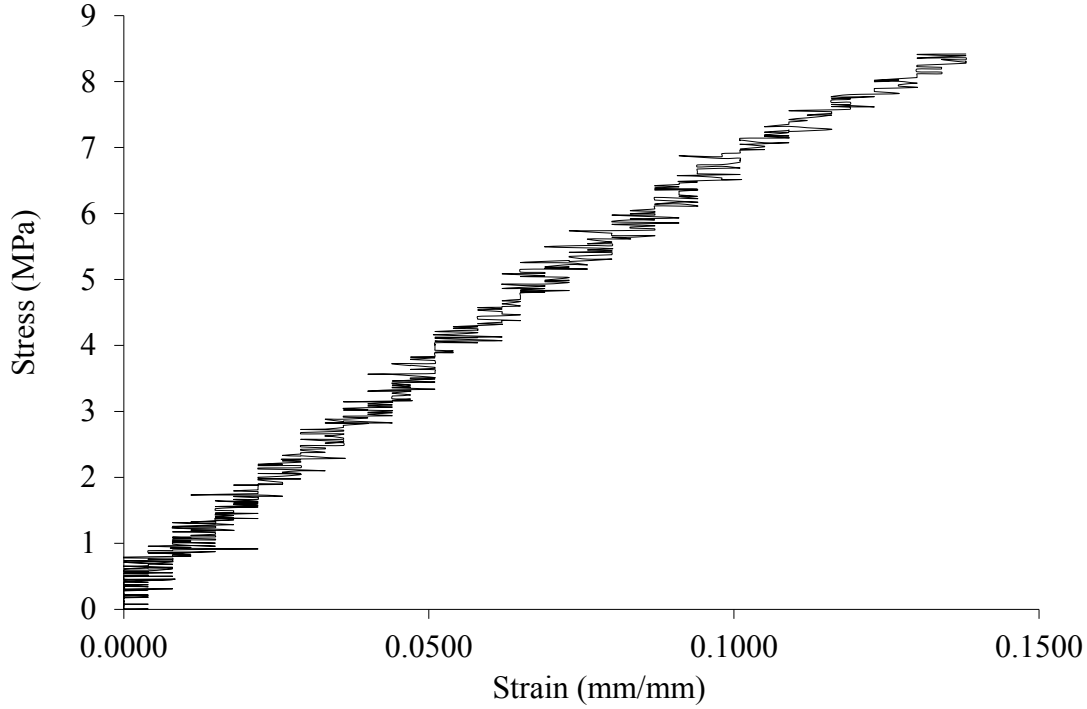

Figure A. 4 Stress-strain curve for prism V4

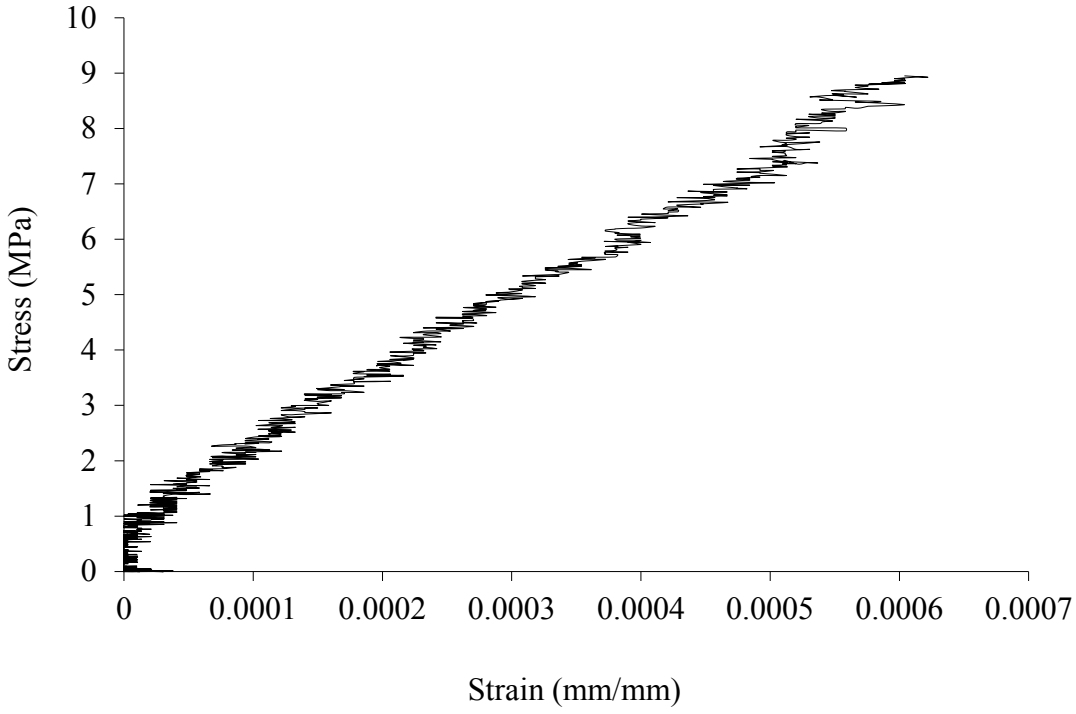

Figure A. 5 Stress-strain curve for prism V5

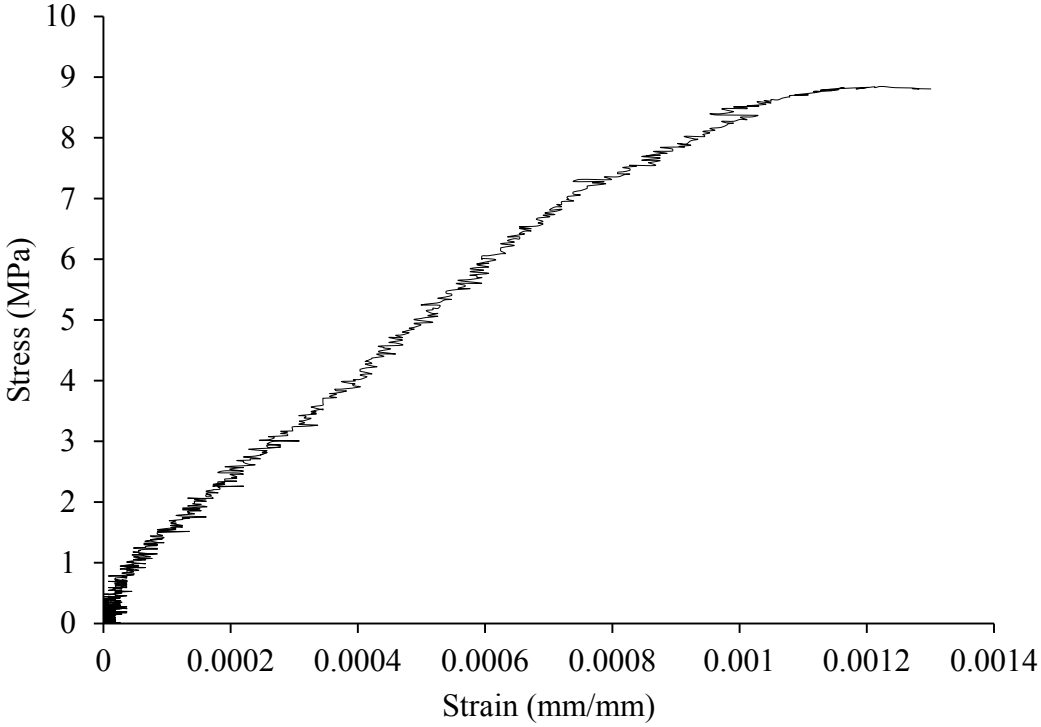

Figure A. 6 Stress-strain curve for prism V6

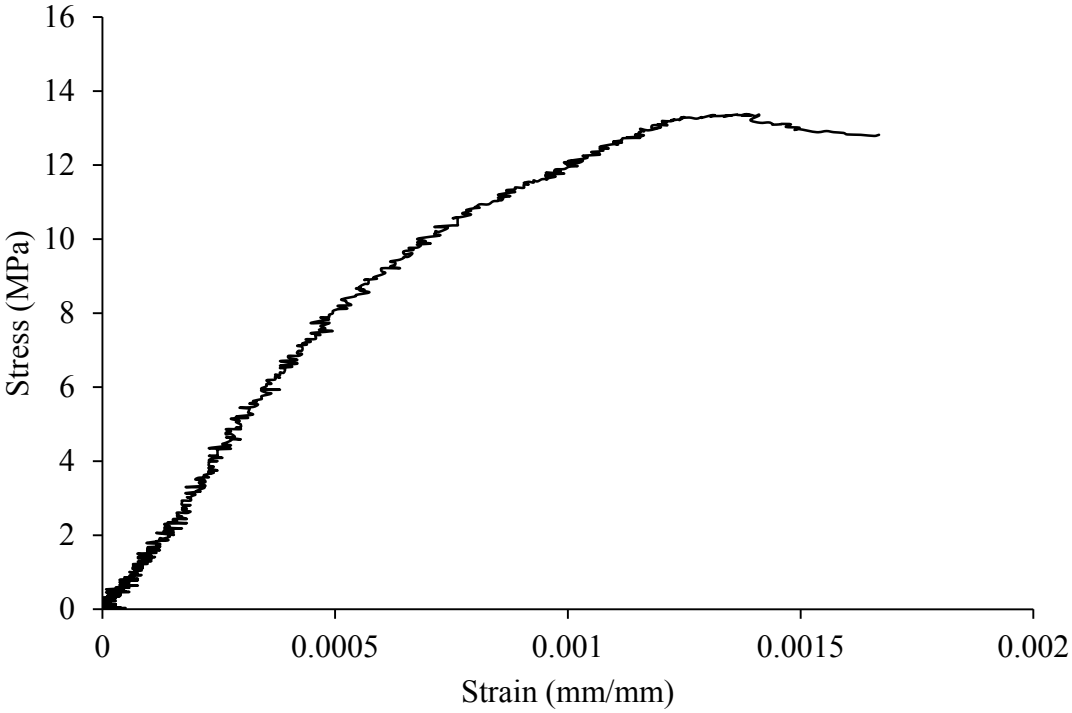

Figure A. 7 Stress-strain curve for prism V8

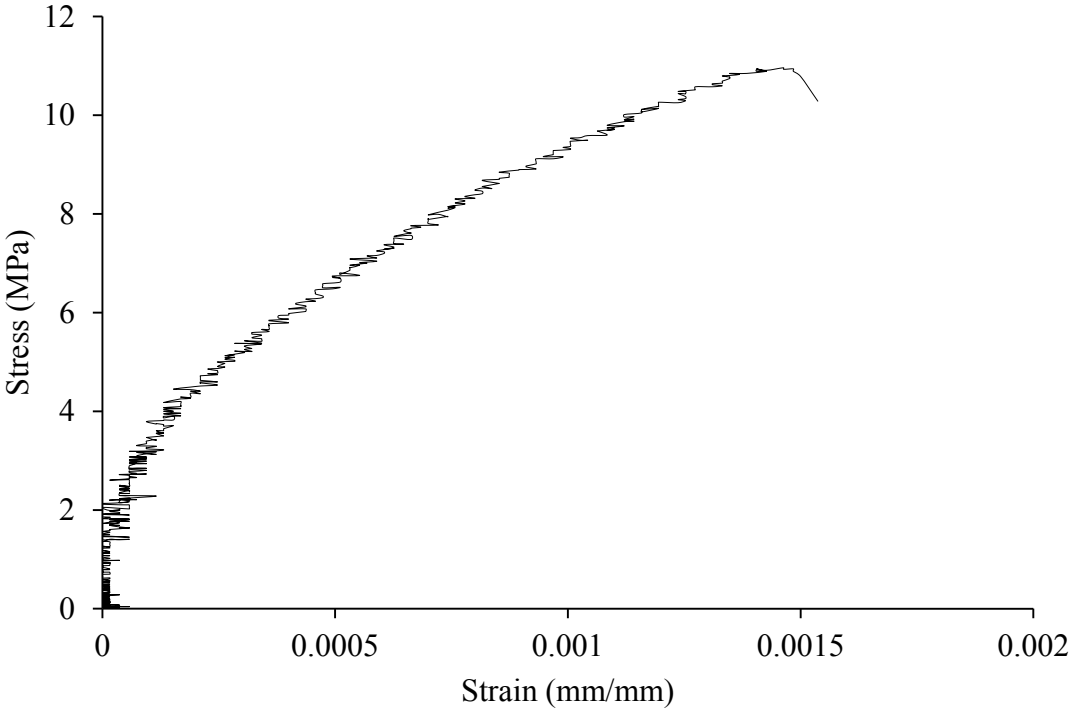

Figure A. 8 Stress-strain curve for prism V9

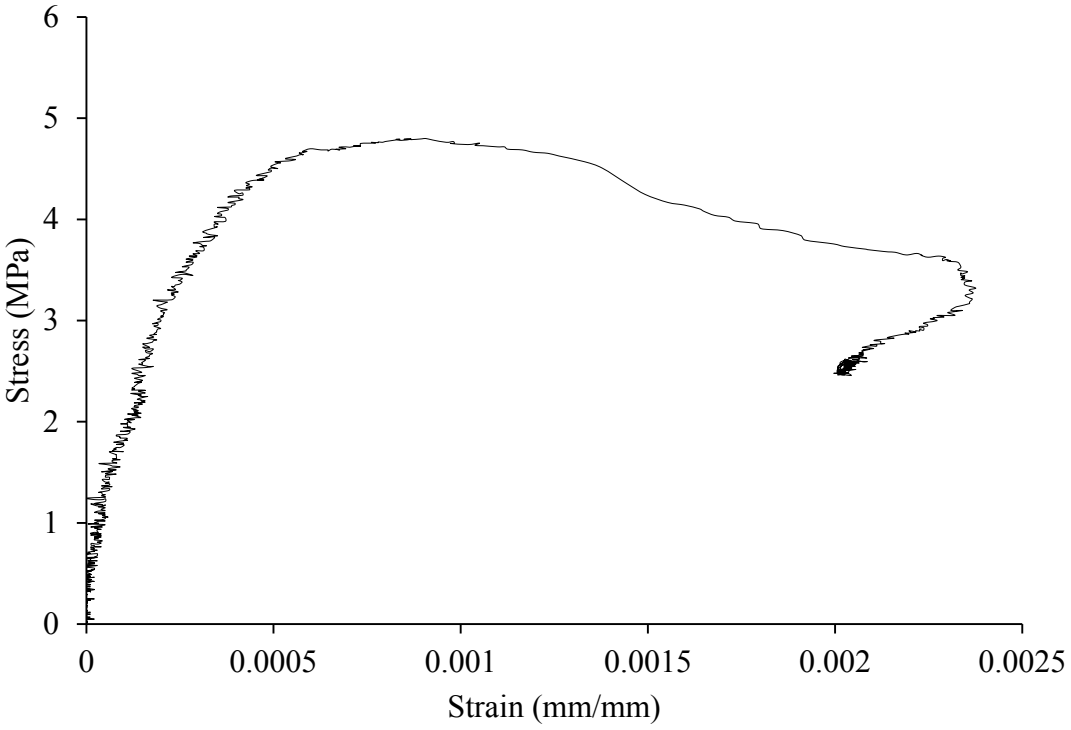

Figure A. 9 Stress-strain curve for prism H1

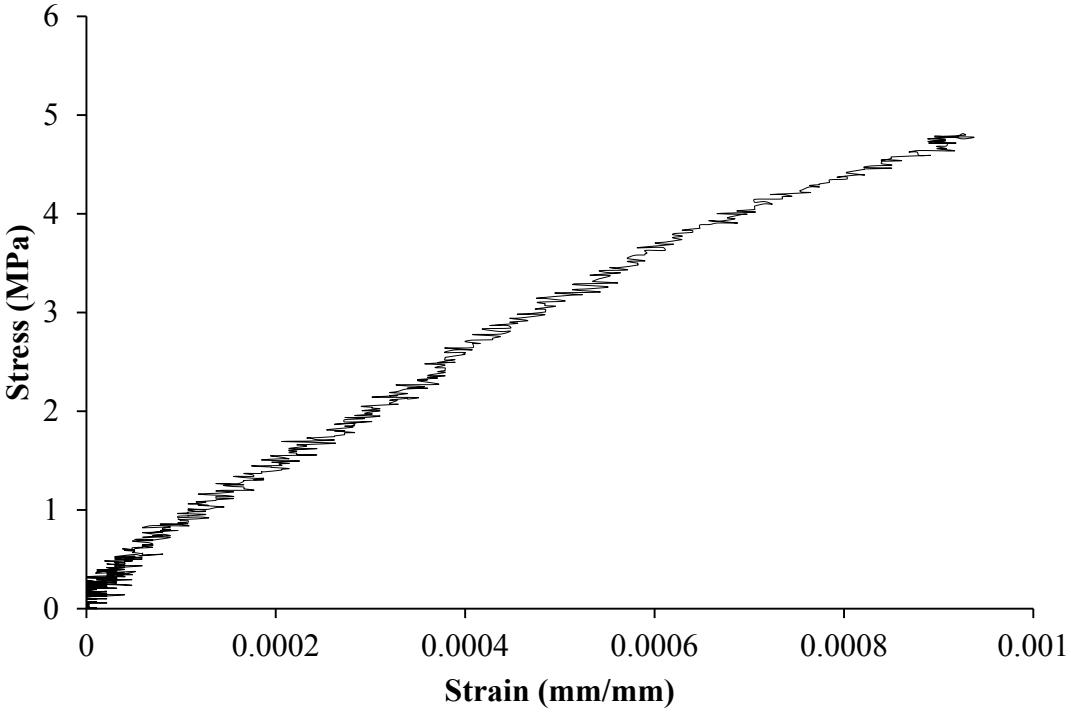

Figure A. 10 Stress-strain curve for prism H2

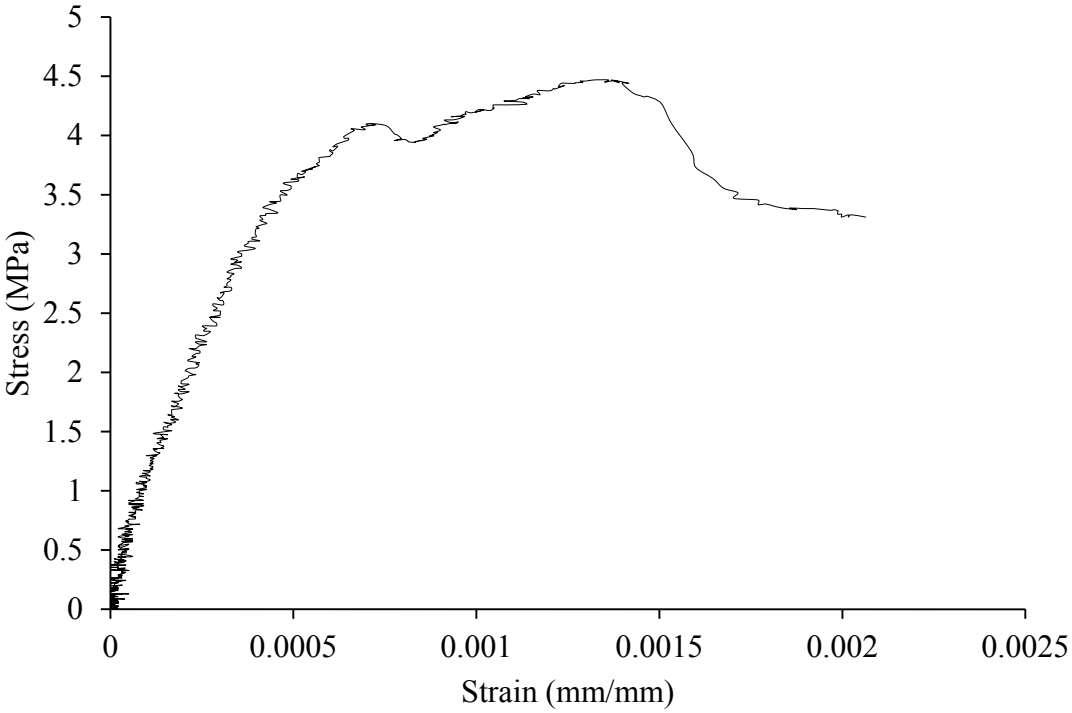

Figure A. 11 Stress-strain curve for prism H4

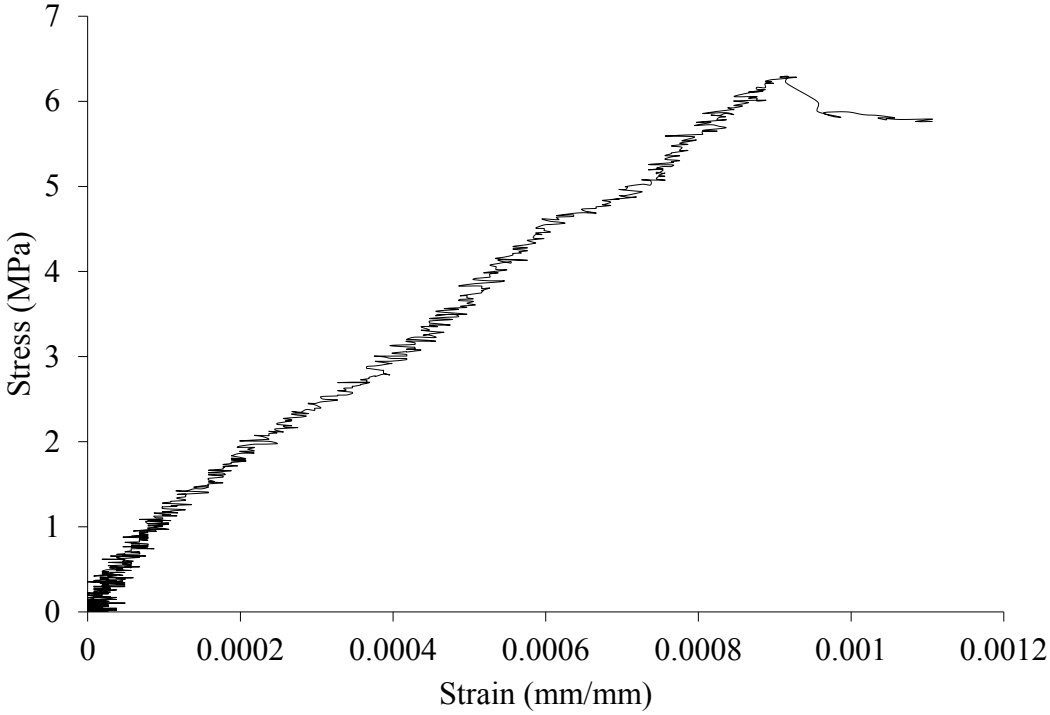

Figure A. 12 Stress-strain curve for prism H5

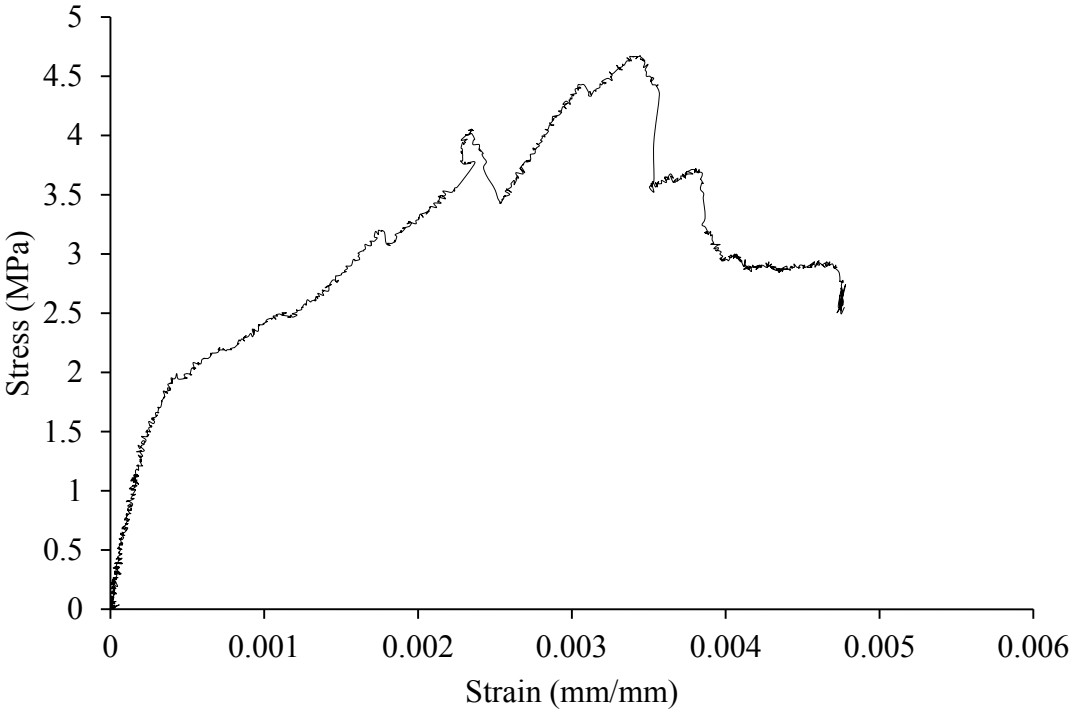

Figure A. 13 Stress-strain curve for prism H7

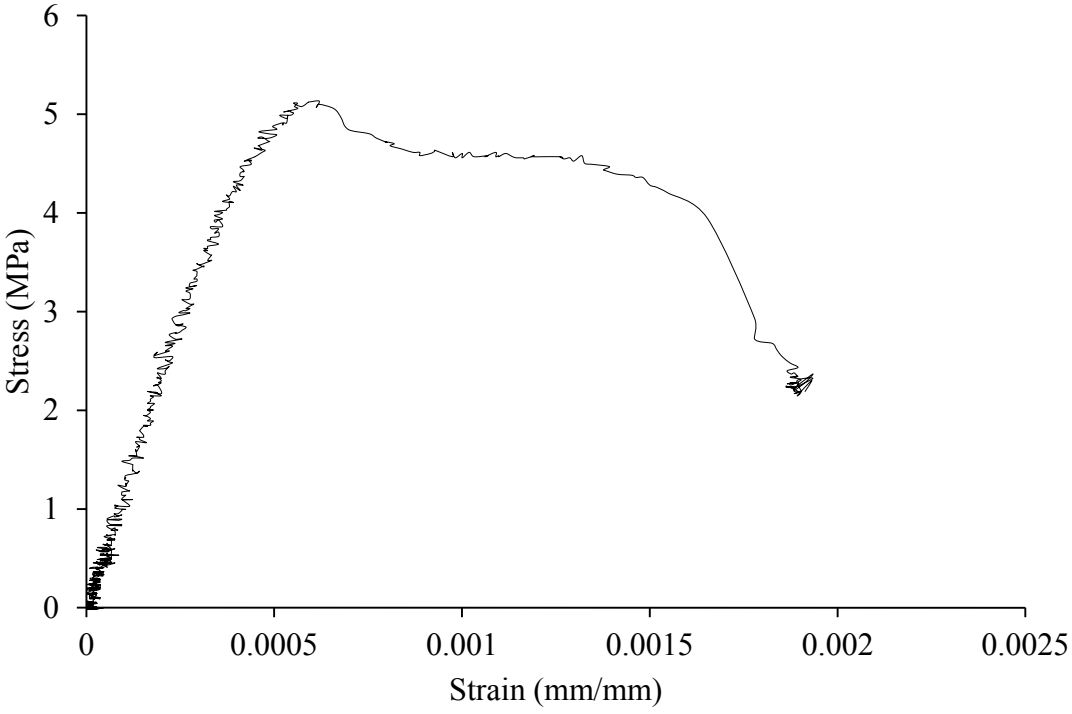

Figure A. 14 Stress-strain curve for prism D1

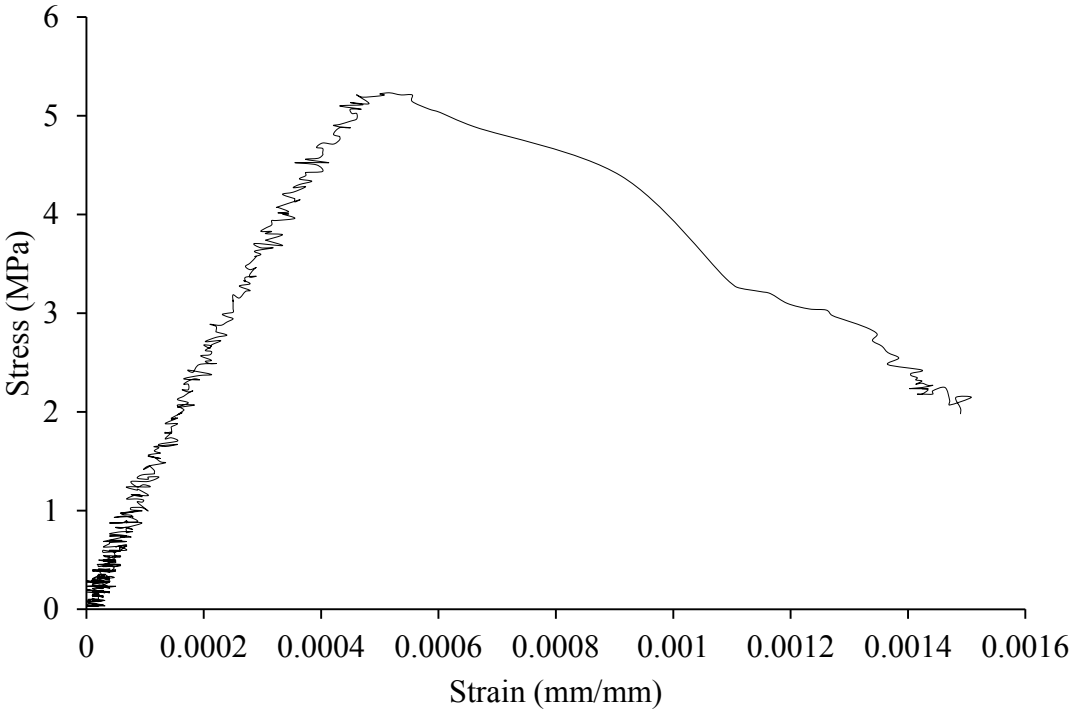

Figure A. 15 Stress-strain curve for prism D2

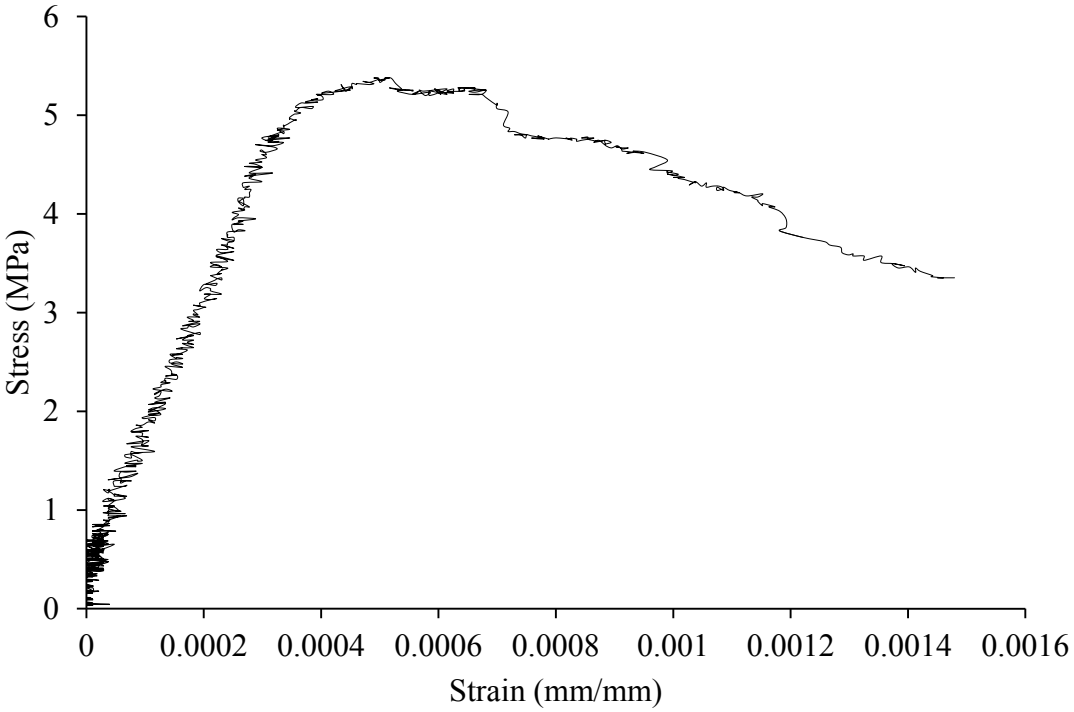

Figure A. 16 Stress-strain curve for prism D3

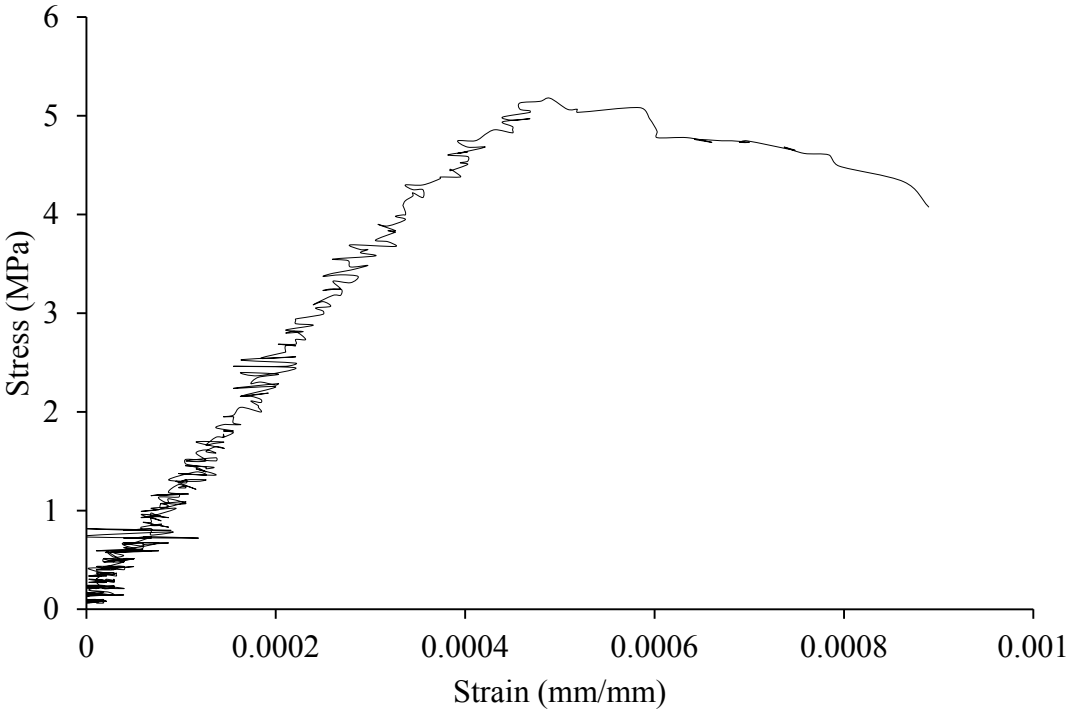

Figure A. 17 Stress-strain curve for prism D4

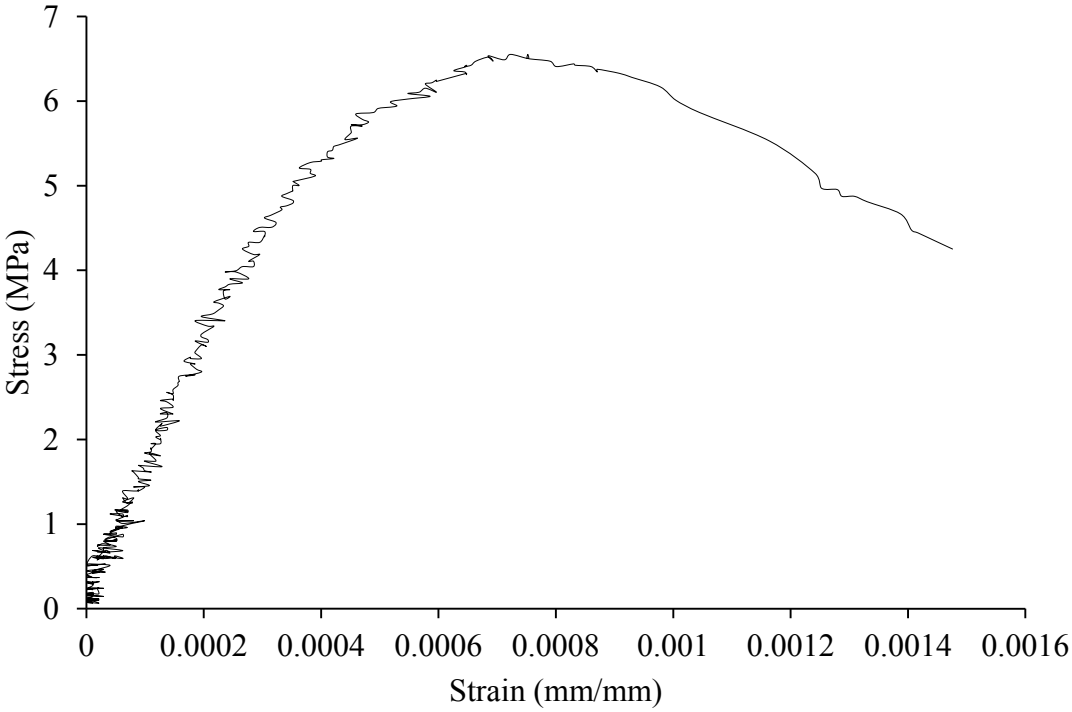

Figure A. 18 Stress-strain curve for prism D5

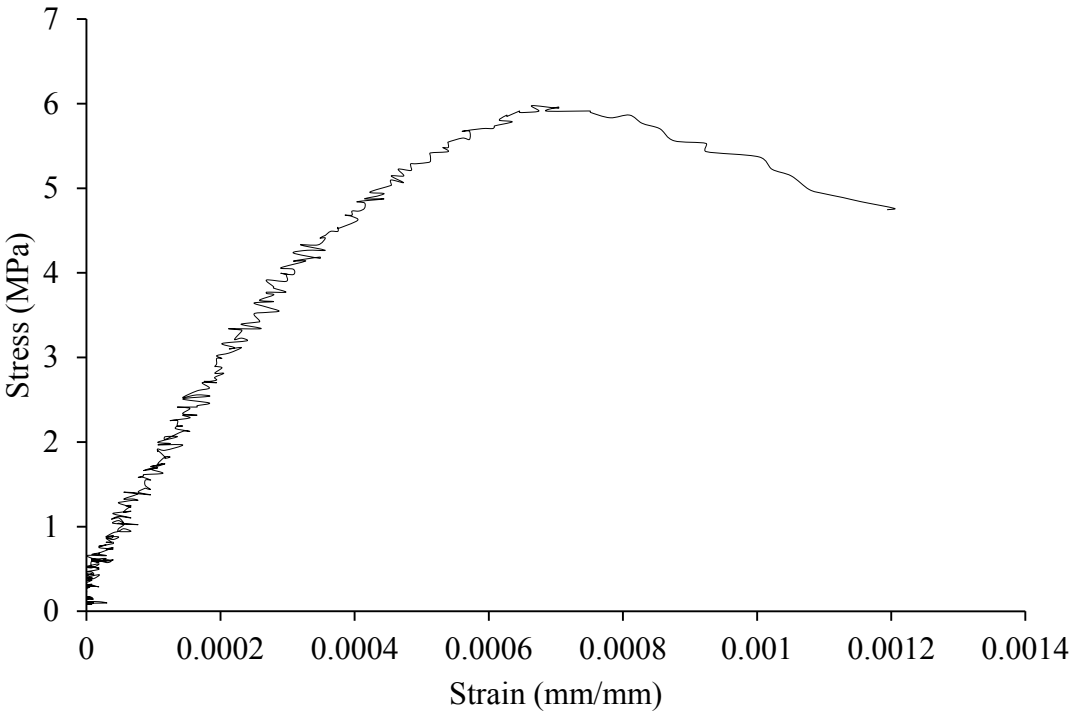

Figure A. 19 Stress-strain curve for prism D6

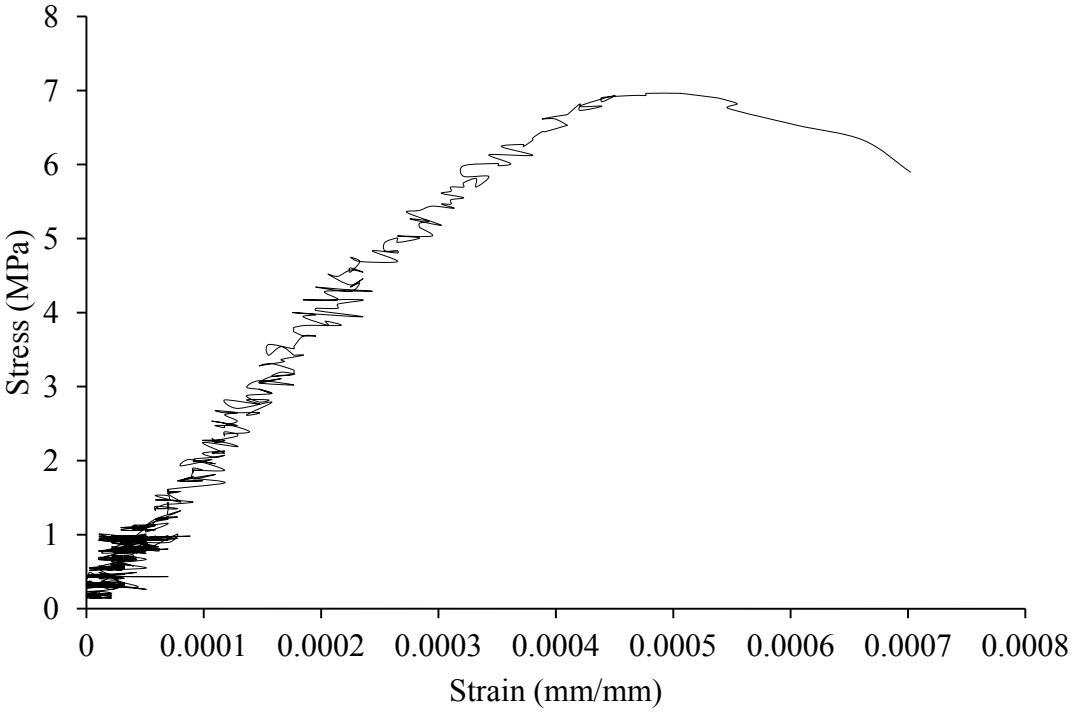

Figure A. 20 Stress-strain curve for prism D8